Ultra-High Performance Concrete Composite Connections for Precast Concrete Bridge Decks

April 2012

NTIS Accession No. PB2012-107569

FHWA Publication No. FHWA-HRT-12-041

U.S. Department of Transportation
Federal Highway Administration

FOREWORD

With the ever increasing congestion and deterioration of our nation's highway system, a need exists to develop highly durable and rapidly constructed infrastructure systems. Durable bridge structures that would require less intrusive maintenance and would exhibit longer life spans thus maximizing the use of the facility are highly desirable. Expediting bridge construction can minimize traffic flow disruptions. Ultra-high performance concrete (UHPC) is an advanced construction material which affords new opportunities to envision the future of the highway infrastructure. The Federal Highway Administration has been engaged in research on the optimal uses of UHPC in the highway bridge infrastructure since 2001 through its Bridge of the Future initiative. This report presents results of a study aimed at assessing the performance of a novel field-cast UHPC composite connection to be used between modular bridge deck components and supporting girder elements. Traditional connection concepts engaged to affix prefabricated deck components to girders have presented construction and performance issues. The novel connection concept investigated herein facilitates simplified construction operations while simultaneously allowing the composite bridge superstructure system to emulate or supersede the performance of conventional precast or cast-in-place systems.

This report corresponds to the TechBrief titled "Ultra-High Performance Concrete Composite Connections for Precast Concrete Bridge Decks" (FHWA-HRT-12-042). This report is being distributed through the National Technical Information Service for informational purposes. The content in this report is being distributed "as is" and may contain editorial or grammatical errors.

TECHNICAL REPORT DOCUMENTATION PAGE

1. Report No. FHWA-HRT-12-041	2. Government Accession No. PB2012-107569	3. Recipient's Catalog No.
4. Title and Subtitle Ultra-High Performance Concrete Composite Connections for Precast Concrete Bridge Decks		5. Report Date April 2012 6. Performing Organization Code:
7. Author(s) Benjamin A. Graybeal		8. Performing Organization Report No.
9. Performing Organization Name and Address Office of Infrastructure Research & Development Federal Highway Administration 6300 Georgetown Pike McLean, VA 22101-2296		10. Work Unit No. 11. Contract or Grant No.
12. Sponsoring Agency Name and Address Office of Infrastructure Research & Development Federal Highway Administration 6300 Georgetown Pike McLean, VA 22101-2296		13. Type of Report and Period Covered Final Report: 2010-2011 14. Sponsoring Agency Code HRDI-40

15. Supplementary Notes

16. Abstract

The demand for accelerated construction of highway bridges and the historically sub-optimal performance of cast-in-place bridge decks has led to a demand for the use of prefabricated concrete bridge decks. Although this decking system presents many advantages, one fundamental hurdle to its use is the field-cast connections which join the panels to the supporting superstructure. The intent of this research project is to redesign the composite connection in a way that provides for simple, constructible details which do not present field fit-up issues and which provide good long-term durability performance. A relatively new construction material, ultra-high performance concrete (UHPC), was engaged for this project. UHPC presents a unique set of rheological, mechanical, and durability properties which are particularly well suited to meeting these goals.

Full-scale girder/deck structural elements were fabricated and tested under cyclic fatigue and static structural loadings. The variables assessed within the study included the performance of both a conventional connection and the novel UHPC connection when installed on both steel and precast concrete girders. The test setup involved loading the 12.2-m (40-foot) long, 1.3-m (51-inch) deep test specimens in four-point bending. The cyclic testing involved application of more than eleven million of cycles fatigue loading, which was followed by static loading of each specimen to failure. The applied loadings surpassed the design loads required by the AASHTO LRFD Bridge Design Specifications. Assessment of performance of the connection and recommendations for future use are based on experience with fabrication of test specimens and on observations and analyses from the structural testing.

This report corresponds to the TechBrief titled "Ultra-High Performance Concrete Composite Connections for Precast Concrete Bridge Decks" (FHWA-HRT-12-042).

17. Key Words	18. Distribution Statement
Ultra-high performance concrete, UHPC, fiber-reinforced concrete, bridges, accelerated construction, connection detail, prefabricated bridge deck, cyclic testing	No restrictions. This document is available through the National Technical Information Service, Springfield, VA 22161.

19. Security Classif. (of this report)	20. Security Classif. (of this page)	21. No. of Pages	22. Price
Unclassified	Unclassified	110	A07

Form DOT F 1700.7 (8-72) Reproduction of completed page authorized

SI* (MODERN METRIC) CONVERSION FACTORS

APPROXIMATE CONVERSIONS TO SI UNITS

Symbol	When You Know	Multiply By	To Find	Symbol
		LENGTH		
in	inches	25.4	millimeters	mm
ft	feet	0.305	meters	m
yd	yards	0.914	meters	m
mi	miles	1.61	kilometers	km
		AREA		
in^2	square inches	645.2	square millimeters	mm^2
ft^2	square feet	0.093	square meters	m^2
yd^2	square yard	0.836	square meters	m^2
ac	acres	0.405	hectares	ha
mi^2	square miles	2.59	square kilometers	km^2
		VOLUME		
fl oz	fluid ounces	29.57	milliliters	mL
gal	gallons	3.785	liters	L
ft^3	cubic feet	0.028	cubic meters	m^3
yd^3	cubic yards	0.765	cubic meters	m^3
		NOTE: volumes greater than 1000 L shall be shown in m^3		
		MASS		
oz	ounces	28.35	grams	g
lb	pounds	0.454	kilograms	kg
T	short tons (2000 lb)	0.907	megagrams (or "metric ton")	Mg (or "t")
		TEMPERATURE (exact degrees)		
^oF	Fahrenheit	5 (F-32)/9 or (F-32)/1.8	Celsius	^oC
		ILLUMINATION		
fc	foot-candles	10.76	lux	lx
fl	foot-Lamberts	3.426	candela/m^2	cd/m^2
		FORCE and PRESSURE or STRESS		
lbf	poundforce	4.45	newtons	N
lbf/in^2	poundforce per square inch	6.89	kilopascals	kPa

APPROXIMATE CONVERSIONS FROM SI UNITS

Symbol	When You Know	Multiply By	To Find	Symbol
		LENGTH		
mm	millimeters	0.039	inches	in
m	meters	3.28	feet	ft
m	meters	1.09	yards	yd
km	kilometers	0.621	miles	mi
		AREA		
mm^2	square millimeters	0.0016	square inches	in^2
m^2	square meters	10.764	square feet	ft^2
m^2	square meters	1.195	square yards	yd^2
ha	hectares	2.47	acres	ac
km^2	square kilometers	0.386	square miles	mi^2
		VOLUME		
mL	milliliters	0.034	fluid ounces	fl oz
L	liters	0.264	gallons	gal
m^3	cubic meters	35.314	cubic feet	ft^3
m^3	cubic meters	1.307	cubic yards	yd^3
		MASS		
g	grams	0.035	ounces	oz
kg	kilograms	2.202	pounds	lb
Mg (or "t")	megagrams (or "metric ton")	1.103	short tons (2000 lb)	T
		TEMPERATURE (exact degrees)		
^oC	Celsius	1.8C+32	Fahrenheit	^oF
		ILLUMINATION		
lx	lux	0.0929	foot-candles	fc
cd/m^2	candela/m^2	0.2919	foot-Lamberts	fl
		FORCE and PRESSURE or STRESS		
N	newtons	0.225	poundforce	lbf
kPa	kilopascals	0.145	poundforce per square inch	lbf/in^2

*SI is the symbol for the International System of Units. Appropriate rounding should be made to comply with Section 4 of ASTM E380.
(Revised March 2003)

TABLE OF CONTENTS

CHAPTER 1. INTRODUCTION 1

INTRODUCTION 1
OBJECTIVE 2
SUMMARY OF APPROACH 2
OUTLINE OF REPORT 2

CHAPTER 2. BACKGROUND 3

INTRODUCTION 3
ULTRA-HIGH PERFORMANCE CONCRETE 3
UNREINFORCED SHEAR STRENGTH OF UHPC CONNECTIONS 4
ADDITIONAL RESEARCH ON UHPC COMPOSITE CONNECTIONS 5
HORIZONTAL SHEAR DESIGN AND ANALYSIS 5

CHAPTER 3. SPECIMEN DESIGN, FABRICATION, AND MATERIAL PROPERTIES 8

INTRODUCTION 8
DESIGN CONCEPT 8
SPECIMEN DESIGN 9
SPECIMEN FABRICATION 21
UHPC MATERIAL PROPERTIES 23
CONVENTIONAL GROUT MATERIAL PROPERTIES 25
PRECAST CONCRETE MATERIAL PROPERTIES 25

CHAPTER 4. TEST PROGRAM AND RESULTS 27

INTRODUCTION 27
TEST PROGRAM 27
UHPC COMPOSITE CONNECTION RESULTS 32
Cyclic Testing 32
Static Loading to Failure 37
CONVENTIONAL CONNECTION RESULTS 44
Cyclic Testing 46
Static Loading to Failure 49

CHAPTER 5. DISCUSSION OF RESULTS 62

INTRODUCTION 62
HORIZONTAL INTERFACE SHEAR — CYCLIC LOAD PERFORMANCE 62
HORIZONTAL INTERFACE SHEAR — STATIC LOAD PERFORMANCE 64
HORIZONTAL INTERFACE SHEAR OF MONOLITHIC UHPC 67
PERFORMANCE OF PRECAST CONCRETE GIRDER COMPOSITE CONNECTION 68
ASSESSMENT OF STUD WELDS 68
RESTRAINED SHRINKAGE CRACKING OF FIELD-CAST GROUTS 73

CHAPTER 6. CONCLUSIONS AND RECOMMENDATIONS 81

INTRODUCTION 81
CONCLUSIONS 81

RECOMMENDATIONS....82
FUTURE RESEARCH....84
ACKNOWLEDGEMENTS....86
REFERENCES....87
APPENDIX A....89

LIST OF FIGURES

Figure 1. Illustration. Conventional composite connection: Transverse cross section of emulative steel girder connection. 13
Figure 2. Illustration. Conventional composite connection: Longitudinal cross section of emulative steel girder connection. 14
Figure 3. Illustration. Conventional composite connection: Transverse cross section of concrete girder connection. 15
Figure 4. Illustration. Conventional composite connection: Longitudinal cross section of concrete girder connection. 16
Figure 5. Illustration. UHPC composite connection: Transverse cross section of emulative steel girder connection. 17
Figure 6. Illustration. UHPC composite connection: Longitudinal cross section of emulative steel girder connection. 18
Figure 7. Illustration. UHPC composite connection: Transverse cross section of concrete girder connection. 19
Figure 8. Illustration. UHPC composite connection: Longitudinal cross section of concrete girder connection. 20
Figure 9. Photograph. Composite connection between emulated steel girder and precast concrete deck immediately prior to field-casting of UHPC. 21
Figure 10. Photograph. Composite connection between concrete girder and precast concrete deck immediately prior to field-casting of UHPC. 22
Figure 11. Illustration. Sample load versus lateral expansion result from a split cylinder test completed on a UHPC cylinder. 24
Figure 12. Illustration. Test setup for cyclic loading of test specimens. 29
Figure 13. Photograph. Overall test setup for cyclic test program. 29
Figure 14. Illustration. Cyclic loading program. 30
Figure 15. Illustration. Test setup for static loading of test specimens. 30
Figure 16. Photograph. Overall test setup for static test program. 31
Figure 17. Illustration. Instrumentation plan used throughout test program. 31
Figure 18. Graph. Cyclic loading program for UHPC connection specimen. 32
Figure 19. Graph. Horizontal movement at haunch in portion of UHPC connection specimen which emulated the composite connection to a concrete girder. 34
Figure 20. Graph. Horizontal movement at haunch in portion of UHPC connection specimen which emulated the composite connection to a steel girder. 35
Figure 21. Graph. Internal strain in portion of UHPC connection specimen which emulated the composite connection to a concrete girder. 35
Figure 22. Graph. Internal strain in portion of UHPC connection specimen which emulated the composite connection to a steel girder. 36
Figure 23. Photo. Haunch connection at portion of test specimen which emulated the composite connection to concrete girder (i.e., west end) at conclusion of cyclic testing. 36

Figure 24. Graph. Load-deflection response of UHPC connection specimen under static load to failure. 39
Figure 25. Graph. Horizontal movement between deck and haunch in portion of UHPC connection specimen which emulated the composite connection to a concrete girder when under static load to failure. 39
Figure 26. Graph. Horizontal movement between haunch and girder in portion of UHPC connection specimen which emulated the composite connection to a concrete girder when under static load to failure. 40
Figure 27. Graph. Horizontal movement between deck and haunch in portion of UHPC connection specimen which emulated the composite connection to a steel girder when under static load to failure. 40
Figure 28. Graph. Horizontal movement between haunch and girder in portion of UHPC connection specimen which emulated the composite connection to a steel girder when under static load to failure. 41
Figure 29. Photo. Haunch connection which emulated the composite connection to a concrete girder (i.e., west end) immediately before the attainment of peak applied load. 41
Figure 30. Photo. Haunch connection which emulated the composite connection to a steel girder (i.e., east end) after completion of static testing. 42
Figure 31. Photo. Haunch connection which emulated the composite connection to a concrete girder (i.e., west end) after completion of static testing. 42
Figure 32. Illustration. Cracking apparent on north face of west end of test specimen after completion of static testing. 43
Figure 33. Illustration. Cracking apparent on south face of east end of test specimen after completion of static testing. 43
Figure 34. Photo. Distress in deck concrete at haunch connection near east end of test specimen which emulated the composite connection to a steel girder. Left photo pertains to south face. Right photo pertains to north face. 44
Figure 35. Photo. Distress in core extracted from haunch connection near east end of test specimen. 44
Figure 36. Photo. Cracking apparent on north face of haunch near east end of test specimen. 45
Figure 37. Photo. Cracking apparent on top of deck at grout pocket near east end of test specimen prior to start of structural loading. 46
Figure 38. Photo. Cracking apparent on top of deck at grout pocket near west end of test specimen prior to start of structural loading. 46
Figure 39. Illustration. Cyclic loading program for conventional connection specimen. 47
Figure 40. Graph. Horizontal movement at haunch in portion of conventional connection specimen which emulated the composite connection to a concrete girder. 48
Figure 41. Graph. Horizontal movement at haunch in portion of conventional connection specimen which emulated the composite connection to a steel girder. 49
Figure 42. Graph. Load-deflection response of conventional connection specimen under static load to failure. 52

Figure 43. Graph. Horizontal movement between deck and haunch in portion of conventional connection specimen which emulated the composite connection to a concrete girder when under static load to failure. 53
Figure 44. Graph. Horizontal movement between haunch and girder in portion of conventional connection specimen which emulated the composite connection to a concrete girder when under static load to failure. 53
Figure 45. Graph. Horizontal movement between deck and haunch in portion of conventional connection specimen which emulated the composite connection to a steel girder when under static load to failure. 54
Figure 46. Graph. Horizontal movement between haunch and girder in portion of conventional connection specimen which emulated the composite connection to a steel girder when under static load to failure. 54
Figure 47. Photo. West end and south face of test specimen immediately after completion of test. 55
Figure 48. Photo. Haunch connection on south face at east end of test specimen when applied shear load in east end was equal to 1575 kN (354 kips). 55
Figure 49. Photo. Haunch connection on south face at east end of test specimen when applied shear load in east end was equal to 1846 kN (415 kips). 56
Figure 50. Photo. Haunch connection on south face at east end of test specimen immediately after completion of test. 56
Figure 51. Photo. East end and north face of test specimen immediately after completion of test. 57
Figure 52. Photo. Midspan north face of test specimen immediately after completion of test. 57
Figure 53. Photo. Emulated steel girder composite connection after completion of test and removal of haunch/deck. 58
Figure 54. Photo. Emulated steel girder composite connection after completion of test and removal of haunch/deck. 59
Figure 55. Photo. Easternmost steel plate on top of girder within emulated steel girder composite connection. 60
Figure 56. Photo. Easternmost two rows of shear studs emanating from conventional grout and precast deck. 60
Figure 57. Illustration. Disposition of shear studs after conclusion of structural testing on conventional haunch specimen. 61
Figure 58. Graph. Design values of horizontal shear fatigue range in relation to applied shear ranges. 63
Figure 59. Graph. Comparison of horizontal movement across haunch in test specimens emulating the composite connection to a steel girder. 64
Figure 60. Graph. Horizontal shear per unit length at failure of test specimen in relation to design values and Georgia Tech push-off test results. 66
Figure 61. Graph. Minimum shear planes for horizontal shear transfer in the UHPC composite connection of the emulated steel girder portion of the test specimen. 67
Figure 62. Illustration. Failure surface of typical shear stud in deck panel. 69

Figure 63. Illustration. Failure surface of typical divot in steel plate. 70
Figure 64. Illustration. Typical stud weld cross section (from Chambers 2001 [12]). 71
Figure 65. Photo. Cross section of shear stud weld showing change in crack morphology. 72
Figure 66. Photo. Cross section of adequate shear stud weld. 73
Figure 67. Illustration. Shrinkage cracking observed in haunch of UHPC composite connection specimen prior to start of cyclic testing. 76
Figure 68. Illustration. Shrinkage cracking observed in haunch of conventional composite connection specimen prior to start of cyclic testing. 77
Figure 69. Photo. Shrinkage crack in haunch on north face near west end of conventional grout test specimen. 78
Figure 70. Photo. Shrinkage cracks in haunch on north face near west end of UHPC test specimen. 78
Figure 71. Photo. Surface finish and shrinkage cracks on formed side of precast concrete deck panel. 79
Figure 72. Illustration. Example composite connection details which emanate from the research presented herein. 83

LIST OF TABLES

Table 1. Typical field-cast UHPC mix composition. 3
Table 2. Typical field-cast UHPC material properties. 4
Table 3. NYSDOT Prospect Mountain Project bridges considered for this design concept. 9
Table 4. Cylinder density and compressive strength for the field-cast UHPC used in the haunch of the UHPC composite connection test specimen. 23
Table 5. UHPC split cylinder tensile test results 25
Table 6. Cube compressive strength for the conventional grout used in the haunch of the conventional composite connection test specimen. 25

CHAPTER 1. INTRODUCTION

INTRODUCTION

There is a growing need for durable and resilient highway bridge construction/reconstruction systems which facilitate rapid completion of on-site activities in order to minimize the impact on the traveling public. Modular components can provide higher quality, accelerated, and safer construction; however, greater offsite prefabrication of bridge components necessitates an increased reliance on the long-term performance of field-installed connections between these components. Connections have often proved lacking, resulting in less than desirable overall system performance.

Prefabricated bridge girders are a common and reliable structural component which has been deployed countless times in the highway infrastructure over the past century. In their most common form, these superstructure elements are connected to a cast-in-place concrete deck through the use of discrete steel connectors cast into or welded onto the girder. Construction of such a slab-on-stringer bridge system is quite straightforward, but can progress slowly due to the need for field activities related to the casting and curing of the concrete deck. For this reason, there is an interest in using precast concrete deck elements to accelerate on-site construction activities while simultaneously increasing the quality of the bridge deck concrete.

One primary problem with the use this type of modular decking system is the composite connection which ties the deck panels to the supporting girders. These connections require the interlacement of discrete connecting elements emanating from the prefabricated girders and decks, thus leading to tolerance and fit-up issues in the field. Also, the field-cast grouts which are used to fill the connection voids have at times displayed less than desirable durability performance. Finally, the intermittent full-depth pockets frequently specified for these composite connections can lead to aesthetic, rideability, and/or durability issues in the finished bridge deck.

The intent of this research project is to determine whether is it is feasible to redesign the composite connection in a way that provides for simple details, no interference or field fit-up issues, good long-term durability performance, and reduced aesthetic and rideability concerns. A relatively new construction material, ultra-high performance concrete (UHPC), was engaged for this project. UHPC presents a unique set of rheological, mechanical, and durability properties which are particularly well suited to meeting the goals of this research effort.

Ultra-high performance concrete (UHPC) is an advanced cementitious composite material which has been developed in recent decades. When compared to more conventional cement-based concrete materials, UHPCs tend to exhibit superior properties such as increased strength, durability, and long-term stability. Of particular interest here, UHPCs can exhibit exceptional bond when cast against previously cast concrete, can significantly shorten the development length of embedded discrete steel reinforcement, and can display a both high and sustained level of tensile resistance. These properties facilitated the redesign of the modular component connection, leading to simplified construction and the potential for enhanced long-term system performance.[1]

OBJECTIVE

The objective of this research program was to evaluate the structural response of a novel field-cast UHPC connection linking precast concrete bridge deck components to supporting girder elements.

SUMMARY OF APPROACH

The research discussed herein focuses on the development of a novel composite connection detail for joining precast concrete bridge deck panels to supporting girder elements. In order to assess the performance of this connection detail, full-scale girder/deck structural elements were fabricated and tested under cyclic fatigue and static structural loadings. The variables assessed within the study included the performance of both a conventional connection and the novel UHPC connection when installed on both steel and precast concrete girders. The test setup involved loading the 12.2-m (40-foot) long, 1.3-m (51-inch) deep test specimens in four-point bending. The cyclic testing involved application of more than eleven million of cycles fatigue loading, which was followed by static loading of each specimen to failure. The applied loadings surpassed the design loads required by the AASHTO LRFD Bridge Design Specifications[(2)] for a two-span continuous steel plate girder bridge with 63.6-m (209-foot) long spans and 2-m (79-inch) deep girders. Assessment of the connection performance was based on experience with fabrication of test specimens and on observations and analyses from the structural testing.

OUTLINE OF REPORT

This report is divided into six chapters. Chapters 1 and 2 provide an introduction to the study and relate relevant background information necessary in understanding the study's results. Chapter 3 presents the geometric details of the test specimens along with the mechanical properties of the UHPC and precast concrete included in the study. Chapter 4 presents the test results, while Chapter 5 presents further detailed analysis thereof. Finally, Chapter 6 presents the conclusions and recommendations from this research program.

CHAPTER 2. BACKGROUND

INTRODUCTION

This chapter provides background information relevant to the focus of the research effort. A general discussion of UHPC constituent materials and material properties is presented first. Next, prior research focused on UHPC composite connections is presented. Finally, an overview of some past research relevant to UHPC composite connections is provided.

ULTRA-HIGH PERFORMANCE CONCRETE

The term UHPC refers to a class of advanced cementitious composite materials.[3] Many of the technological advances in the field of cement and concrete science have been brought together in the development of this set of concretes. In general terms, these concretes can be classified as high strength, fiber-reinforced cementitious composites with discontinuous pore structures and enhanced durability properties. These concretes tend to have exceptionally low water-to-cementitious materials ratios and an optimized gradation of granular materials.

Although the general concepts which lead to the advanced performance characteristics of UHPC are well known, the commercial availability of UHPC and the development of locally-sourced UHPC mixes have been limited in the United States. The availability of UHPC has developed differently in other parts of the world, most notably Europe, where multiple prebagged and locally-sourced UHPCs are available. The specific UHPC investigated in this study is a product of a major worldwide construction materials manufacturer and supplier. It is currently the only product of this type that is widely available in the U.S. in the quantities necessary for large scale infrastructure applications. Table 1 provides a typical UHPC composition.[4]

Table 1. Typical field-cast UHPC mix composition.

Material	Amount (kg/m^3 (lb/yd^3))	Percent by Weight
Portland Cement	712 (1,200)	28.5
Fine Sand	1,020 (1,720)	40.8
Silica Fume	231 (390)	9.3
Ground Quartz	211 (355)	8.4
Superplasticizer	30 (51)	1.2
Steel Fibers	156 (263)	6.2
Water	130 (218)	5.2

As reported in reference (4), the constituent material proportions were determined, in part, based on an optimization of the granular mixture. This method allows for a finely graded and highly homogeneous concrete matrix. Fine sand, generally between 150 and 600 micrometers (0.006 and 0.024 inch), is dimensionally the largest granular material. The next largest particle is cement with an average diameter of approximately 15 µm (0.0006 inch). Of similar size is the crushed quartz with an average diameter of 10 µm (0.0004 inch). The smallest particle, the silica fume, has a diameter small enough to fill the interstitial voids between the cement and the

crushed quartz particles. Dimensionally, the largest constituent in the mix is the steel fiber reinforcement. In this study, the fibers in the mix had a diameter of 0.2 mm (0.008 inch), a length of 12.7 mm (0.5 inch), and a minimum tensile strength of 2600 MPa (377 ksi). The fibers were included in the mix at two percent by volume. Given the relative sizes of the sand and the fibers, the steel fibers are able to reinforce the concrete matrix on the micro level.

The research program associated with reference (4) characterized the material properties of a similar UHPC product produced by the same manufacturer as the UHPC investigated in this study. A brief summary of the relevant material property results is presented in Table 2. Note that, as with the UHPC in the specimens tested in this study, these results pertain to UHPC which was cast and cured in an ambient environment.

Table 2. Typical field-cast UHPC material properties.

Material Characteristic	Average Result
Density	2,480 kg/m^3 (155 lb/ft^3)
Compressive Strength (ASTM C39; 28-day strength)	126 MPa (18.3 ksi)
Modulus of Elasticity (ASTM C469; 28-day modulus)	42.7 GPa (6200 ksi)
Split Cylinder Cracking Strength (ASTM C496)	9.0 MPa (1.3 ksi)
Prism Flexure Cracking Strength (ASTM C1018; 305-mm (12-in.) span)	9.0 MPa (1.3 ksi)
Mortar Briquette Cracking Strength (AASHTO T132)	6.2 MPa (0.9 ksi)
Direct Tension Cracking Strength (Axial tensile load)	5.5–6.9 MPa (0.8–1.0 ksi)
Prism Flexural Tensile Toughness (ASTM C1018; 305-mm (12-in.) span)	I_{30} = 48
Long-Term Creep Coefficient (ASTM C512; 77 MPa (11.2 ksi) load)	0.78
Long-Term Shrinkage (ASTM C157; initial reading after set)	555 microstrain
Total Shrinkage (Embedded vibrating wire gage)	790 microstrain
Coefficient of Thermal Expansion (AASHTO TP60–00)	14.7 x10^{-6} mm/mm/ºC (8.2 x10^{-6} in./in./ºF)
Chloride Ion Penetrability (AASHTO T277 (ASTM C1202); 28-day test)	360 coulombs
Chloride Ion Permeability (AASHTO T259; 12.7-mm (0.5-in.) depth)	< 0.06 kg/m^3 (< 0.10 lb/yd^3)
Scaling Resistance (ASTM C672)	No Scaling
Abrasion Resistance (ASTM C944 2x weight; ground surface)	0.73 grams lost (0.026 oz. lost)
Freeze-Thaw Resistance (ASTM C666A; 600 cycles)	RDM = 112%
Alkali-Silica Reaction (ASTM C1260; tested for 28 days)	Innocuous

UNREINFORCED SHEAR STRENGTH OF UHPC CONNECTIONS

A research investigation recently completed at the Georgia Institute of Technology (Georgia Tech) focused on the shear performance of UHPC as applicable to bridge girders.[5] This study, titled “Shear and Shear Friction of Ultra-High Performance Concrete Bridge Girders” was authored by C. Kennan Crane under the advisement of Dr. L. Kahn. Of particular interest to the present study, the Georgia Tech study investigated the shear performance of girder/deck composite connections by conducting push-off tests of monolithic UHPC specimens.

These test specimens were composed of the same type of UHPC from the same manufacturer; however, a different formulation was used. Specifically, these tests were completed on the standard set version of this UHPC which is intended for use in precasting operations. Additionally, these specimens were steam treated to accelerate their curing.

The test program included two relevant testing schemes. The first type of monolithic UHPC specimen was structurally intact and uncracked at the start of the testing. The second type of monolithic UHPC specimen was subjected to splitting tensile forces along the eventual shear plane prior to the start of the interface shear test, thus generating a specimen which was precracked along the shear plane. In both cases, the specimens contained only steel fiber reinforced UHPC crossing the shear plane; no discrete reinforcement crossed the plane.

These tests demonstrated that UHPC, whether precracked parallel to the applied shear forces or uncracked, can exhibit exceptionally high interface shear capacities. The three precracked specimen results all exceeded 11 MPa (1600 psi) of interface shear capacity. The three uncracked specimen results all exceeded 17.5 MPa (2550 psi) of interface shear capacity. For reference, the AASHTO LRFD Bridge Design Specification assumes an interface shear capacity of 2.76 MPa (400 psi) for monolithic concrete when calculating resistance to interface shear loads.

ADDITIONAL RESEARCH ON UHPC COMPOSITE CONNECTIONS

Three additional research studies which engaged UHPC as part of a composite connection system were identified. None of these studies focuses on the specific application of using UHPC as a field-cast grout in otherwise unreinforced connection regions subjected to high shear loads. However, each one does advance the concept that the exceptional mechanical properties of UHPC are relevant to enhancing the performance of discrete connections with steel members.

A study by Hegger, Rauscher, and Goralski (6) investigated the use of UHPC collars surrounding steel shear studs. The study demonstrated that these collars were capable of enhancing the local performance of the cast-in-place concrete into which the studs were embedded.

Two additional studies, one by Hegger and Raucher (7) and one by Jungwirth, Seidl, Schmitt, and Ungermann (8), investigated the use of composite beam systems composed of steel T-sections embedded into UHPC. The embedded portion of the T-section was deformed in a “puzzle” or “saw-tooth” shape in order to facilitate bonding with the UHPC. These studies demonstrated the feasibility of novel composite systems which engage the best mechanical properties of multiple construction materials.

HORIZONTAL SHEAR DESIGN AND ANALYSIS

The horizontal shear resistance across a horizontal interface in a beam element is the critical performance measure being investigated in this research project. From mechanics of materials, the horizontal shear per unit length is determined from Equation 1.

$$V_{sr} = \frac{V_f Q}{I}$$ Equation 1

In Equation 1, V_{sr} is the horizontal shear per unit length of beam. V_{sr} is sometimes referred to as shear flow. V_f refers to that vertical shear force on the beam element, Q refers to that first moment with respect to the neutral axis of the area of the cross section beyond the interface of interest, and I is the moment of inertia of the beam about the neutral axis.

This equation can be used both from a design and from an analysis standpoint. Specifically, during initial design of a bridge, the loads and cross-sectional properties of the line girders can be used to determine the required V_{sr} resistance. During the analysis of the structural response of a test specimen, the known vertical shear loads and known cross-sectional properties can be used to determine the applied V_{sr}.

In this research program, the test specimens were designed based on preliminary New York State Department of Transportation designs of specific slab-on-stringer bridges. These bridges were determined to have a particular requirement for V_{sr}. This V_{sr} requirement was then assumed to apply to the test specimen, and its composite connection was designed accordingly.

The service limit state design of the shear stud composite connectors was completed according to Equation 2 which is reproduced from AASHTO LRFD Equation 6.10.10.1.2-1. In this equation, p is the pitch of the shear connectors, n is the number of shear connectors in a cross section, and Z_r is the shear fatigue resistance of an individual shear connector.

$$p \leq \frac{nZ_r}{V_{sr}}$$ Equation 2

The strength limit state design of the shear stud composite connectors was completed according to Equation 3 which is reproduced from AASHTO LRFD Equation 6.10.10.4.3-1. In this equation, Q_n is the nominal shear resistance of one shear connector embedded in the concrete deck, A_{sc} is the cross-sectional area of one stud connector, and F_u is the specified minimum tensile strength of a shear stud connector. f_c' is the deck concrete compressive strength and E_c is the deck concrete modulus of elasticity.

$$Q_n \leq 0.5 A_{sc} \sqrt{f_c' E_c} \leq A_{sc} F_u$$ Equation 3

Normally, Equation 2 controls the design of the shear stud connectors. This was the case within this test program.

The AASHTO LRFD Bridge Design Specifications does not speak to the service load level fatigue resistance of concrete-on-concrete horizontal shear interfaces wherein reinforcing bars cross the interface. For this type of detail, the LRFD solely focuses on the strength limit state in terms of determining the details of these composite connections. Equation 4 provides the relationship with V_{ni} being the nominal shear resistance of the interface plane, c being a cohesion factor, A_{cv} being the area of concrete engaged in interface shear transfer, μ being a friction factor, A_{vf} being the area of shear reinforcement crossing the interface, f_y being the reinforcement yield strength, and P_c being the permanent net compressive force normal to the shear plane. Within this research program, the values for c and m at an intentionally roughened surface were assumed to apply for the interface at the top of the prestressed girder. The non-intentionally roughened values were chosen for the haunch to deck interface in the UHPC novel connection specimen.

$$V_{ni} = cA_{cv} + \mu\left(A_{vf}f_y + P_c\right) \qquad \text{Equation 4}$$

Due to the specific focus of this research program on the service level fatigue resistance of these connections, it was decided that an equivalent amount of steel would be specified to cross the horizontal shear interfaces at the top of the concrete girders as was specified to be in place at the top of the steel girders. In effect, this decision forced a significant increase in the amount of reinforcing bar crossing the interface since this interface was now designed according to the fatigue provisions of AASHTO LRFD Section 6.10.10.4.

In the novel UHPC composite connection test specimen, the connection detail joining the precast deck panel to the haunch was not designed for any specific service or ultimate level loading condition. The deck to haunch reinforcing plan coincided with the transverse reinforcement which would commonly be placed in the bottom mat of reinforcement in a concrete bridge deck. As such, the total amount of reinforcement crossing the horizontal shear interface between the field-cast haunch and the precast deck was significantly less than the steel which crosses the interface between the girder top flange and the field-cast haunch.

CHAPTER 3. SPECIMEN DESIGN, FABRICATION, AND MATERIAL PROPERTIES

INTRODUCTION

The physical details of the full-scale test specimens, as well as the fabrication of these specimens, are described in this chapter. Material properties for the UHPC and the conventional grout used in the haunches, and the high performance concrete (HPC) used in the precast girders and panels, are also presented.

DESIGN CONCEPT

The intent of this research program was to investigate the structural performance of conventional and novel details for creating the composite connection between prefabricated bridge girders and prefabricated bridge deck panels. In order to assess this performance, it was deemed necessary to conduct full-scale structural tests of bridge members subjected to both cyclic and static loadings commensurate with those normally considered during the design of highway bridges. Since this research program emanated from discussions between FHWA and NYSDOT, and NYSDOT was partnering with FHWA on the conduct of the program, NYSDOT was engaged to assist in determining the structural configuration of the test specimens and the structural loads to be applied.

The design of the test specimens was based on preliminary structural designs completed by NYSDOT as part of the Prospect Mountain Interchange Project. This project aims to rehabilitate eleven bridges in the Binghamton, New York area, including six bridges in the I-81/I-86/US-17 interchange over the Chenango River. As part of NYSDOT's preliminary studies for this construction project, they investigated opportunities for accelerating the construction process by engaging accelerated bridge construction technologies. NYSDOT was interested in allowing the use of precast bridge deck panels on various bridges in this construction project, while also addressing past concerns with the constructability of said systems. Specifically, NYSDOT was interested in allowing for simplified composite connection details between steel or concrete girders and precast concrete deck panels, made possible by the use of a novel UHPC connection detail.

NYSDOT identified the six bridges in the I-81/I-86/US-17 interchange as being potentially viable candidates for the use of this particular accelerated bridge construction technology and as being appropriate structures on which to base the experimental test program. Each of these bridges was likely to be constructed in multi-span continuous slab-on-stringer configurations with steel plate girders. All of these bridges were considered to include composite action between the bridge deck and the underlying girders. Basic details from these six bridges are presented in Table 3. Note that, although all of these structures are multispan steel stringer bridges, NYSDOT and FHWA were interested in demonstrating the viability of the concept for both steel and concrete superstructure bridges in single and multiple span configurations.

Through the preliminary design of these structures, NYSDOT identified a likely structural configuration for each bridge and, according to the AASHTO LRFD Bridge Design Specifications, determined the design loads to be attributed to interior and exterior girder lines in each span of each structure. Through this design process, the maximum horizontal shear fatigue range on any girder in each bridge was determined. These values are provided in Table 3. The overall maximum value is 0.164 kN/mm (0.937 kip/in.). This maximum value became the critical parameter engaged in the design of the test specimen and the structural loading program.

Table 3. NYSDOT Prospect Mountain Project bridges considered for this design concept.

Bridge	Spans	Maximum Span (m (ft))	Girder Lines	Girder Depth (mm (in.))	Girder Spacing (m (ft))	Maximum Horizontal Shear Fatigue Range (kN/mm (kip/in.))
SBEBR	2	63.6 (209)	9	2000 (79)	2.33 (7.6)	0.164 (0.937)
NBWB	2	53.5 (176)	10	1860 (73)	2.53 (8.3)	0.135 (0.771)
SB	4	49.7 (163)	5	1300 (51)	2.78 (9.1)	0.076 (0.436)
EBR	3	68.4 (224)	5	2200 (87)	2.78 (9.1)	0.067 (0.384)
NB	3	63.8 (209)	6	2200 (87)	2.73 (9.0)	0.056 (0.322)
WB	4	68.3 (224)	5	1750 (69)	2.78 (9.1)	0.054 (0.311)

SPECIMEN DESIGN

The test program included two full-scale test specimens, each of which contained details representative of two different types of composite connections. One test specimen was designed to emulate the types of composite connection details commonly implemented when precast concrete bridge deck panels are installed on prefabricated steel or concrete girders. In this type of connection system, the composite connection connectors are included as part of the prefabricated girder. The connectors emanate from the top flange of the girder and are designed to pass through the haunch into intermittent voids cast into the precast deck elements. The connectors are clustered and, commensurately, the voids in the deck panels are spaced and sized to accommodate the clustered connectors.

The conventional composite connection specimen was composed of a 991 mm (39 in.) deep prestressed girder, a 76 mm (3 in.) tall haunch, and 216 mm (8.5 in.) thick precast concrete deck panels. This specimen used a conventional grout, selected from the NYSDOT approved materials list, to fill the haunch and complete the composite connection.

The east end of this test specimen simulated the steel girder connection. A 19 mm (3/4 in.) thick steel plate was cast into the top of the top flange of the prestressed girder. This plate had rows of four transversely spaced 19 mm (3/4 in.) diameter shear studs welded onto its surface at a 321 mm (12.63 in.) longitudinal spacing. This composite connector design amounts to 3560 mm^2 of

steel per meter (1.68 in^2 of steel per foot) along the length of the test specimen. According to section 6.10.10.2 of the AASHTO LRFD Bridge Design Specifications, this composite connection design is sufficient to provide an infinite design life when subjected to a 0.189 kN/mm (1.080 kip/inch) maximum horizontal shear fatigue range at the service limit state. At the strength limit state, this design is capable of carrying an unfactored horizontal shear of 1.263 kN/mm (7.215 kip/inch) according to LRFD section 6.10.10.4 assuming a stud ultimate strength of 345 MPa (50 ksi). The details pertaining to the emulative steel girder connection end of this test specimen can be found in Figure 1 and Figure 2.

The west end of this test specimen simulated the concrete girder connection. D-108 Dowel-In bars with a size of 19M (No. 6) and a length of 305 mm (12 in.) were used in the connection. Rows of four D-108 Dowel-In bars were cast into the top flange of the girder at a 300 mm (11.81 in.) longitudinal spacing. This composite connector design amounts to 3790 mm^2 of steel per meter (1.79 in^2 of steel per foot) along the length of the test specimen. If these bars are treated as welded shear studs subjected to fatigue loads, section 6.10.10.2 of the AASHTO LRFD Bridge Design Specifications suggests that this composite connection design is sufficient to provide an infinite design life when subjected to a 0.184 kN/mm (1.053 kip/in.) maximum horizontal shear fatigue range. At the strength limit state, this design is capable of carrying an unfactored horizontal shear of 2.448 kN/mm (13.99 kips/inch) according to LRFD section 5.8.4 with 0.882 kN/mm (5.04 kips/inch) attributed to the cohesion of the cementitious materials along the roughened surface of the precast girder. The details pertaining to the concrete girder connection end of this test specimen can be found in Figure 3 and Figure 4.

The second test specimen was designed to emulate a novel type of composite connection detail being considered for use when installing precast concrete bridge deck panels on prefabricated steel or concrete girders. This novel connection detail engages the advanced mechanical properties of field-cast UHPC to simplify both the component fabrications as well as the field construction of the superstructure/deck system. The clustering of shear connectors and the intermittent pockets in the precast panels are eliminated in favor of evenly spaced shear connectors and an exposed bottom mat of deck reinforcement in the haunch region. The shear connectors do not intersect with the bottom mat of deck reinforcement and thus conflicts between the two are eliminated and field fit-up is greatly simplified.

As with the first test specimen, the second test specimen also simulated both steel and concrete girder composite connections. The same type of prestressed girder and the same types of precast deck panels were used. The haunch height was increased to 102 mm (4 in.) to create a more severe condition as compared to the conventional connection test specimen. The connection was filled with field-cast UHPC.

The east end of this test specimen emulated the steel girder composite connection with pairs of 19 mm (3/4 in.) diameter shear studs spaced at 161.9 mm (6.38 in.). This composite connector design amounts to 3510 mm^2 of steel per meter (1.66 in^2 of steel per foot) along the length of the girder at the girder to haunch interface. According to section 6.10.10.2 of the AASHTO LRFD Bridge Design Specifications, this composite connection design is sufficient to provide an infinite design life with when subjected to a 0.187 kN/mm (1.069 kip/in.) maximum horizontal shear fatigue range. At the strength limit state, this design is capable of carrying an unfactored

horizontal shear of 1.263 kN/mm (7.215 kip/inch) according to LRFD section 6.10.10.4 assuming a stud ultimate strength of 345 MPa (50 ksi). The details pertaining to the emulative steel girder connection end of this test specimen can be found in Figure 5 and Figure 6.

The west end of this test specimen emulated the concrete girder composite connection with pairs of 13M (No. 4) hairpin rebar spaced at 130 mm (5.13 in.). This composite connector design amounts to 3960 mm^2 of steel per meter (1.87 in^2 of steel per foot) along the length of the girder at the girder to haunch interface. If these bars are treated as welded shear studs subjected to fatigue loads, section 6.10.10.2 of the AASHTO LRFD Bridge Design Specifications suggests that this composite connection design is sufficient to provide an infinite design life when subjected to a 0.188 kN/mm (1.072 kip/in.) maximum horizontal shear fatigue range. At the strength limit state, this design is capable of carrying an unfactored horizontal shear of 2.52 kN/mm (14.39 kips/inch) according to LRFD section 5.8.4 with 0.882 kN/mm (5.04 kips/inch) attributed to the cohesion of the cementitious materials along the roughened surface of the precast girder. The details pertaining to the concrete girder connection end of this test specimen can be found in Figure 7 and Figure 8.

Given that the composite connection reinforcement details in this test specimen terminate within the haunch, the composite connection reinforcement at the haunch to deck interface also becomes a critical location at which a design check must be completed. Over the entire length of this test specimen, the bottom mat of deck reinforcement was exposed so as to pass through and be engaged by the field-cast UHPC. The exposed bottom layer of 13M (No. 4) transverse deck reinforcement was longitudinally spaced at 200 mm (7.88 in.) along the length of the test specimen. This deck reinforcement design amounts to 1530 mm^2 of steel per meter (0.724 in^2 of steel per foot) crossing the haunch to deck interface along the length of the girder. It is noted that none of the longitudinal reinforcing bars in the bottom mat of steel in the deck panels exist within the haunch. Using a similar design concept to that used for the design at the girder to haunch horizontal shear interface with the rebar being treated as though it had the fatigue performance of welded shear studs, section 6.10.10.2 of the AASHTO LRFD Bridge Design Specifications indicates that this composite connection design is sufficient to provide an infinite design life when subjected to a 0.061 kN/mm (0.349 kip/inch) maximum horizontal shear fatigue range. At the strength limit state, this design is capable of carrying an unfactored horizontal shear of 0.616 kN/mm (3.52 kips/inch) according to LRFD section 5.8.4 with 0.236 kN/mm (1.35 kips/inch) attributed to the cohesion of the cementitious materials along the non-roughened surface at the top of the haunch connection blockout.

Clearly, the intent of the research program is to investigate the performance of the composite connection between the girder and the precast deck panel. As such, the remainder of the test specimen must be designed so as to afford a reasonable level of overstrength against alternate failure mechanisms. However, these overstrength features must be implemented in such a way as to not create unrealistic stress conditions on the features of interest within the test. Given that the test specimens were to be loaded in four-point bending, it was of critical importance to ensure that the test specimen had excess flexural tensile strength, flexural compressive strength, and shear strength. To ensure these conditions were met, the overall width of the girder was increased, a large number of prestressing strands were specified, and high concrete compressive strengths were specified in the precast girder and the precast deck.

Through this design of the test specimen, it was possible to create a test specimen which both appeared similar to the type of composite connection design which would be expected for a common slab-on-stringer bridge and would be capable of being stressed through a range of loadings which simulated a variety of span ranges and loading configurations. The implemented loadings, which will be discussed in detail in the next chapter, were designed to offer insight into the service fatigue loadings which might be experienced by a variety of bridges. The initial cyclic load level was based on the service fatigue design stresses which would be imparted onto the composite connection in bridge SESBR of the NYSDOT Prospect Mountain Interchange Project. The initial cyclic load levels generated a fatigue shear stress in the connection which was 20 percent larger than that required for this moderately large steel plate girder bridge whose overall details were presented in Table 3. Subsequent cyclic load ranges were increased by 33 percent per stage, with the fourth (i.e., final) stage imparting a fatigue shear stress range that was 140 percent larger than that required for this bridge.

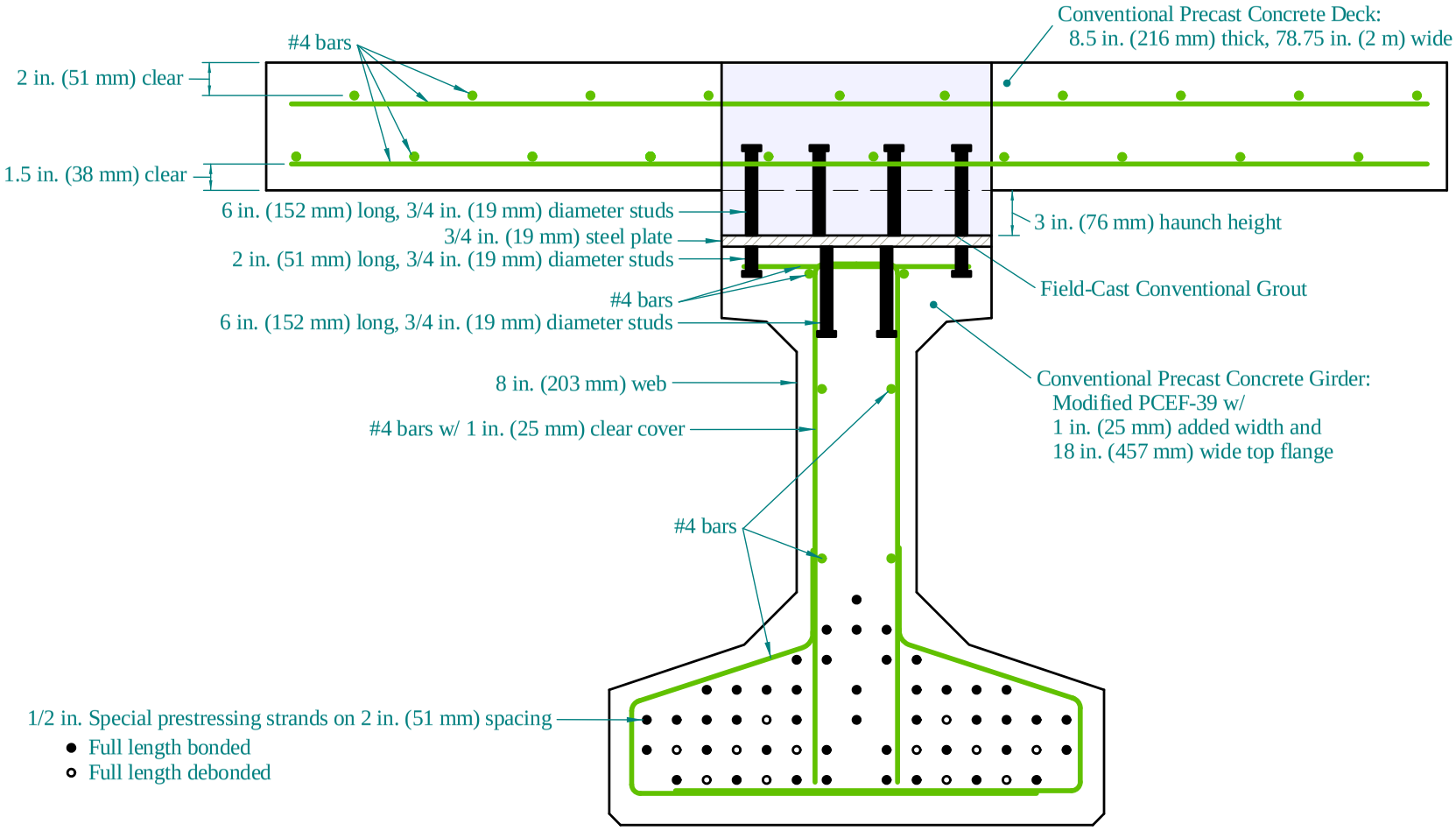

Figure 1. Illustration. Conventional composite connection: Transverse cross section of emulative steel girder connection.

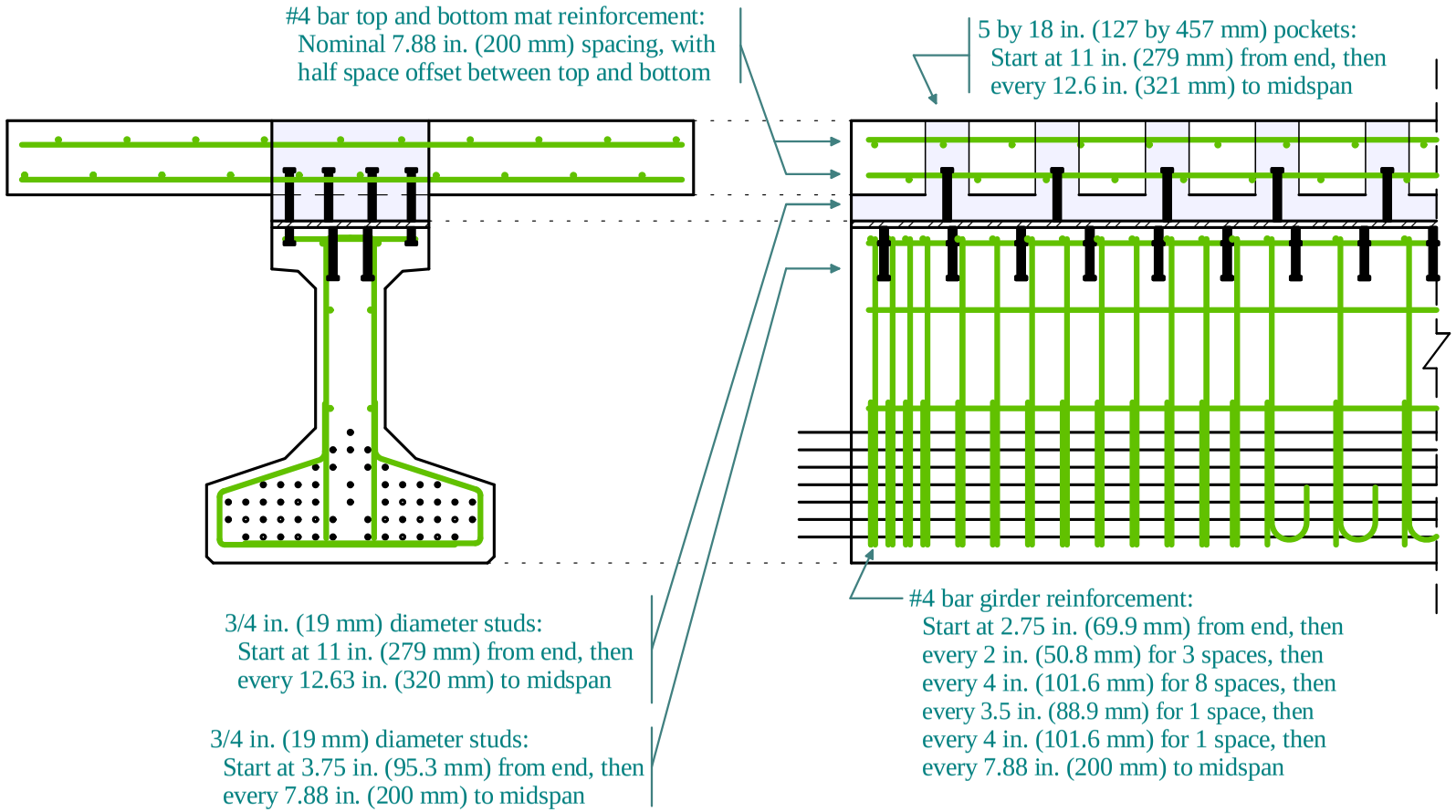

Figure 2. Illustration. Conventional composite connection: Longitudinal cross section of emulative steel girder connection.

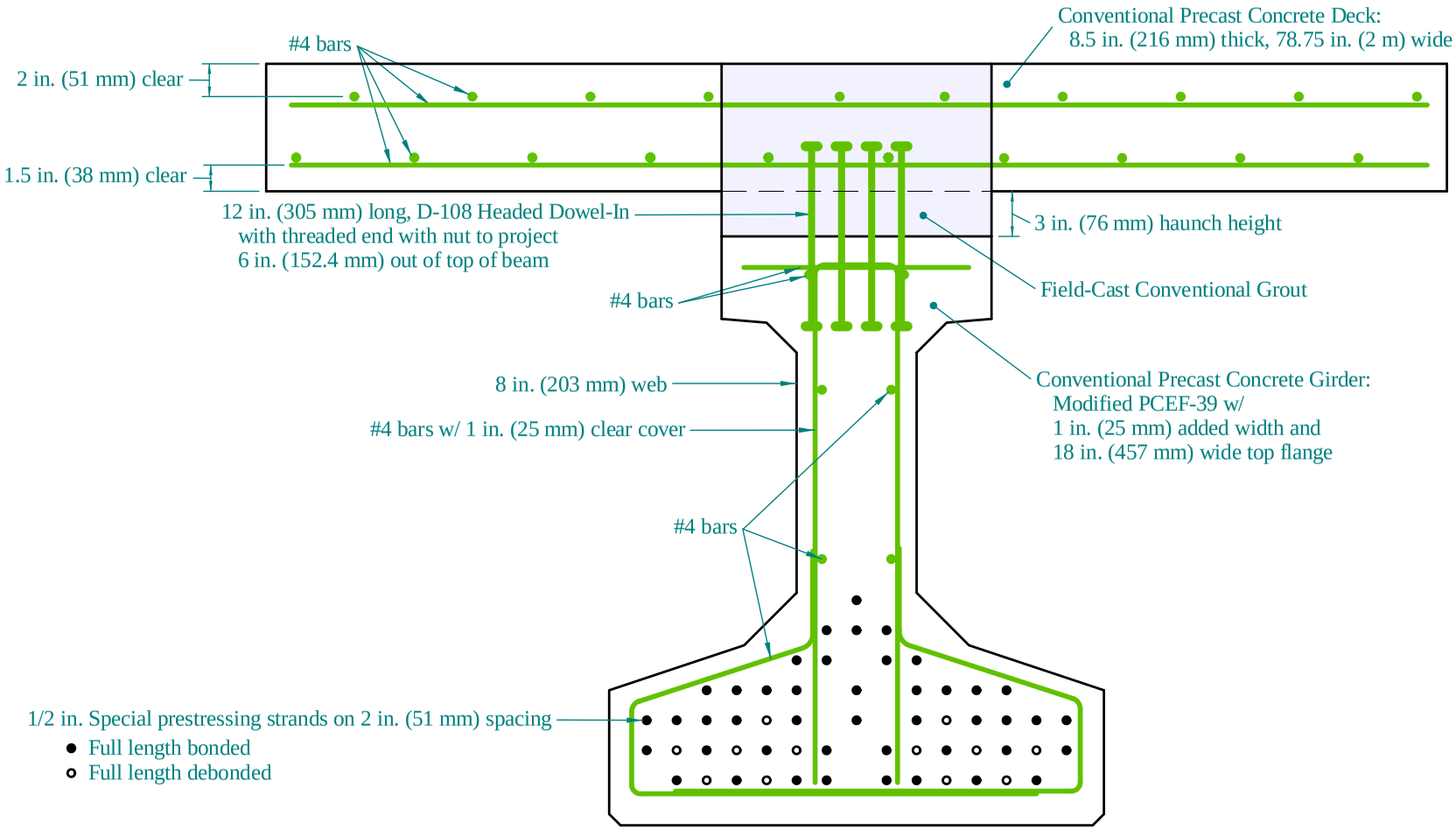

Figure 3. Illustration. Conventional composite connection: Transverse cross section of concrete girder connection.

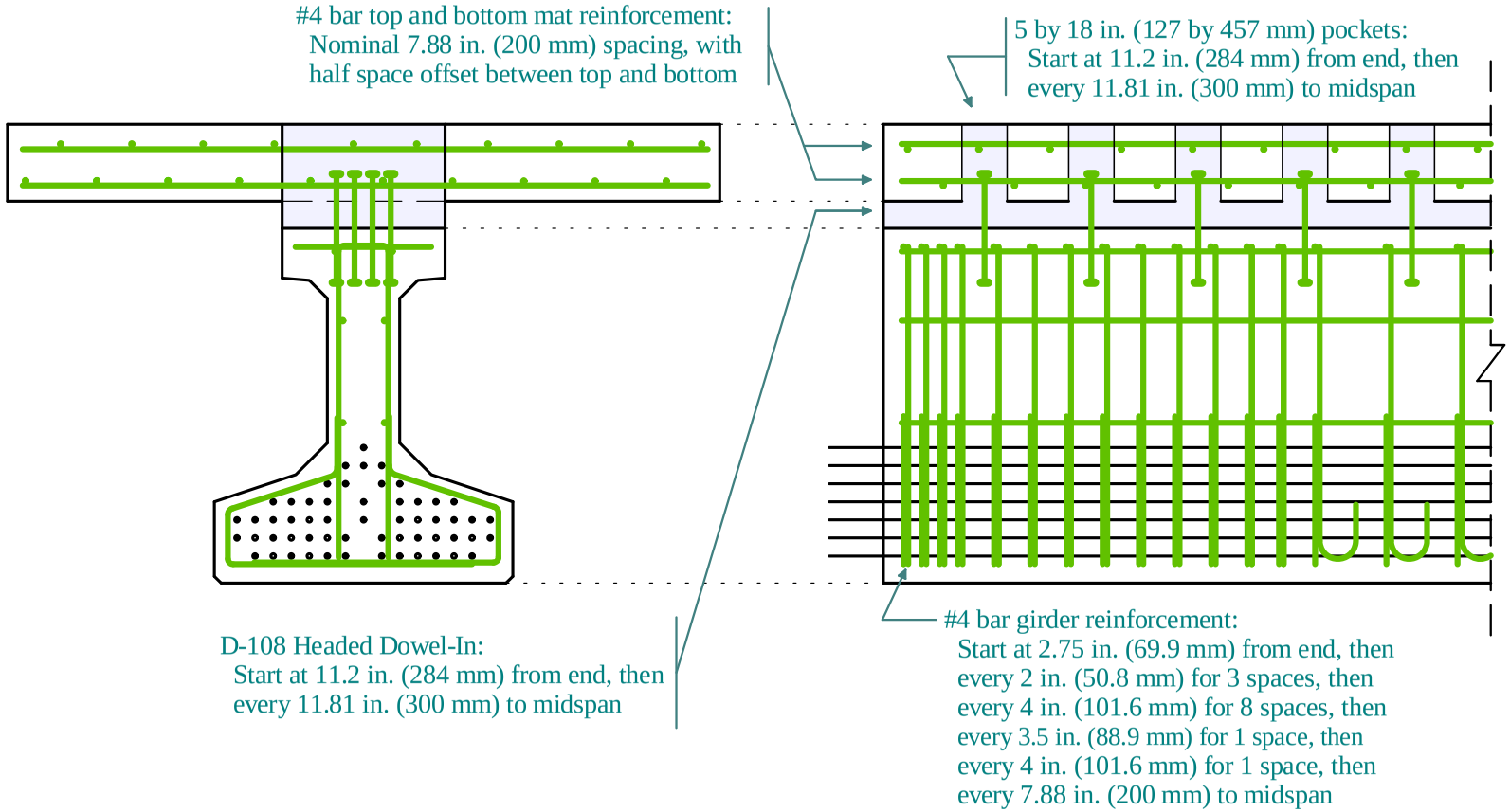

Figure 4. Illustration. Conventional composite connection: Longitudinal cross section of concrete girder connection.

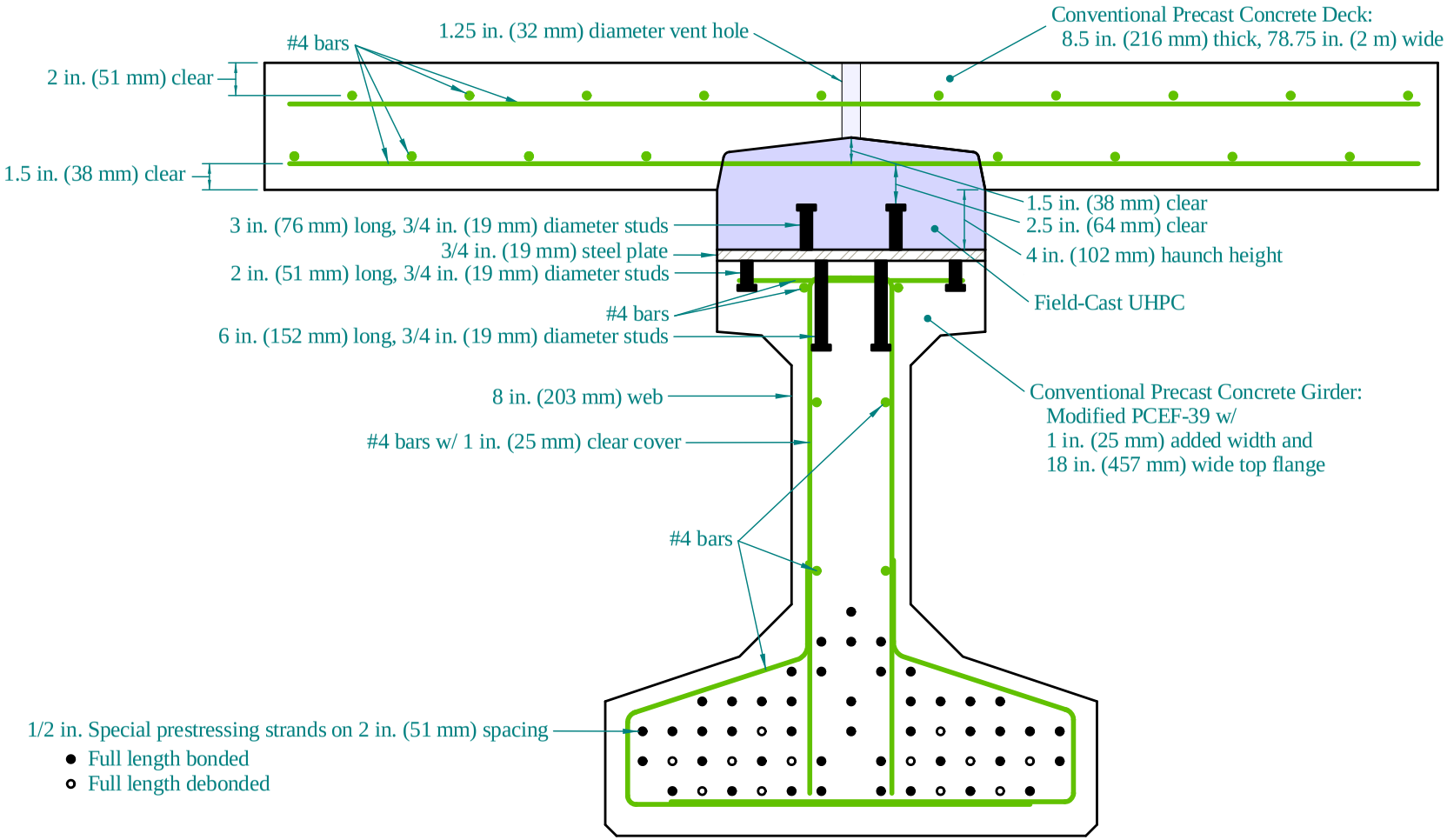

Figure 5. Illustration. UHPC composite connection: Transverse cross section of emulative steel girder connection.

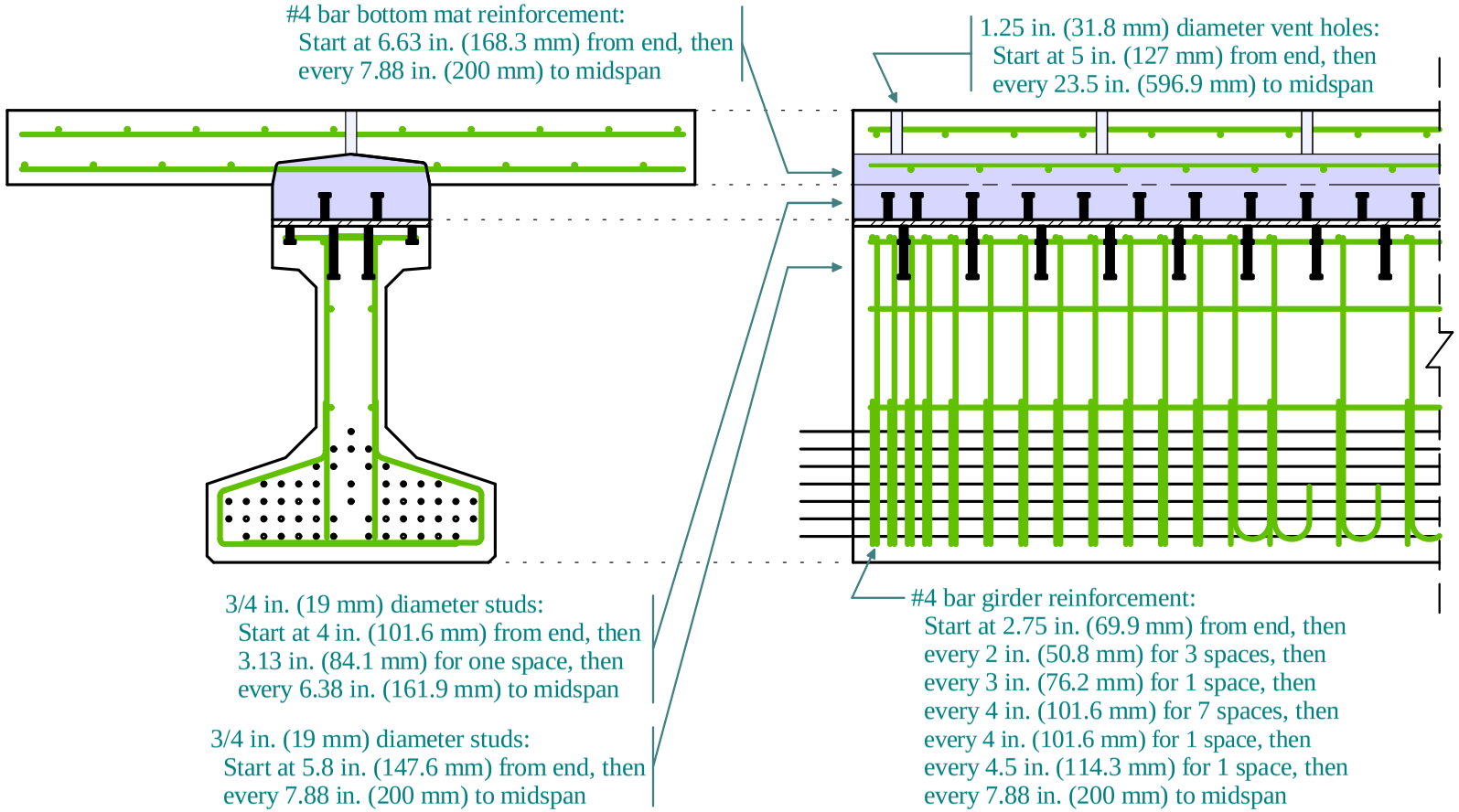

Figure 6. Illustration. UHPC composite connection: Longitudinal cross section of emulative steel girder connection.

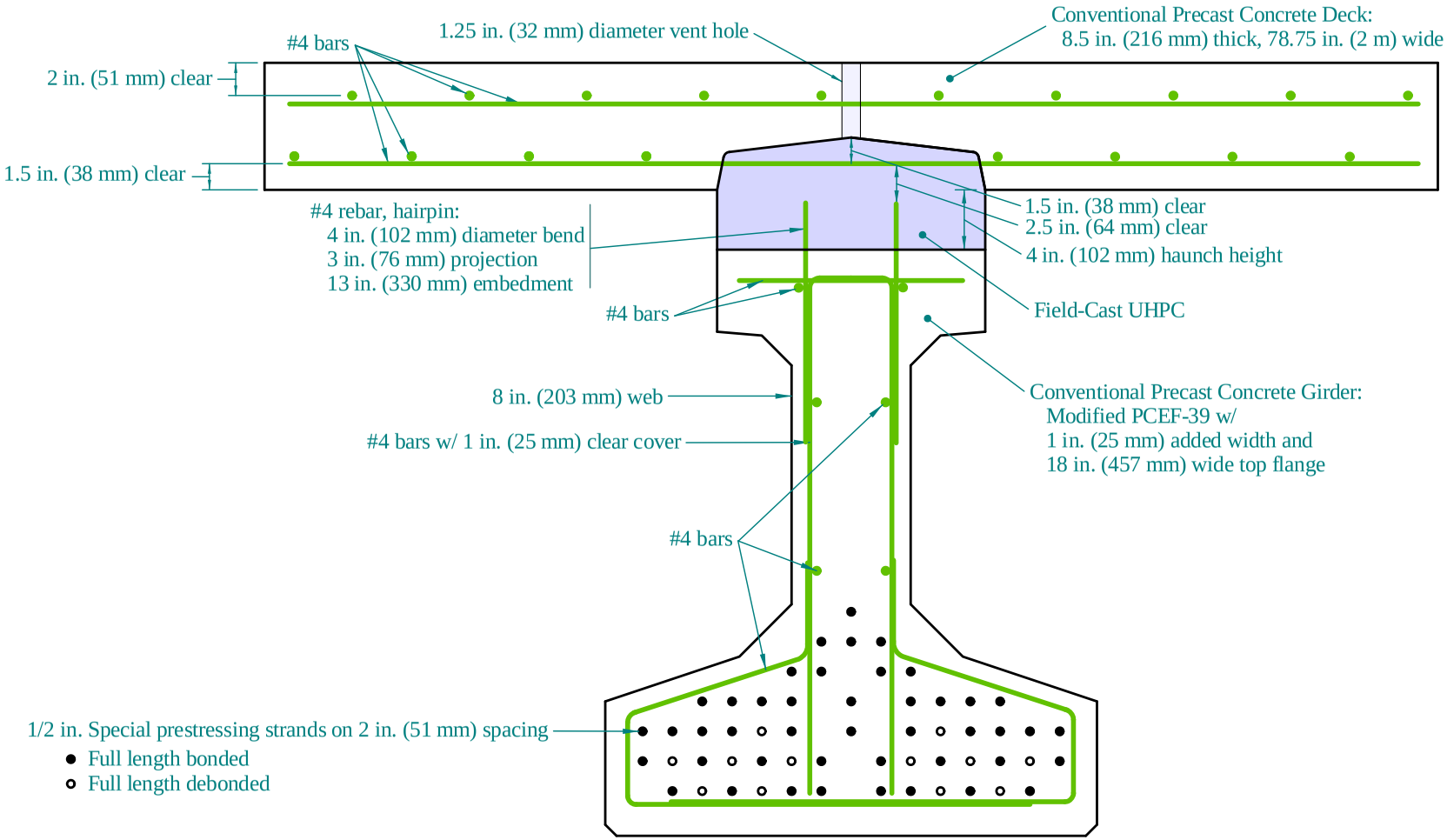

Figure 7. Illustration. UHPC composite connection: Transverse cross section of concrete girder connection.

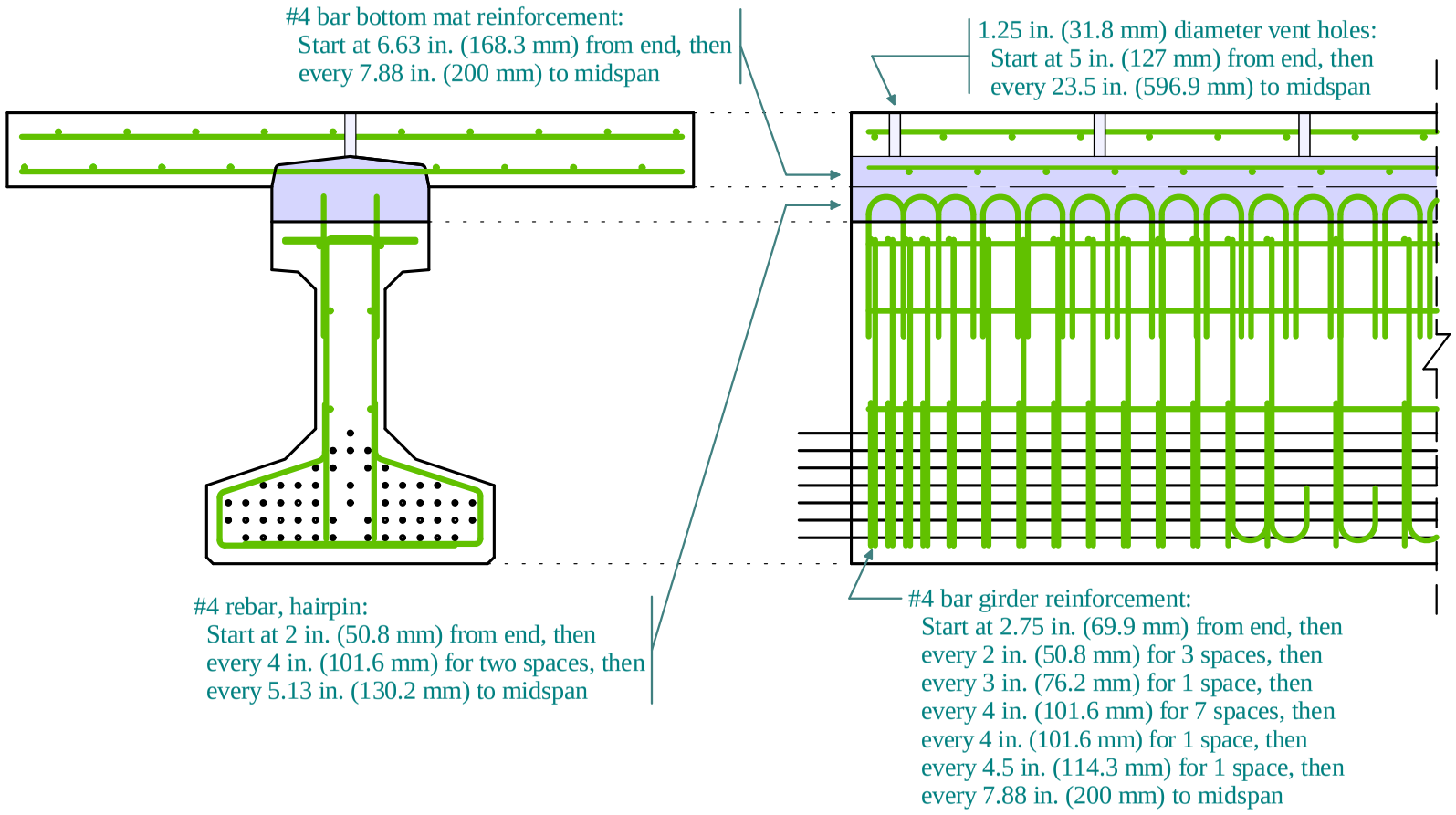

Figure 8. Illustration. UHPC composite connection: Longitudinal cross section of concrete girder connection.

SPECIMEN FABRICATION

The precast components were fabricated by a precast concrete component manufacturer, Northeast Prestressed Products, LLC, of Cressona, Pennsylvania. The two prestressed girders and the four precast deck panels were all fabricated during the week of January 10, 2011. All components were cast indoors and remained indoors for at least 24 hours prior to being moved to an outdoor storage area. Supplemental additional of heat/steam accelerated the concrete curing during the first 24 hours after casting. After reaching sufficient strength, the six precast pieces were shipped to a warehouse in Binghamton, New York.

Lancaster Development, Inc. assembled the precast pieces and cast the grouts in an indoor facility in Binghamton, New York, in February 2011. The novel composite connection detail specimen was assembled first. The two precast deck panels were staged on top of the precast girder, and then the haunch forms were installed. Immediately before UHPC casting, photographs were captured showing the composite connection space between the girder and the deck. Figure 9 pertains to the connection between the emulated steel girder and the precast concrete deck. Figure 10 pertains to the connection between the concrete girder and the precast concrete deck.

Figure 9. Photograph. Composite connection between emulated steel girder and precast concrete deck immediately prior to field-casting of UHPC.

Figure 10. Photograph. Composite connection between concrete girder and precast concrete deck immediately prior to field-casting of UHPC.

The UHPC was mixed in approximately 0.14 m^3 (5 ft^3) batches and poured into the haunch through the midspan connection between the two deck panels. As such, the UHPC was required to flow 6.1 m (20 ft) in each direction from the midspan insertion point. Ten batches were mixed and cast over the course of 5 hours during the afternoon of February 4, 2011. The mix design for each batch included 317.5 kg (700 lbs) of Ductal premix, 20.3 kg (44.8 lbs) of water, 4.3 kg (9.5 lbs) of Chryso Premia 150 superplasticizer, and 22.6 kg (50 lbs) of 12.7 mm long by 0.2 mm diameter (0.5 in. long by 0.008 in. diameter) straight steel fibers.

The conventional composite connection specimen was assembled in the same facility. The connection was cast on February 23, 2011. The field-cast haunch connection used Harris Construction Grout, a prebagged, non-shrink construction grout. The grout was specified to be mixed to a flowable consistency, thus allowing the grout to fill the connection and reach appropriate strength levels. The first batch of grout included insufficient water and thus, when it was used to fill the easternmost portion of this test specimen, it did not appropriately consolidate and fully fill the connection void spaces. All subsequent batches expressed appropriate fluidity. The unfilled void spaces on the easternmost end of this test specimen were subsequently filled with a cementitious patching compound upon demolding of the test specimen.

UHPC MATERIAL PROPERTIES

During the placement of the UHPC into the composite connection test specimen, 76-mm (3-inch) diameter cylinder specimens were cast in order to allow for material property characterization. These cylinders were stored with the larger test specimens in order to simulate the characteristics of the UHPC cast into the haunch. The cylinders were prepared for testing by grinding both ends to create parallel surfaces through the use of a fixed end grinder. After preparation, the cylinders exhibited length to diameter ratios of approximately 1.9. Density and compressive strength tests were completed on the cylinders. Density measurements were obtained through conventional means by measuring the weight of each cylinder and dividing by the volume. The average density of the UHPC was 2550 kg/m^3 (159 lb/ft^3).

The compressive strength tests were completed according to ASTM C39[9]. The test method was modified by increasing the load rate to 1 MPa/sec (150 psi/sec). The test results are presented in Table 4. The average compressive strength of the UHPC ranged from 152 MPa (22.1 ksi) at the start of cyclic testing to 186 MPa (27.0 ksi) on the day of the static test to failure of the full-scale test specimen.

Table 4. Cylinder density and compressive strength for the field-cast UHPC used in the haunch of the UHPC composite connection test specimen.

Days After Casting	Density†, kg/m^3 (lb/ft^3)	Compressive Strength†, MPa (ksi)	Note
21	2563 (160.0)	152 (22.1)	Start of girder cyclic testing
97	2537 (158.4)	186 (27.0)	Girder static test to failure
180	2549 (159.1)	191 (27.7)	6 months after casting
270	2558 (159.7)	205 (29.7)	9 months after casting

† Each presented result represents the average of three cylinders.

The split cylinder test is a commonly applied test method for indirectly assessing the tensile cracking strength of concrete. This test method relies on the unique mechanical property set of concrete, with the compressive strength generally in the vicinity of an order of magnitude higher than the tensile strength. In the test, two compressive line loads are applied along opposing sides of a concrete core or cylinder. The compressive force generates a lateral expansion of the cylinder. The elastic lateral expansive stresses are nearly uniform along the loaded plane, allowing for an estimation of the tensile cracking strength of the concrete.

The ASTM C496 Standard Test Method for Splitting Tensile Strength of Cylindrical Concrete Specimens[10] was modified for use in this test program. This standardized test method is generally applicable for conventional concretes, but is not necessarily applicable for fiber reinforced concretes. In the standard test method, the tensile cracking strength is calculated based on the peak applied load and the geometry of the test specimen. However, the post-cracking tensile strength of fiber reinforced concrete, combined with the biaxial state-of-stress generated in this test method, present the possibility that the peak stress carried by the specimen

may not coincide with the cessation of elastic behaviors. As such, the test method must be supplemented to facilitate the capture of the load at first cracking of the specimen.

Two specific modifications to the standard test method were implemented. First, the lateral expansion of the cylinder perpendicular to the loaded plane was electronically measured and captured throughout the entire test. The measurement allowed for an assessment of the cessation of elastic behavior and thus an indication of first cracking. The second modification was an increase in the load rate. The load rate was increased from 1.0 MPa/min to 3.5 MPa/min (150 psi/min to 500 psi/min) splitting tensile stress. This modification allows for reasonable test duration. This modified test procedure is discussed more fully in reference (11).

Figure 11 provides an illustration of the type of result captured during the completion of this test method. Although first cracking of the specimen may or may not be apparent through visual or audible indications, the electronically captured data clearly indicates a discontinuity in the lateral expansion consistent with the cessation of elastic behaviors.

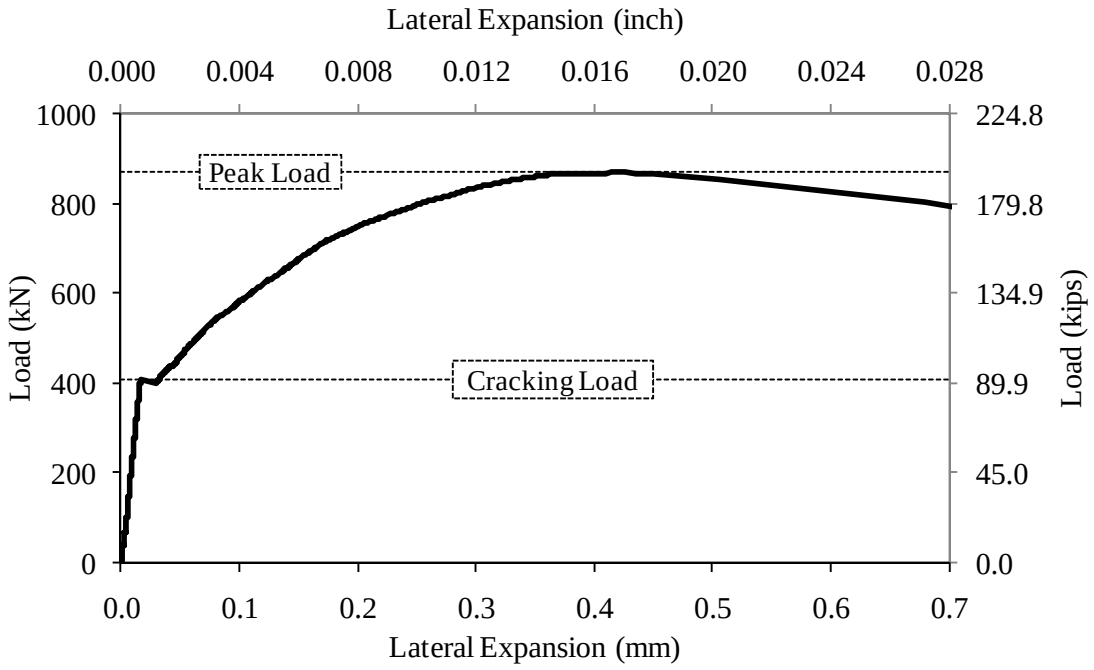

Figure 11. Illustration. Sample load versus lateral expansion result from a split cylinder test completed on a UHPC cylinder.

Six cylinders were cast at the time of the UHPC haunch connection casting. The cylinders were 102-mm (4-inch) diameter. The ends of the cylinders were ground plane prior to testing. The length-to-diameter ratio of each cylinder was approximately 1.9.

The test results for the cylinders are presented in Table 5. The tests were completed at two ages, namely 21 days after casting and 97 days after casting. These timeframes coincide with the start of cyclic testing and the static test to failure of the full-scale UHPC connection test specimen, respectively.

The average density at 21 days was 2551 kg/m^3 (159.2 lb/ft^3). The average density at 97 days was 2561 kg/m^3 (159.9 lb/ft^3).

The split cylinder test results are presented in Table 5. At 21 days, the average cracking strength was 9.0 MPa (1.31 ksi) and the average peak strength was 19.0 MPa (2.76 ksi). At 97 days, the average cracking strength was 5.7 MPa (0.83 ksi) and the average peak strength was 21.9 MPa (3.19 ksi).

Table 5. UHPC split cylinder tensile test results.

Days after Casting	Cyl. #	Density, kg/m^3 (lb/ft^3)	Cracking Strength, MPa (ksi)	Peak Strength, MPa (ksi)
21	1	2555 (159.5)	7.72 (1.12)	16.8 (2.44)
	2	2561 (159.8)	10.7 (1.55)	19.8 (2.87)
	3	2537 (158.4)	8.67 (1.26)	20.4 (2.96)
97	1	2561 (159.9)	5.43 (0.79)	22.0 (3.20)
	2	2557 (159.6)	5.60 (0.81)	21.7 (3.15)
	3	2565 (160.1)	6.12 (0.89)	22.1 (3.21)

CONVENTIONAL GROUT MATERIAL PROPERTIES

During the placing of the conventional grout used in the conventional composite connection specimen, 51 mm (2 in.) cubes were cast for determination of the compressive strength. These cubes were cured alongside the larger test specimens in order to simulate the characteristics of the grout cast into the haunch. These compressive strength tests were completed according to ASTM C109[(12)]. The results are presented in Table 6, with the grout expressing 55 MPa (8 ksi) of strength at the start of cyclic testing.

Table 6. Cube compressive strength for the conventional grout used in the haunch of the conventional composite connection test specimen.

Days After Casting	Compressive Strength†, MPa (ksi)	Note
28	54.8 (7.95)	4 weeks after casting
106	55.1 (7.99)	Start of cyclic testing

† Each presented result represents the average of three cubes.

PRECAST CONCRETE MATERIAL PROPERTIES

The two prestressed girders were cast using a standard concrete mix frequently mixed and cast by the precaster. Briefly, this mix can be described as a self-consolidating concrete with 389 kg/m^3 (655 lbs/yd^3) of cement and 29.7 kg/m^3 (50 lbs/yd^3) of silica fume. The concrete was specified to have a compressive strength of 49 MPa (7.10 ksi) at strand transfer and of 70 MPa

(10.15 ksi) at 56 days. The concrete was reported by the precaster to have a compressive strength of 52.7 MPa (7.65 ksi) at 19 hours after casting.

The four precast deck panels were cast using a standard concrete mix frequently mixed and cast by the precaster. Briefly, this mix can be described as a 203 mm (8 in.) slump concrete with 390 kg/m^3 (658 lbs/yd^3) of cement and a 0.36 water/cement ratio. The concrete was specified to have a compressive strength of 34.5 MPa (5 ksi) before the panels could be lifted. The precaster reported that the panels used in the conventional composite connection test specimen exhibited a compressive strength of 39.2 MPa (5.4 ksi) at 19 hours after casting. The precaster reported that the panels used in the UHPC composite connection test specimen exhibited a compressive strength of 40.8 MPa (5.9 ksi) at 15 hours after casting.

CHAPTER 4. TEST PROGRAM AND RESULTS

INTRODUCTION

The test results and observations from the physical testing of the composite connection specimens are presented in this chapter. The overall test program is presented first. The results from the novel UHPC composite connection specimen follow. Finally, the results from the conventional composite connection test specimen are presented.

TEST PROGRAM

Two full-scale test specimens were designed to mimic the type of slab-on-stringer construction commonly used throughout the U.S. for highway bridge construction. Although composed of precast deck panels on prestressed concrete girders, the specimens were designed to emulate the composite connections between precast concrete deck elements and both steel and concrete girders. The design of the test specimens mimicked the line-girder design concept commonly implemented in U.S. highway bridge superstructure design. In this test program, individual superstructure elements (i.e., girder-deck systems) were simply supported and subjected to four-point bending. This test setup allowed for the generation of realistic flexure and shear stresses within the entirety of the test specimen. In short, the test specimens were subjected to loads simulating the types of truck and lane structural loadings which are the primary basis for a large proportion of the structural design of bridge superstructures.

The test program for each specimen included two phases. First, each test specimen was subjected to cyclic loads in order to simulate the type of service level fatigue loadings commonly applied to highway bridge structures. Figure 12 shows the elevation view illustration of the test setup that was used for the cyclic testing. Figure 13 shows a photograph of this test setup. Each test specimen was supported on an 11.89 m (39 ft) span by roller supports. Vertical loads were applied symmetrically at 4.11 m (13.5 ft) from each roller. Loads were applied by servo-hydraulic controlled actuators operated under load control. The pair of 445-kN (100-kip) capacity actuators applied loads to the top of the deck along the centerline of the girder through 0.3 by 0.3 m (12 by 12 in.) elastomeric pads backed by steel plates.

The cyclic loading program was designed to generate large horizontal shear force ranges within the composite connection between the girder and the deck. This loading program is shown in Figure 14. The loading program included four stages. The first three stages each subjected a test specimen to more than 2 million cycles of structural loading. The final stage subjected a test specimen to more than 5 million additional cycles of structural loading. The lower end of the load cycles was set at an applied load of 13.3 kN (3 kips) per load point. The upper end of the first stage was 222 kN (50 kips) per load point, thus generating a vertical shear force range of 209 kN (47 kips) within each end of the test specimen. The vertical shear force range was increased by approximately one-third at each successive stage, resulting in the final stage applying twice the vertical shear force range as the initial stage. In this final stage, the vertical shear force range was 418 kN (94 kips).

The loads followed a sinusoidal path through each loading cycle. The frequency of the cyclic loading varied. The maximum achievable frequency of loading was influenced by the desired load levels, the stiffness of the specimen, and the stiffness of the reaction system. The cyclic loading program was initiated at a frequency of 3 Hz. The frequency was periodically decreased during the testing of each specimen until the final cyclic load ranges were completed at a frequency of 2 Hz.

During the cyclic load program, the loading was periodically stopped to allow for the capture of data emanating from slow-response instrumentation. Specifically, the vibrating wire gages embedded in each specimen require multiple seconds per reading and thus they cannot be used to capture response during cyclic loading. To capture data from these gages, the cyclic loading was paused, the load level was decreased to the lower limit of the cyclic program, and then the load was increased in a step-wise fashion until the upper load limit of the cyclic program was reached. After the data was captured at each load step, the cyclic loading program was restarted.

After the completion of the cyclic loading program, each specimen was subjected to static loading. This portion of the test program provided insight into the structural capacity of the system after being subjected to over 11 million cycles of structural loading. The basic loading setup was the same as that used for the cyclic loading, with additional static hydraulic actuators added to the loading system in order to facilitate the achievement of higher loads. Eight additional static jacks were used, with four located adjacent to each of the two servo-hydraulic actuators. This test setup is illustrated in Figure 15 and shown in Figure 16. Pairs of static actuators applied force to loading beams which spanned across each test specimen at locations 0.23 m (9 in.) east and west of each servo-hydraulic actuator. During the static testing, the load per load point was initially increased to 445 kN (100 kips) through the use of servo-hydraulic jacks. Then, with the servo-hydraulic jacks maintaining that force, the static jacks were engaged to incrementally increase the load until structural failure of the specimen occurred. The load steps were initially approximately 180 kN (40 kips) per load point, with this value decreasing as the specimen sustained increasing levels of damage.

The structural response of each specimen was captured through the use of electronic instrumentation and visual/audible observations. The electronic instrumentation on each end of the each test specimen included seven electrical resistance strain gages mounted on the concrete, five LVDTs monitoring the horizontal movement at the haunch to deck and haunch to girder interfaces, five vibrating wire gages embedded in the precast elements, and two potentiometers measuring vertical deflection of the specimen at the load points. Load cells were also used at each actuator to monitor the applied load. The locations for the strain gages, LVDTs, and potentiometers are shown in Figure 17. The LVDTs and strain gages were all oriented along the length of the specimen in order to measure longitudinal behaviors. The LVDTs were affixed adjacent to the shear interfaces so as to allow for the capture of discrete movements occurring along the interfaces. Aside from the vibrating wire gages which were cast into the precast components, all instrumentation was affixed in the laboratory immediately prior to testing. The data from these electronic instruments was collected by data acquisition systems. A high-speed data acquisition system was used for the capture of data from the electric resistance strain gages, the load cells, and the LVDTs during the cyclic loading. This data acquisition system, as well as a dedicated, low speed system for the vibrating wire gages, was used during static loadings.

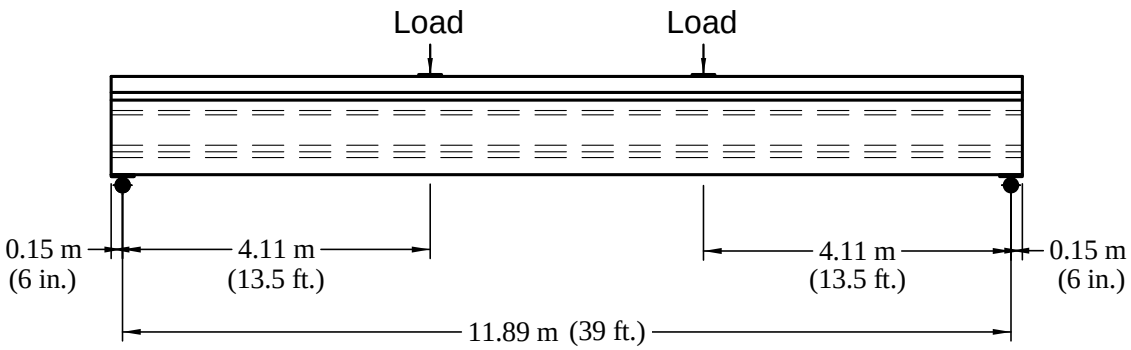

Figure 12. Illustration. Test setup for cyclic loading of test specimens.

Figure 13. Photograph. Overall test setup for cyclic test program.

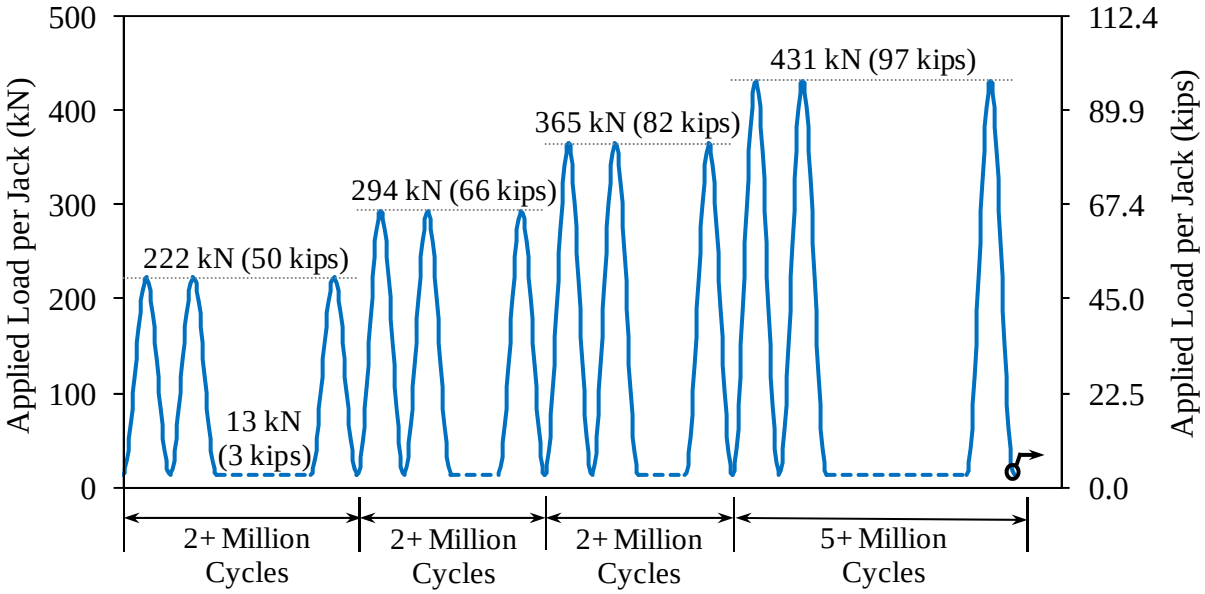

Figure 14. Illustration. Cyclic loading program.

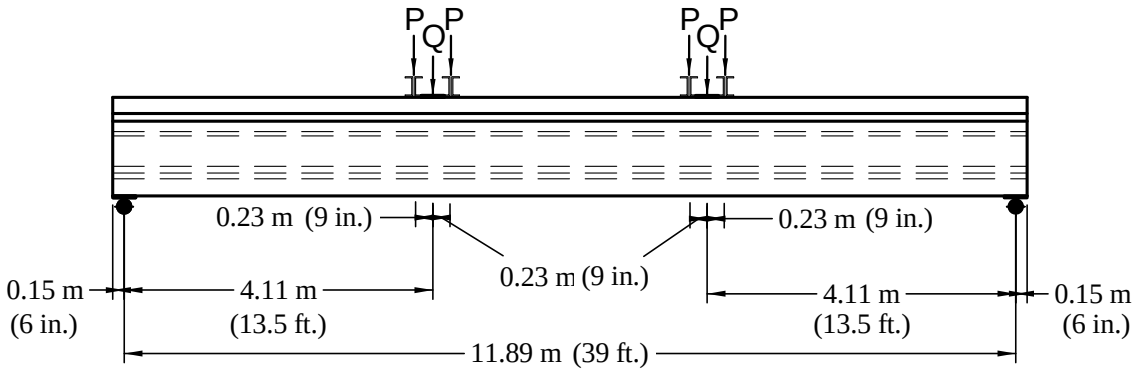

Note: Each load "P" can be up to 890 kN (200 kips).
Each load "Q" can be up to 445 kN (100 kips).
Loads "P" applied first, followed by "Q".

Figure 15. Illustration. Test setup for static loading of test specimens.

Figure 16. Photograph. Overall test setup for static test program.

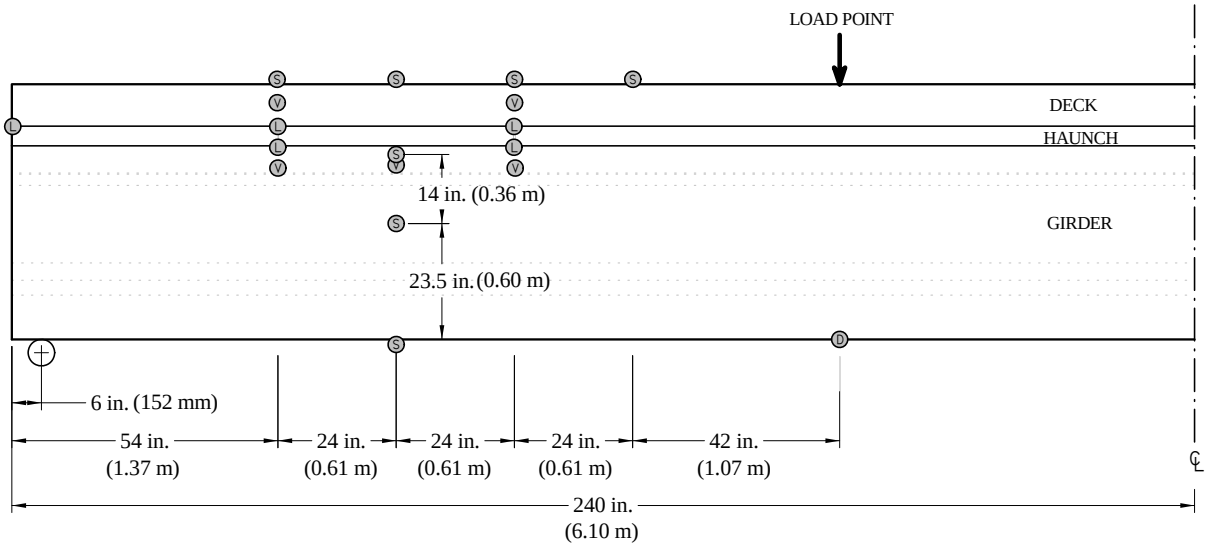

Ⓛ LVDT measuring horizontal movement across shear plane
Ⓢ Electrical resistance strain gage measuring longitudinal strain on concrete surface
Ⓥ Vibrating wire gage measuring longitudinal strain along transverse centerline of specimen
Ⓓ String potentiometer measuring vertical displacement of specimen relative to floor

Figure 17. Illustration. Instrumentation plan used throughout test program.

UHPC COMPOSITE CONNECTION RESULTS

The first test specimen used the novel composite connection detail, with field-cast UHPC playing a critical role in carrying horizontal shear forces between the girder and the deck. The results of the cyclic and static loadings of this specimen are presented below.

Cyclic Testing

The cyclic testing of the UHPC composite connection specimen was conducted according to the testing program previously described. The cyclic loading was completed over a two month timeframe beginning in February 2011. The specific number of cycles applied at each loading stage is detailed in Figure 18. The results obtained during this testing are generally reported in terms of the total number of cycles completed at the time a particular reading was captured. As such, a result reported as occurring at ten million cycles occurred at the ten millionth cycle according to the loading program in Figure 18.

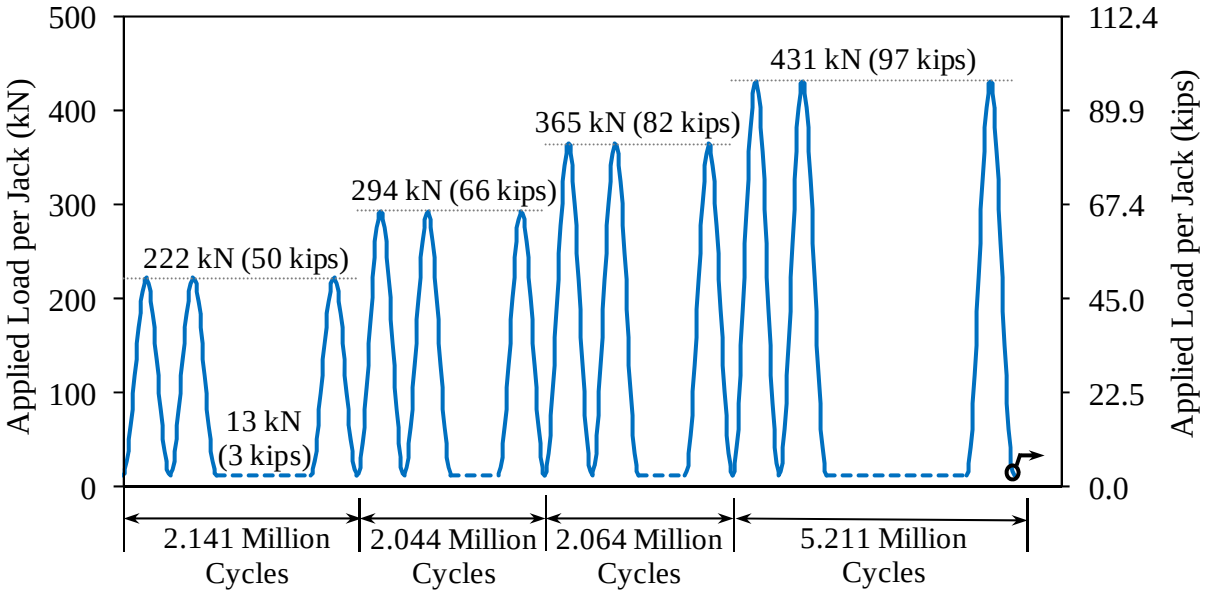

Figure 18. Graph. Cyclic loading program for UHPC connection specimen.

The LVDTs which monitored horizontal movement along the shear interfaces above and below the haunch provided the clearest indication of the performance of the structural system throughout the duration of the cyclic testing. These LVDTs were located on the south face of the test specimen at four locations on each end of the test specimen. These LVDTs report relative movements of the haunch to the girder and of the deck to the haunch. Movements are reported as positive when the haunch or the deck expressed relative movement toward the end of the test specimen. In order to normalize the results, relative movements are reported as horizontal

movement per load with the load being both the applied point load and the applied vertical shear in an end of the test specimen.

Figure 19 presents the horizontal movement results for the concrete girder composite connection. The results from the LVDTs at the haunch to girder interface clearly demonstrate that this interface remained intact throughout the entirely of the cyclic loading. No differential movement was observed electronically or visually at this interface. The UHPC remained well bonded to the surface of the prestressed girder with no indication of cracking, delamination, or debonding. This plot also shows that relative movement did occur at the haunch to deck interface and that this movement increased with increasing cycles. Also note that there was greater movement closer to the support point and that the relative difference between the movement at 1.22 m (4 ft) and at 2.44 m (8 ft) increases with increasing cycles. At the conclusion of this testing, the maximum total relative movement observed at the deck to haunch interface at 1.22 m (4 ft) from the support was 0.191 mm (0.0075 in.) over the course of a 431 kN (97 kip) load range.

Figure 20 presents the horizontal movement results for the emulated steel girder composite connection. The results from these LVDTs clearly demonstrate that both interfaces expressed relative movement from the beginning of the cyclic loading. This was visually apparent at the haunch to girder interface from the beginning of the testing, with any chemical bond between the UHPC and the steel plate being broken by the initial cyclic loads. This plot shows that greater movement and increasing movement occurred at the deck to haunch interface, and that the movement at the haunch to girder interface showed less tendency to increase in magnitude as cycling progressed. Clearly, there was greater movement closer to the support point and that the relative difference between the movement at 1.22 m (4 ft) and at 2.44 m (8 ft) increased with increasing cycles. At the conclusion of this testing, the maximum total relative movement observed at the deck to haunch interface at 1.22 m (4 ft) from the support was 0.173 mm (0.0068 in.) over the course of a 431 kN (97 kip) load range.

Figure 21 and Figure 22 provide the results obtained from the vibrating wire gages embedded in this specimen. Recall that there were ten vibrating wire gages in the specimen, with two in the precast deck and three in the precast girder in each end of the specimen. These gages were installed to provide an indication of the longitudinal strain within the specimen immediately above and below the horizontal shear interfaces. Similar response can be observed in both Figure 21 which is from the end of the specimen simulating the concrete girder connection and in Figure 22 which is from the end of the specimen simulating the steel girder connection. In both cases, the strain in the top flange of the girder trends toward increasing compressive strain per unit of applied load as the cyclic loading progresses. The strains in the precast deck can be observed to be either constant or trending toward decreasing compressive stresses per unit of applied load as the cyclic loading progresses. This combination of behaviors is indicative of a slight loss of composite action between the girder and the deck, thus leading to the girder top flange carrying additional flexural compressive forces. In total, the largest change in strain observed from the start to the conclusion of the cyclic testing amounted to 0.043 με/kN (-0.19

με/kip). Given an applied vertical shear of 222 kN (50 kips) and an assumption of elastic behavior with a 33 GPa (4500 ksi) concrete modulus of elasticity, this amounts to an induced stress change of -0.3 MPa (-43 psi) in the top flange of the prestressed girder over the duration of this loading regime.

In summary, the over 11 million cycles of cyclic loading applied within this test program created little apparent damage in the composite connections or the adjacent precast elements. Small movements were observed across the horizontal shear interfaces in some locations. No visible damage was observed on the exterior surfaces of either the UHPC or the precast elements. Figure 23 provides a photograph showing the end face of the composite connection at the west end of the test specimen after the conclusion of the cyclic loading. This photograph demonstrates that the horizontal interface between the girder and the haunch remained uncracked, while the horizontal interface between the UHPC and the deck exhibited small movements.

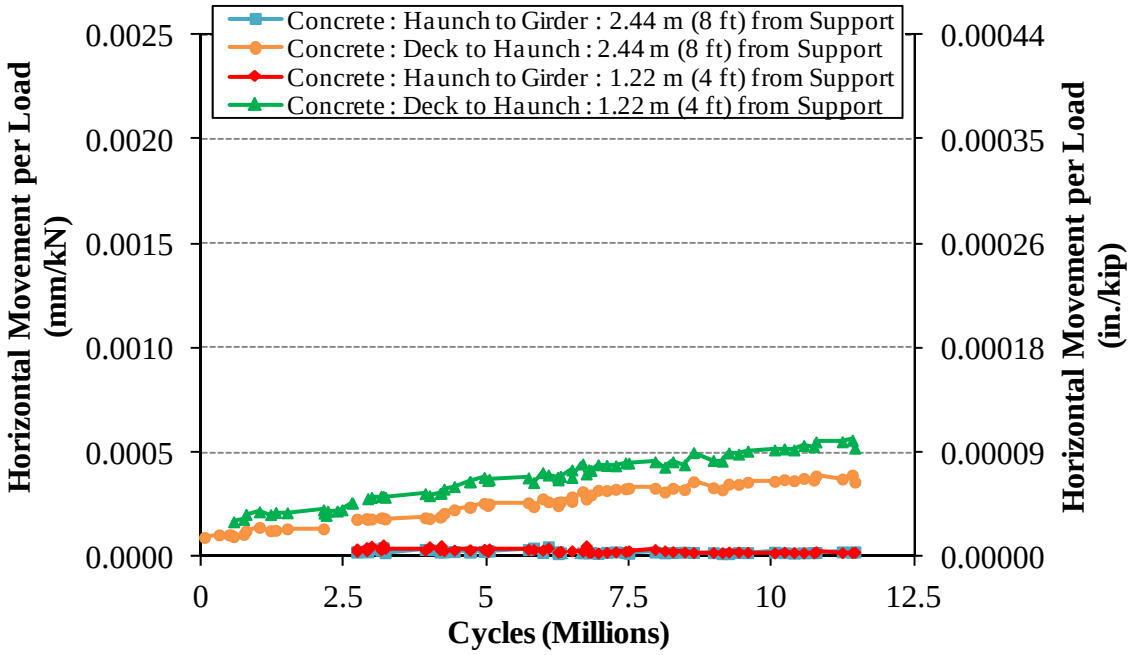

Figure 19. Graph. Horizontal movement at haunch in portion of UHPC connection specimen which emulated the composite connection to a concrete girder.

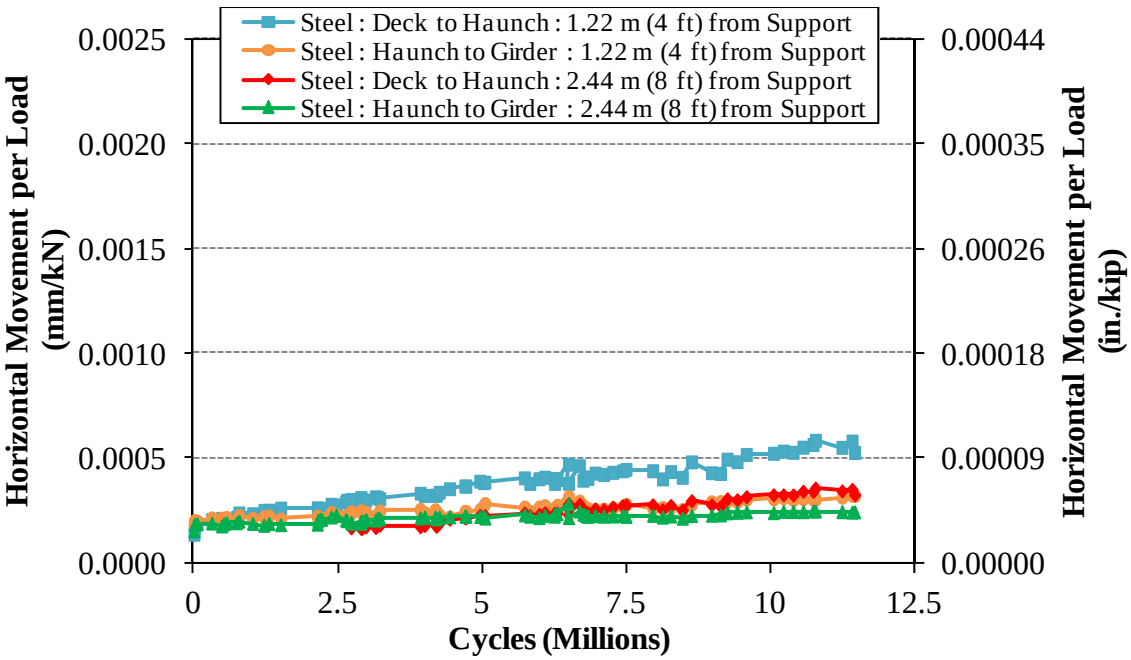

Figure 20. Graph. Horizontal movement at haunch in portion of UHPC connection specimen which emulated the composite connection to a steel girder.

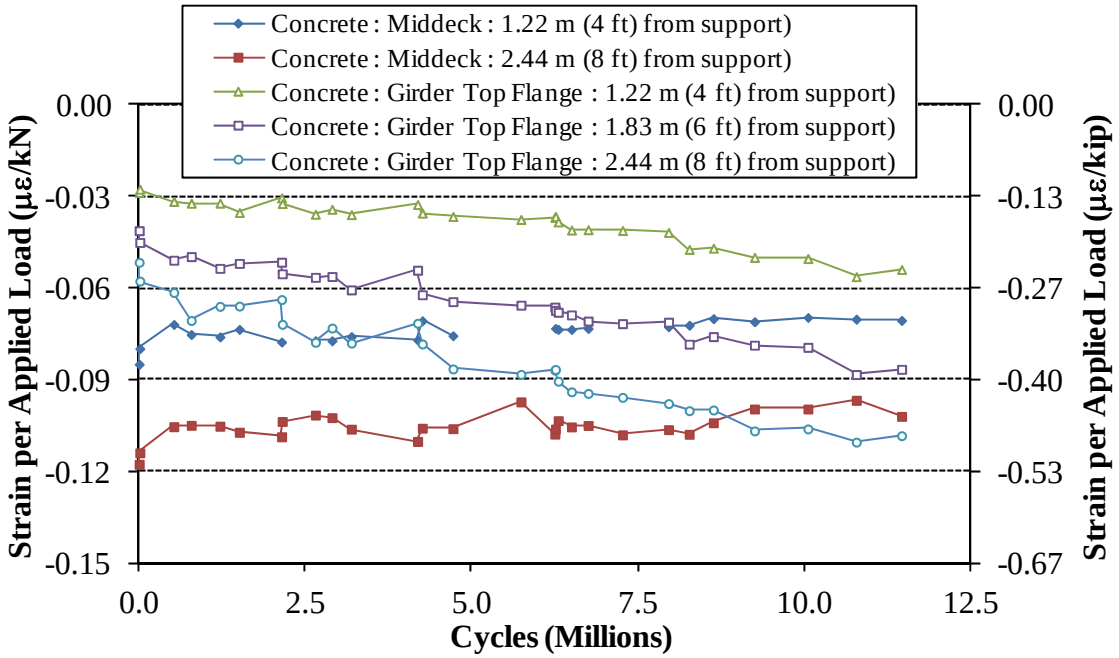

Figure 21. Graph. Internal strain in portion of UHPC connection specimen which emulated the composite connection to a concrete girder.

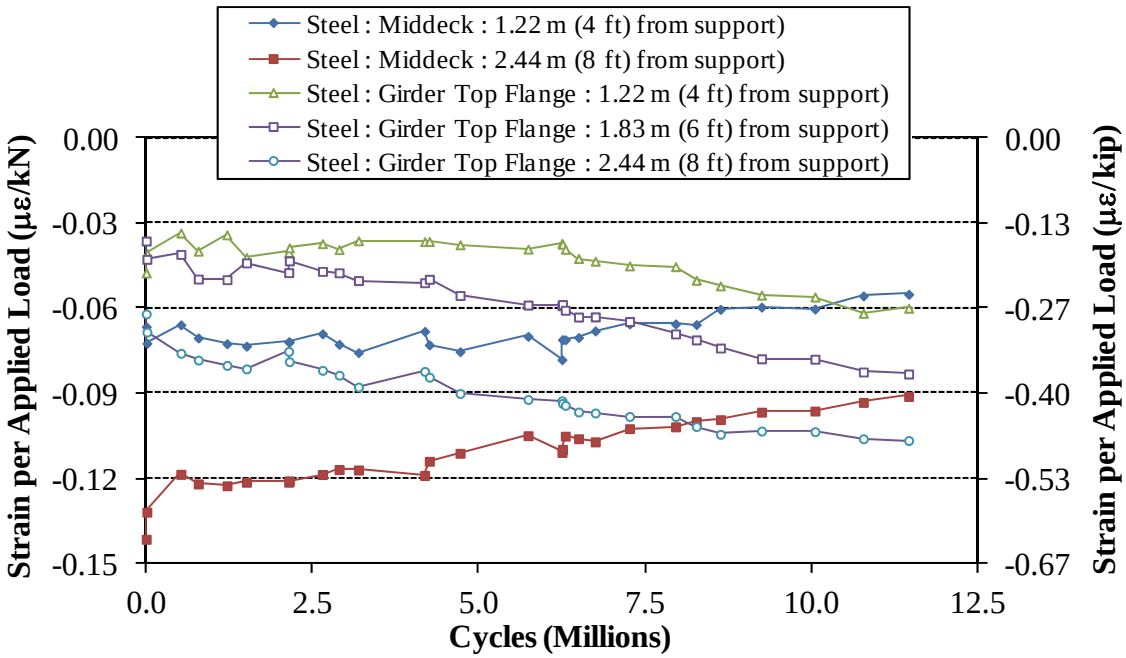

Figure 22. Graph. Internal strain in portion of UHPC connection specimen which emulated the composite connection to a steel girder.

Figure 23. Photo. Haunch connection at portion of test specimen which emulated the composite connection to concrete girder (i.e., west end) at conclusion of cyclic testing.

Static Loading to Failure

The static loading of this test specimen was completed according to the loading program previously described. This portion of the loading program was completed over the course of two hours in May 2011. The overall response of the specimen is shown in Figure 24. This and subsequent plots use applied vertical shear load, which is commensurate with the applied load at each load point, on the vertical axis. The load versus displacement responses are nearly identical for the two load points. The test specimen presented a linear response until the applied vertical shear load surpassed 890 kN (200 kips). A slight softening was then observed until the applied vertical shear load surpassed 1500 kN (337 kips). The test specimen then exhibited significantly decreased stiffness until the peak loading resistance was encountered at an applied vertical shear of 2215 kN (498 kips) at each load point.

Visual and audible observations were also compiled throughout the static test. The first shear cracks in the web of the prestressed girder were audibly observed at an applied vertical shear load of 1155 kN (260 kips) and were clearly visually apparent at 1335 kN (300 kips). The first flexural cracks were observed near midspan in the test specimen at an applied vertical shear load of 1600 kN (360 kips).

Horizontal movement along the horizontal shear interfaces was also monitored throughout the static testing. Figure 25 and Figure 26 provide the results from the western half of the test specimen which simulated the concrete girder composite connection. Throughout the static test, no movement was observed at the horizontal interface between the girder and the UHPC. This interface remained uncracked through global failure of the test specimen. All horizontal interface shear movement on this end of the test specimen occurred at the precast deck to UHPC interface. The observed movements were similar at each of the three data collection locations. Less than 0.3 mm (0.012 in.) of movement was observed at vertical applied shear loads below 890 kN (200 kips). At an applied load of 1690 kN (380 kips) the horizontal movement was approximately 1.6 mm (0.063 in.). At the peak load, the observed movement at the end of the test specimen was 6.6 mm (0.26 in.). Figure 29 provides a photograph showing this end of the test specimen immediately before failure of the test specimen.

Figure 27 and Figure 28 provide the horizontal shear interface horizontal movements for the eastern half of the test specimen which simulated the steel girder composite connection. Movement was observed at both the girder to UHPC and the UHPC to deck interfaces. Less than 0.22 mm (0.009 in.) of movement was observed at any of the data collection points at vertical applied shear loads below 890 kN (200 kips). By the time the applied load had reached 1690 kN (380 kips) the horizontal movements had diverged, with slightly more deformation being observed at the gages closer to midspan. At the peak load, the total observed movement between both gages at the collection point closer to midspan amounted to 9.1 mm (0.36 in.).

The failure of the test specimen can be attributed to a horizontal shear failure of the conventional concrete both in the prestressed girder and in the precast deck elements. Figure 30 and Figure 31 show the haunch connections at each end of the test specimen immediately after completion of the test. The deck can be observed to be extended relative to the haunch and the underside of the deck shows structural cracking and spalls beginning at the location of the first bottom mat reinforcing bars. Figure 32 and Figure 33 provide illustrations indicating the locations of the observed structural cracking in each end of the test specimen at the conclusion of testing. The cracks have been drawn onto the photographs in order to facilitate easy viewing. Figure 33, showing the end of the girder which emulated the steel girder connection, shows a small amount of structural cracking in the underside of the deck and a significant amount of shear cracking in the prestressed girder. This shear cracking in the girder web extends into the top flange of the prestressed girder and runs horizontally parallel to the steel plate embedded into the top of the girder. Figure 32, focusing on the end of the girder which emulated the concrete girder connection, shows a somewhat different response. A greater amount of structural cracking is observed in the underside of the deck, while the shear cracking in the prestressed girder is confined to the web and web transitions.

The distress apparent at the conclusion of the static test is also shown in Figure 34 and Figure 35. Two cores were extracted from the east end of the test specimen, each one drilled downward through the top of the deck to the top of the steel plate. The cores were aligned so that half of each hole would penetrate the haunch. One of the cores intersected the easternmost transverse bar in the bottom mat of reinforcement immediately above the south face of the girder. The other core intersected the second bottom mat transverse bar from the east end immediately above the north face of the girder. Views down into the core holes are provided in Figure 34. The distress in the conventional concrete in the vicinity of the UHPC haunch can be observed in each core hole. Figure 35 shows one of the cores after extraction. The transverse bar was firmly embedded in the UHPC with no indication of UHPC or rebar degradation. The conventional concrete which was immediately adjacent to this transverse bar has failed, allowing the bar and haunch to move relative to the concrete. Identical behaviors were observed in both cores.

In summary, the conventional concrete failed locally in the vicinity of the discrete shear connectors (i.e., rebar and shear studs) within the conventional precast concrete above and below the UHPC composite connection. The UHPC composite connection and the connectors emanating therefrom remained intact.

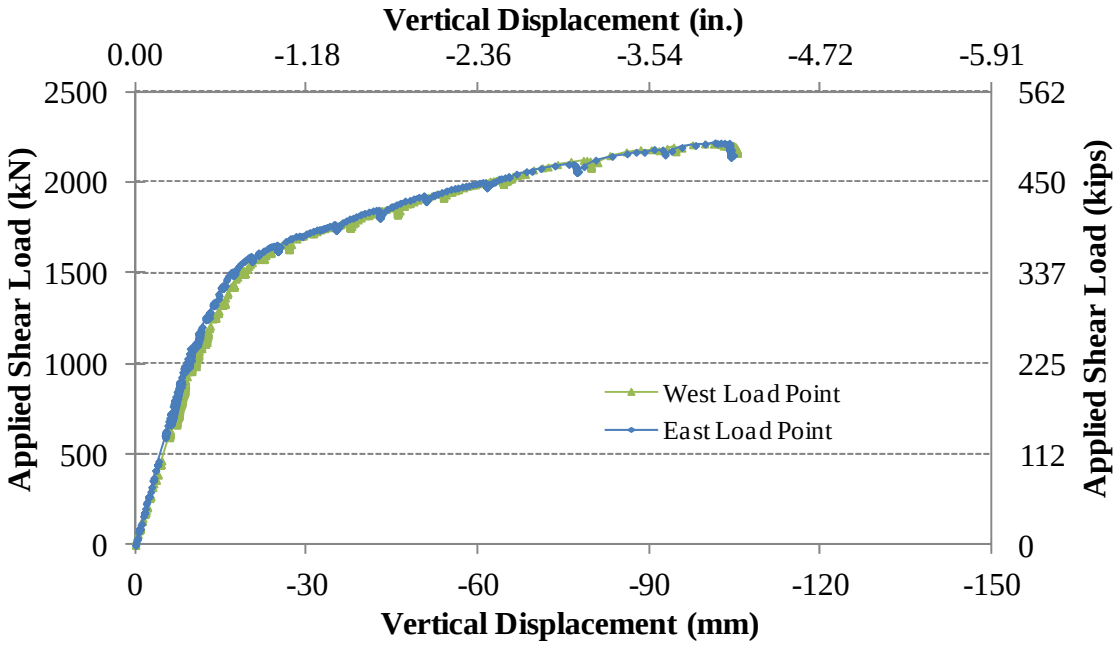

Figure 24. Graph. Load-deflection response of UHPC connection specimen under static load to failure.

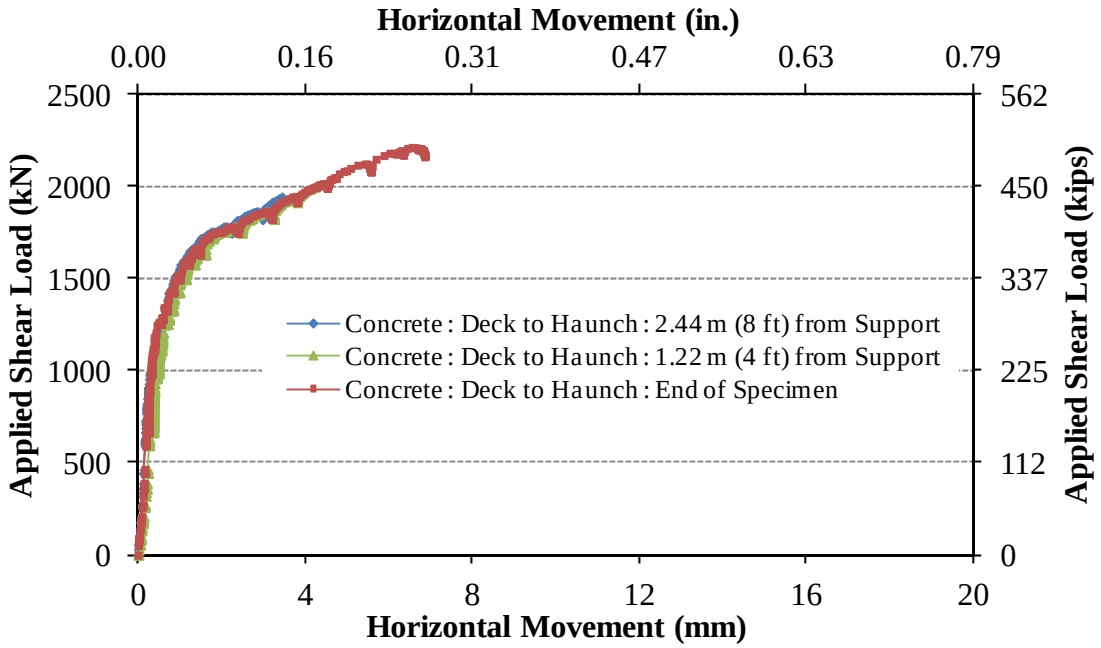

Figure 25. Graph. Horizontal movement between deck and haunch in portion of UHPC connection specimen which emulated the composite connection to a concrete girder when under static load to failure.

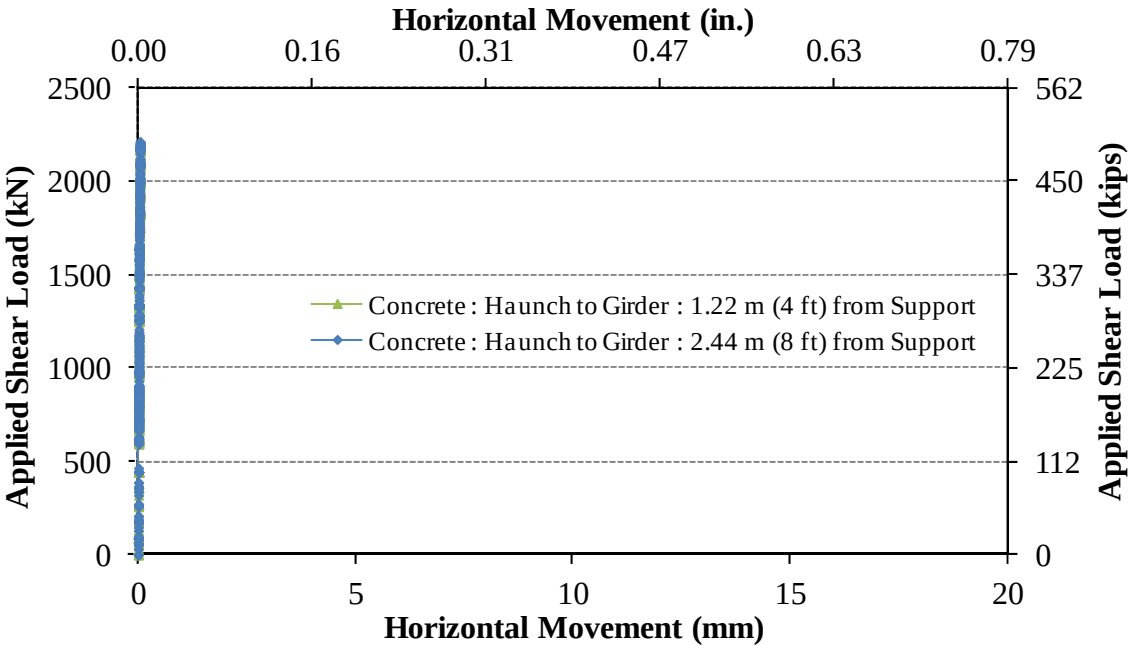

Figure 26. Graph. Horizontal movement between haunch and girder in portion of UHPC connection specimen which emulated the composite connection to a concrete girder when under static load to failure.

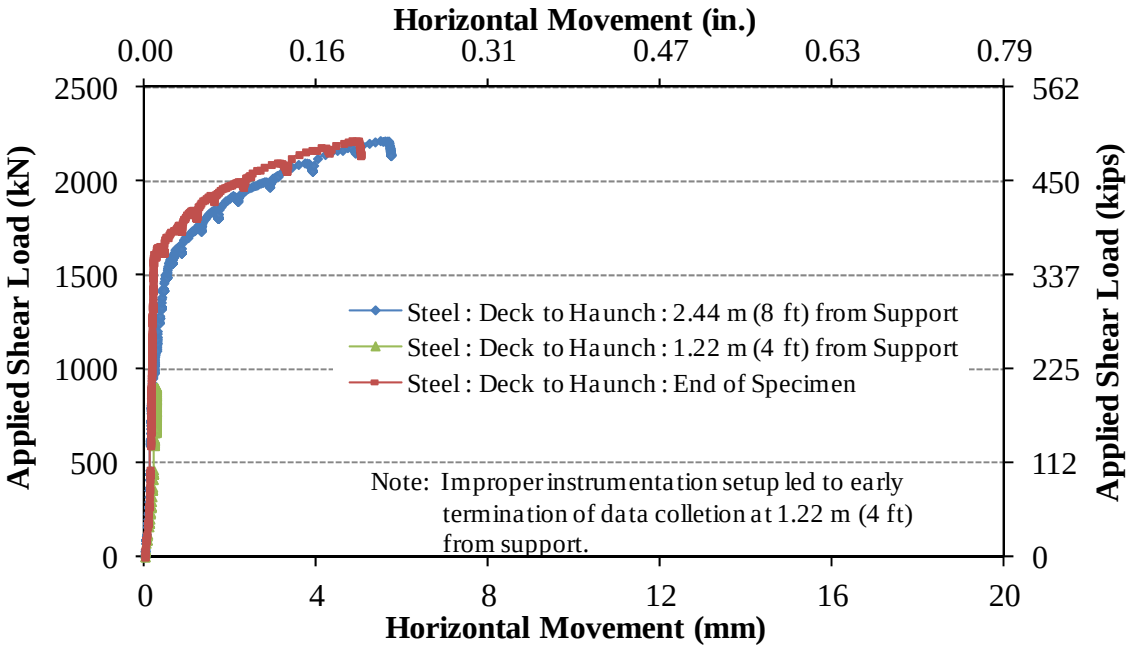

Figure 27. Graph. Horizontal movement between deck and haunch in portion of UHPC connection specimen which emulated the composite connection to a steel girder when under static load to failure.

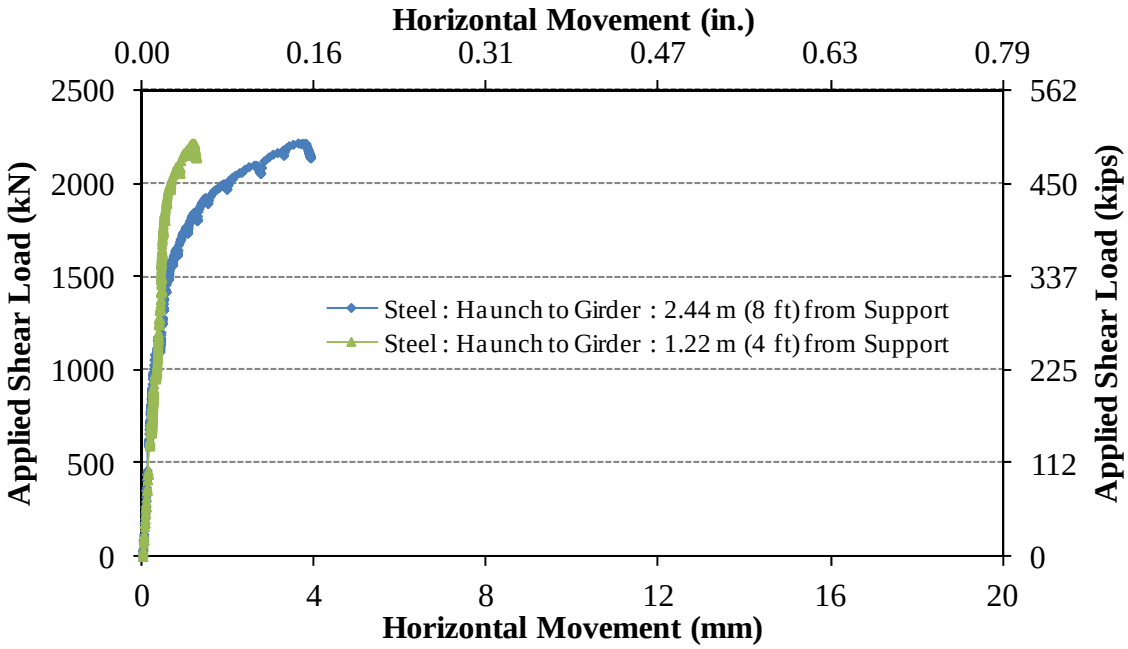

Figure 28. Graph. Horizontal movement between haunch and girder in portion of UHPC connection specimen which emulated the composite connection to a steel girder when under static load to failure.

Figure 29. Photo. Haunch connection which emulated the composite connection to a concrete girder (i.e., west end) immediately before the attainment of peak applied load.

Figure 30. Photo. Haunch connection which emulated the composite connection to a steel girder (i.e., east end) after completion of static testing.

Figure 31. Photo. Haunch connection which emulated the composite connection to a concrete girder (i.e., west end) after completion of static testing.

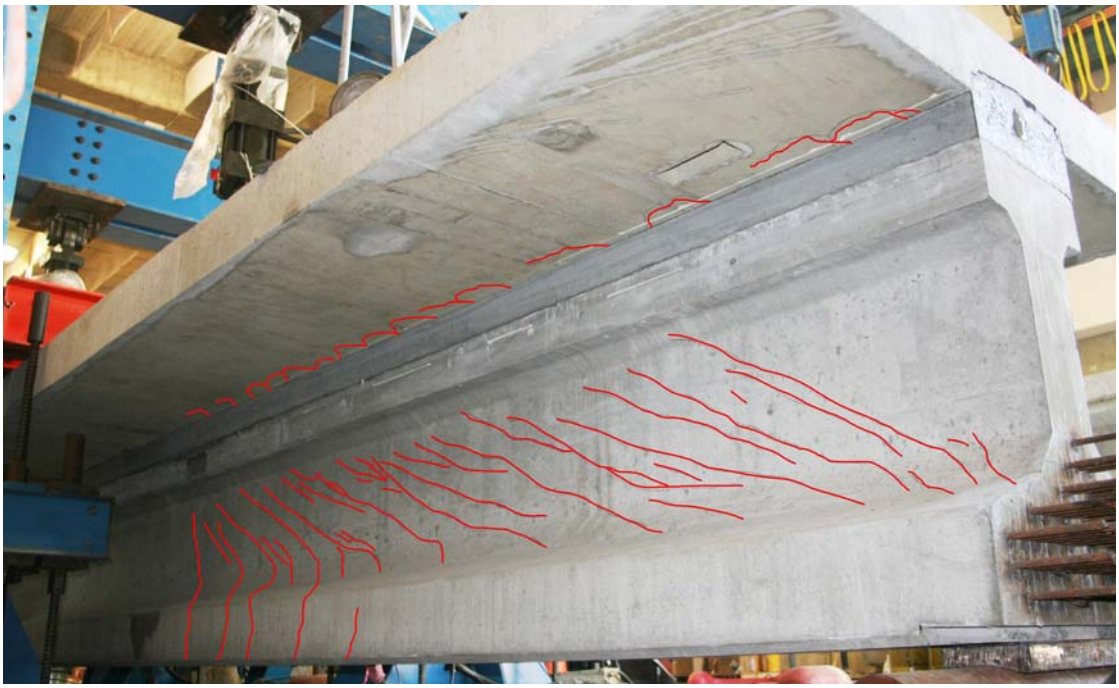

Figure 32. Illustration. Cracking apparent on north face of west end of test specimen after completion of static testing.

Figure 33. Illustration. Cracking apparent on south face of east end of test specimen after completion of static testing.

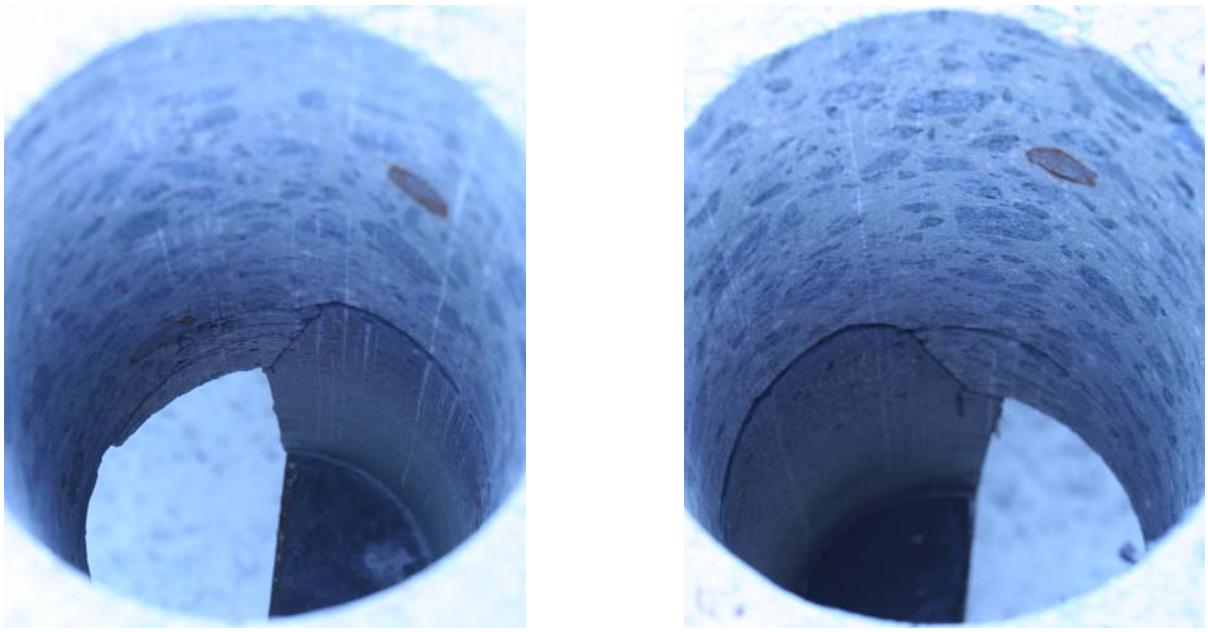

Figure 34. Photo. Distress in deck concrete at haunch connection near east end of test specimen which emulated the composite connection to a steel girder. Left photo pertains to south face. Right photo pertains to north face.

Figure 35. Photo. Distress in core extracted from haunch connection near east end of test specimen.

CONVENTIONAL CONNECTION RESULTS

The second test specimen used the conventional composite connection detail, with field-cast conventional grout filling the void space in the composite connection and assisting in carrying horizontal shear forces between the girder and the deck. The results of the cyclic and static loadings of this specimen are presented below.

As initially noted in the specimen fabrication section of Chapter 3, the first batch of conventional grout placed into the connection had an inappropriate rheology and thus was not able to be fully consolidated to fill all of the void space. The grout was too stiff, and thus it filled the blockouts in the deck panels and the areas immediately around the stud clusters, but left some voids in areas farther away from the stud clusters. This issue was encountered on the easternmost 2.4 m (8 ft) of the test specimen, with the grout for the remainder of the specimen being of appropriate consistency. After the initial placement had set, void spaces were filled by placing fluid grout into the void spaces laterally via accessible areas on the sides and ends of the haunch.

The inappropriate consistency and the secondary grout casting both resulted in greater than anticipated shrinkage cracking of the grout in the haunch connection within the easternmost 2.4 m (8 ft) of the test specimen. Figure 36 and Figure 37 provide representative examples of the cracking observed in the haunch connection grout near the east end of the specimen. Map cracking was apparent in the surface of the fluid patching grout on the sides and end of the haunch. In the deck blockouts, the overly stiff grout exhibited relatively large shrinkage cracks around the perimeter of the blockouts as well as across the short direction of the blockout. For comparison, a deck blockout located near the western end of the test specimen is shown in Figure 38. Blockouts in this area displayed a similar cracking patter, but the shrinkage cracks were much narrower.

Figure 36. Photo. Cracking apparent on north face of haunch near east end of test specimen.

Figure 37. Photo. Cracking apparent on top of deck at grout pocket near east end of test specimen prior to start of structural loading.

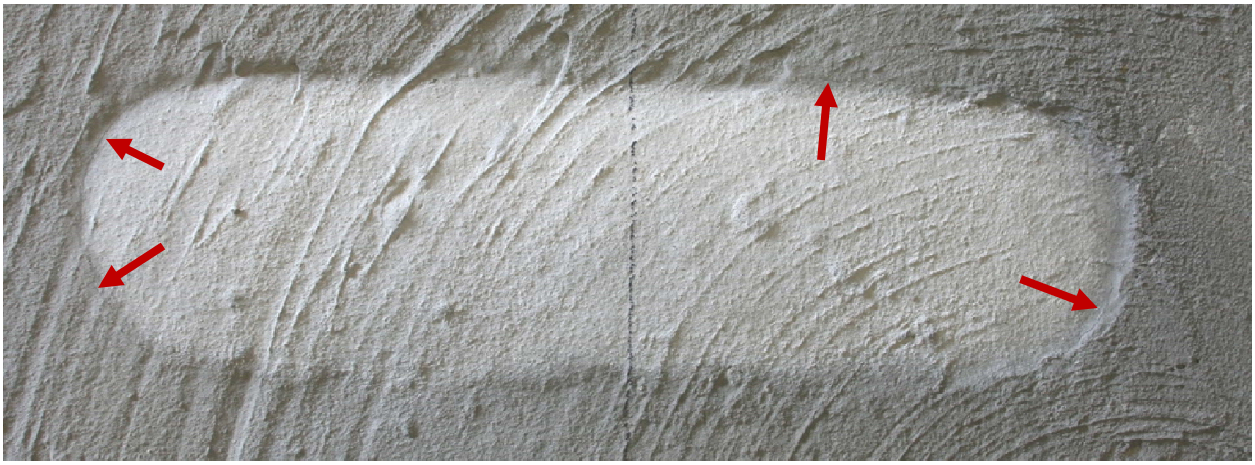

Figure 38. Photo. Cracking apparent on top of deck at grout pocket near west end of test specimen prior to start of structural loading.

Cyclic Testing

The cyclic testing of the conventional composite connection specimen was conducted according to the testing program previously described. The cyclic loading was completed over a nine week timeframe beginning in late June 2011. The specific number of cycles applied at each loading stage is detailed in Figure 39. The results obtained during this testing are generally reported in terms of the total number of cycles completed at the time a particular reading was captured. As such, a result reported as occurring at ten million cycles occurred at the ten millionth cycle according to the loading program in Figure 39.

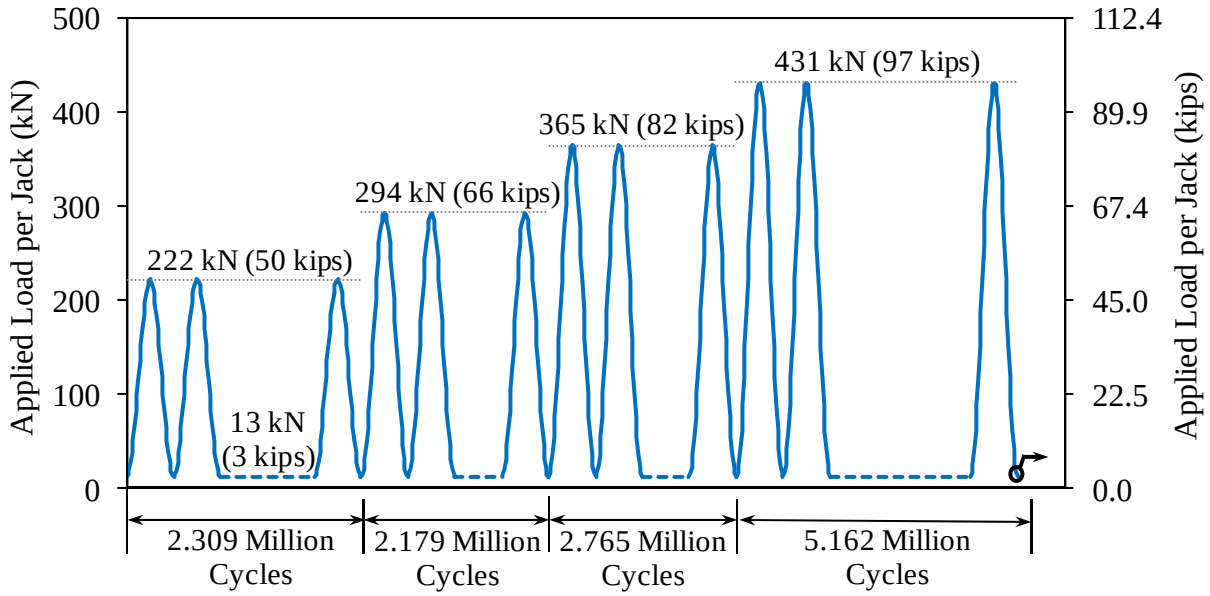

Figure 39. Illustration. Cyclic loading program for conventional connection specimen.

The LVDTs which monitored horizontal movement along the shear interfaces above and below the haunch provided the clearest indication of the performance of the structural system throughout the duration of the cyclic testing. As with the first test specimen, these LVDTs were located on the south face of the test specimen at four locations on each end of the test specimen. These LVDTs report relative movements of the haunch to the girder and of the deck to the haunch. Movements are reported as positive when the haunch or the deck expressed relative movement toward the end of the test specimen. In order to normalize the results, relative movements are reported as horizontal movement per load with the load being both the applied point load and the applied vertical shear in an end of the test specimen.

Figure 40 presents the horizontal movement results for the concrete girder composite connection. These results clearly demonstrate that both interfaces remained intact throughout the entirely of the cyclic loading. No differential movement was observed electronically or visually at these interfaces. The conventional grout remained well bonded to the precast surfaces with no indication of cracking, delamination, or debonding.

Figure 41 presents the horizontal movement results for the emulated steel girder composite connection. The results from these LVDTs clearly demonstrate that the shear interface movement occurred only at the girder to haunch interface and that it began with the first cycles of cyclic loading. This was visually apparent at the haunch to girder interface from the beginning of the testing, with any chemical bond between the conventional grout and the steel plate being broken by the initial cyclic loads. This plot shows that greater movement occurred closer to the end of the test specimen and that the difference between the movement magnitudes

increased as the cyclic progressed. At the conclusion of this testing, the maximum total relative movement observed at the girder to haunch interface at 1.22 m (4 ft) from the support was 0.57 mm (0.023 in.) over the course of a 431 kN (97 kip) load range. Note that the largest measured horizontal movement per load at the start of the conventional grout specimen cyclic testing is of similar magnitude to the largest measured horizontal movement per load measured at the conclusion of the UHPC specimen cyclic testing.

The results obtained from the vibrating wire and electrical resistance strain gages for this specimen were not of value in interpreting the results of the test. The configuration of the test specimen with numerous blockouts and other discontinuities located in the vicinity of the gages resulted in spurious results being obtained throughout the testing.

In summary, the over 12 million cycles of cyclic loading applied within this test program created little apparent damage in the composite connections at the deck to haunch interfaces or at the haunch to concrete girder interface. Interface shear movements were concentrated at the interface between the steel plate and the haunch on the eastern half of the test specimen.

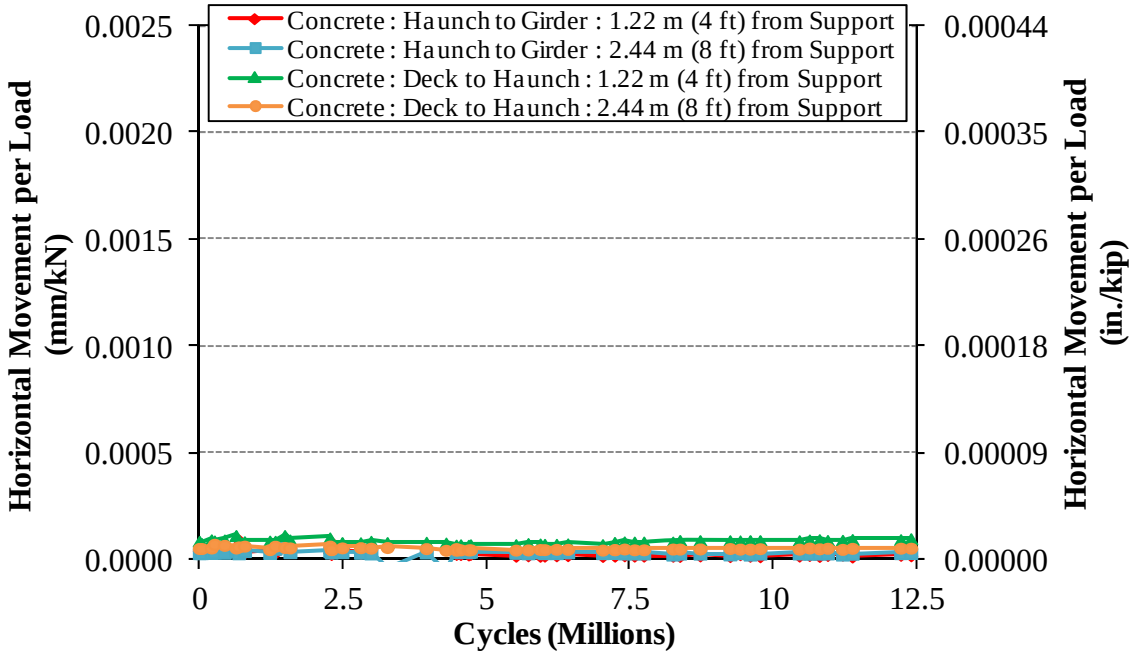

Figure 40. Graph. Horizontal movement at haunch in portion of conventional connection specimen which emulated the composite connection to a concrete girder.

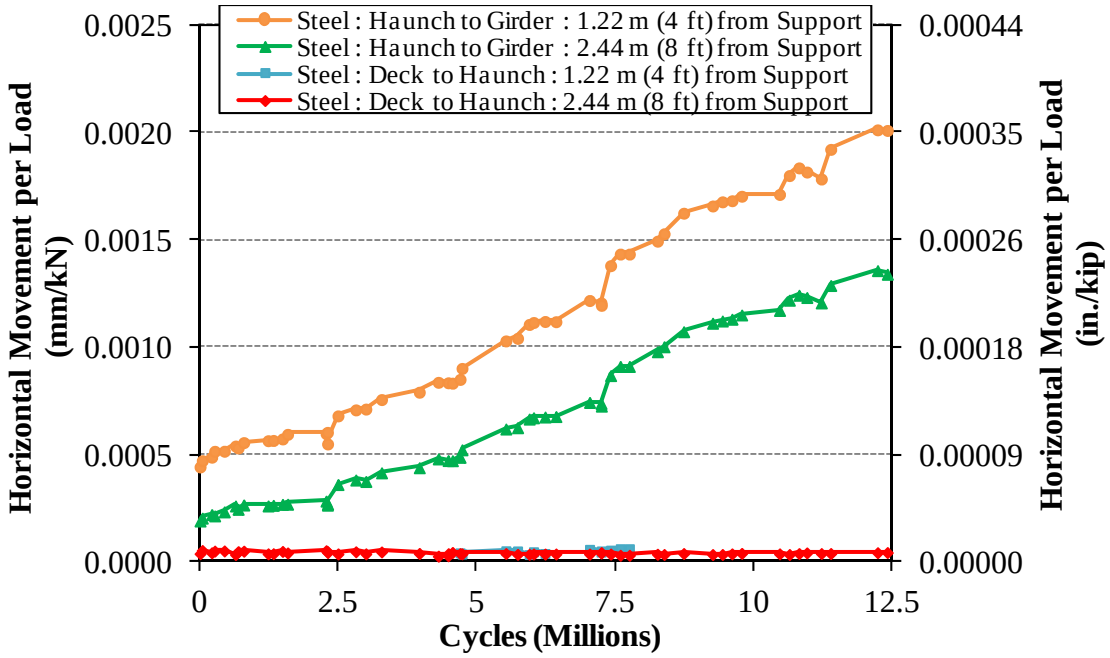

Figure 41. Graph. Horizontal movement at haunch in portion of conventional connection specimen which emulated the composite connection to a steel girder.

Static Loading to Failure

The static loading of the test specimen was completed according to the loading program previously described. This portion of the loading program was completed over the course of one hour in November 2011. The overall response of the specimen is shown in Figure 42. As with the UHPC test specimen, this and subsequent plots use applied vertical shear load, which is based on the applied load at each load point, on the vertical axis. The load versus displacement responses are very similar for the two load points until the specimen approached failure. The test specimen presented a linear response until the applied vertical shear load surpassed 890 kN (200 kips). The specimen then began to soften until the applied vertical shear load surpassed 1500 kN (337 kips). After this, the test specimen exhibited a significantly decreased stiffness until the peak loading resistance was encountered at an applied vertical shear of 1980 kN (445 kips) in the eastern portion of the span.

Visual and audible observations were also compiled throughout the static test. The first shear cracks in the web of the prestressed girder were audibly observed at an applied vertical shear load of 1110 kN (250 kips) and were clearly visually apparent at 1220 kN (275 kips). The first onset of flexural cracking was not noted, but flexural cracks were noted to be prevalent near midspan in the test specimen at an applied vertical shear load of 1820 kN (410 kips).

Horizontal movement along the horizontal shear interfaces was also monitored throughout the static testing. Figure 43 and Figure 44 provide the results from the western half of the test

specimen which simulated the concrete girder composite connection. Throughout the static test, no rigid body movement was observed across the horizontal interface between the deck and the haunch. This interface remained uncracked through global failure of the test specimen. No movement was observed at the haunch to girder interface measurement 1.22 m (4 ft) from the support roller. Small interface shear movement was observed at the 2.44 m (8 ft) measurement location between the girder and haunch. These movements, which only occurred near the end of the static test as the eastern end of the test specimen was beginning to fail, are attributed to the entire haunch and deck element moving eastward from a fixed point in the middle of the western span. Figure 47 provides a photograph showing this end of the test specimen immediately after failure of the test specimen.

Figure 45 and Figure 46 provide the horizontal shear interface horizontal movements for the eastern half of the test specimen which simulated the steel girder composite connection. Movement was significantly concentrated at the girder to haunch interface, with only smaller movements occurring later in the loading at the deck to haunch interface. The shape of the response observed at the girder to haunch interface is indicative of the weakening which occurred along this connection plane during the cyclic loading. At applied static vertical shear loads below 445 kN (100 kips), the stiffness of the response is reduced as compared to the stiffness at applied vertical shear loads between 445 kN (100 kips) and 890 kN (200 kips). At the higher loads, the shear connectors crossing this plane were engaged more firmly. Soon thereafter, the stiffness of the response began to again decrease with 4 mm (0.16 in.) of movement being observed by the time the applied vertical shear force had reached 1500 kN (337 kips). By the time the applied load had reached 1815 kN (408 kips), more than 16 mm (0.63 in.) of movement was observed at the measurement point 1.22 m (4 ft) from the support point. The stroke capacity of the LVDTs was exhausted by this point, thus no specific measurements along this plane could be made thereafter.

The south face of the eastern end of the test specimen as observed during the static test is shown in Figure 48, Figure 49, and Figure 50. This series of photos, including Figure 50 showing the specimen after failure, shows that the deck/haunch element moved horizontally along the top of the girder and also vertically away from the girder.

The failure of the test specimen occurred when the composite connection between the steel plate on the top of the precast girder and the haunch connected thereto became completely disconnected from midspan to the east end of the test specimen. As this connection disconnected, the eastern half of the specimen ceased to be a composite beam and began functioning as a significantly shallower member. The compressive flexural capacity of this remaining cross-section was superseded by the applied load, resulting in compressive failure of the top flange of the prestressed girder at midspan. Figure 51 shows the east end and part of the north face of the girder immediately after failure. Figure 52 shows the failure location as viewed from the north side. The termination point of the steel plate just under the haunch area coincides with midspan of the test specimen.

The precast deck element and the still connected haunch details on the eastern end of the test specimen were removed in order to inspect the failure plane. Since all 72 shear stud connectors on the top of the steel plate had either failed by pullout or failed at their bases, the removal of the deck element only required cutting the deck-to-deck connection at midspan. Figure 53 provides a view of the steel plate side of the composite connection on the eastern half of the test specimen. A corresponding view of the haunch/deck side of the connection is provided in Figure 54. Close-up photographs of the easternmost four stud row locations on the steel plate and the easternmost two stud row locations on the haunch are provided in Figure 55 and Figure 56, respectively.

Examination of the failure surfaces at the bases of the shear studs indicates that some studs failed during the cyclic loading program. Although many of the studs displayed fracture surfaces indicative with combined shear/tensile loading, others displayed smooth fracture surfaces which had been polished by repeated cyclic shearing of two mating surfaces against one another. These polished surfaces tended to be surrounded by fretting rust particles which had accumulated on both the steel plate and on the underside of the haunch grout.

The performance of the 72 studs was cataloged and the results are presented in Figure 57. Each of the studs was cataloged into one of seven categories based on a qualitative assessment of the failure of the stud. These categories ranged from “Cyclic Loading Fracture at Base of Stud” indicating that the stud became disconnected from the plate during the cyclic loading program, to “Static Fracture at Base of Stud” indicating that the stud fractured at its based with no indication of damage having occurred prior to the static loading of the test specimen, to “Stud Remained Attached to Plate” indicating that the stud remained with the steel plate and pulled out of the grout. For the intermediate categories describing studs which showed indications of damage occurring during cyclic loading that was followed by static fracture of the non-fatigue-damaged remaining cross section, the categorical assignment was based on the percentage of the total fracture surface which could be attributed to each failure mechanism.

Given that steel fatigue failure is driven by stress range, it is reasonable to assume that the studs which failed during cyclic loading may have been subjected to higher cyclic stress ranges than those that failed under static loading. The stud failure pattern indicates that the cyclic stresses may have been higher immediately east of the load point and as well as at the eastern end of the test specimen. More significantly, the results also indicate that the cyclic stresses were likely higher on the middle two studs of each row of four. All ten studs which failed entirely during the cyclic loading portion of the load program were located in the middle stud positions. Twelve of the 13 studs located east of the load point which failed in static fracture entirely during the static loading were located in the outer stud positions.

Further discussion of the fracture performance of the stud shear connectors is provided in Chapter 5.

Based on the recognition that stud connectors were beginning to fail during the cyclic loading, the observed horizontal movements along this interface during the cyclic loading program were reassessed. Recall that these results are presented in Figure 41. The first load range was applied until nearly 2.5 million cycles had been accumulated, the second load range until nearly 5 million, and the third load range until nearly 7.5 million. These results show that this horizontal shear interface was approaching a nearly steady state of movement per load at the conclusion of the first loading range. In each of the subsequent loading ranges, the movement per load does not seem to stabilize, indicating that cyclic damage was progressively accumulating.

In summary, the conventional grout haunch connection detail failed locally at the interface between the emulated steel girder top flange shear connectors and the conventionally grouted haunch. Neither the connections between the precast deck elements and the haunch nor the connection between the precast girder and the haunch showed any significant distress throughout the entirely of the cyclic and static loading programs. The horizontal shear interface failure at the emulated steel girder connection began during the cyclic loading program. There are indications that this progressive failure may have begun during the second stage of the cyclic loading program.

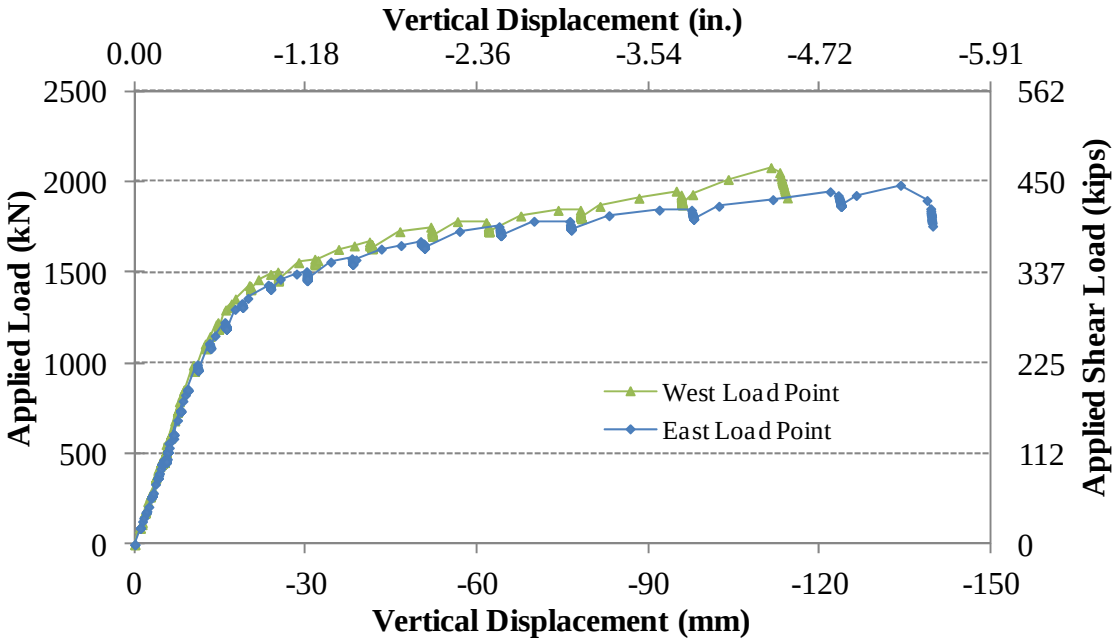

Figure 42. Graph. Load-deflection response of conventional connection specimen under static load to failure.

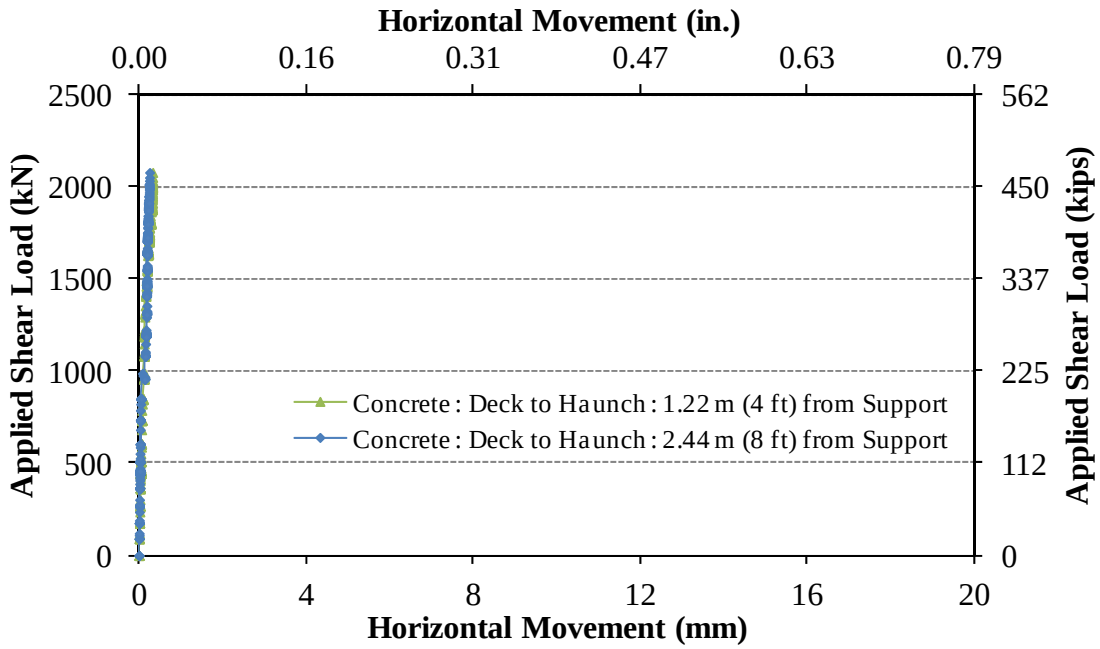

Figure 43. Graph. Horizontal movement between deck and haunch in portion of conventional connection specimen which emulated the composite connection to a concrete girder when under static load to failure.

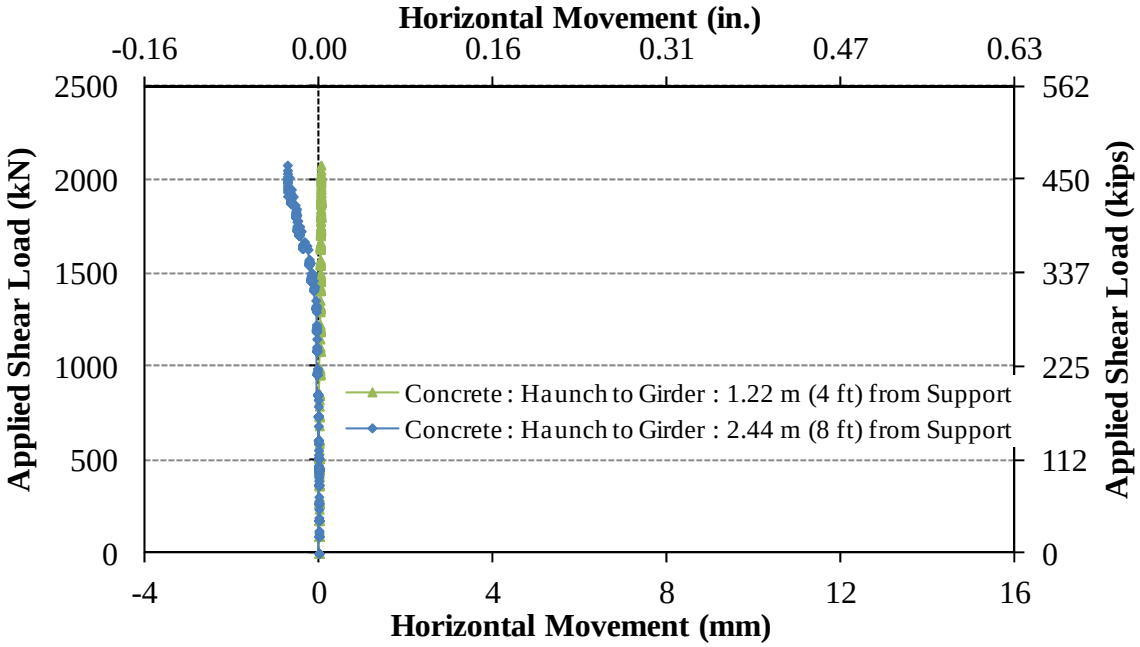

Figure 44. Graph. Horizontal movement between haunch and girder in portion of conventional connection specimen which emulated the composite connection to a concrete girder when under static load to failure.

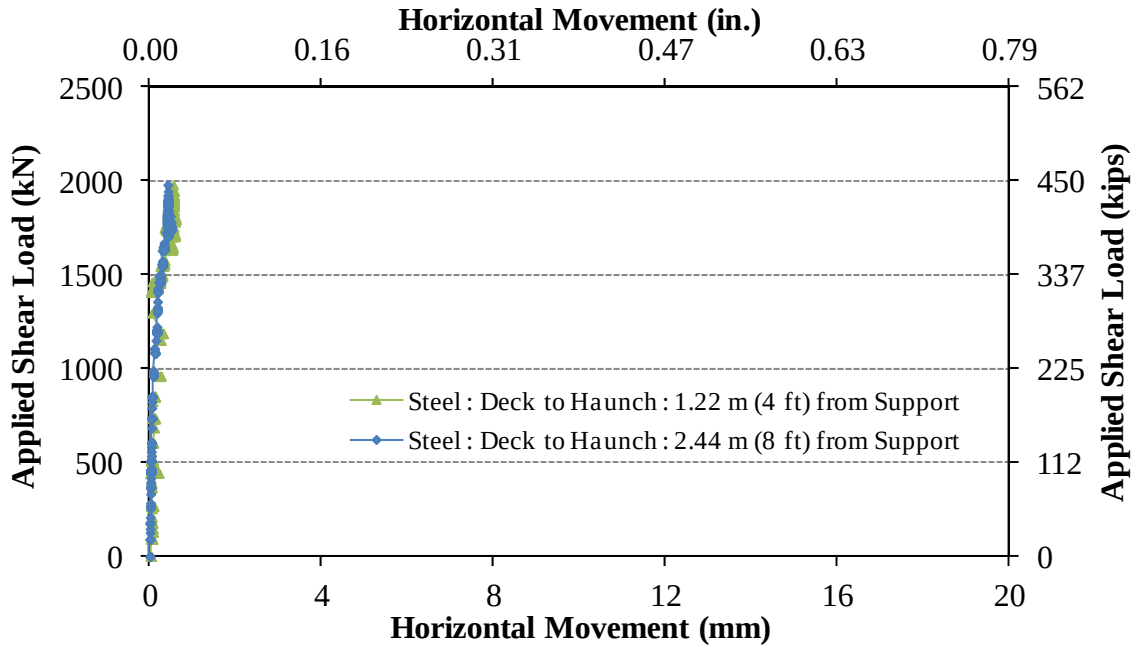

Figure 45. Graph. Horizontal movement between deck and haunch in portion of conventional connection specimen which emulated the composite connection to a steel girder when under static load to failure.

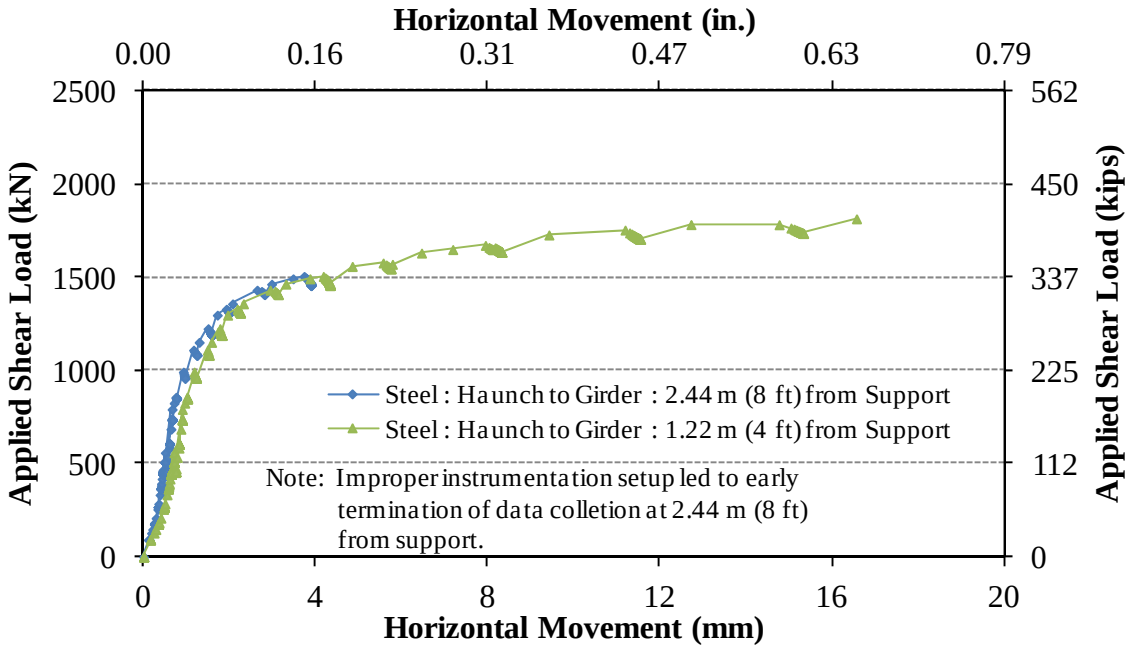

Figure 46. Graph. Horizontal movement between haunch and girder in portion of conventional connection specimen which emulated the composite connection to a steel girder when under static load to failure.

Figure 47. Photo. West end and south face of test specimen immediately after completion of test.

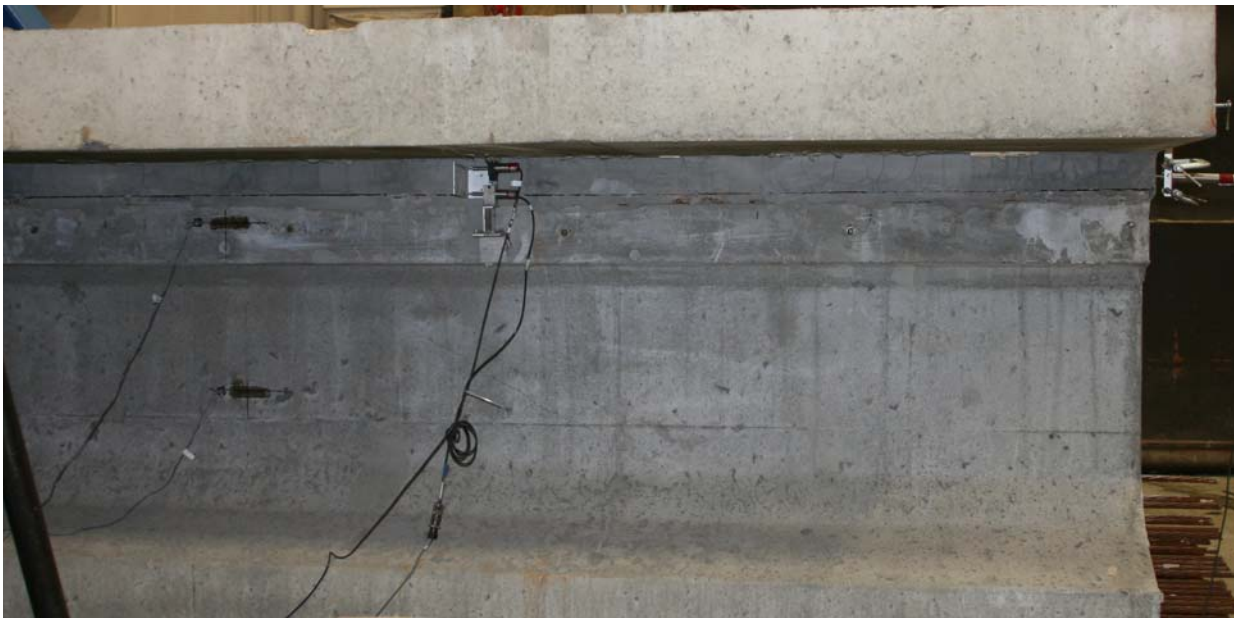

Figure 48. Photo. Haunch connection on south face at east end of test specimen when applied shear load in east end was equal to 1575 kN (354 kips).

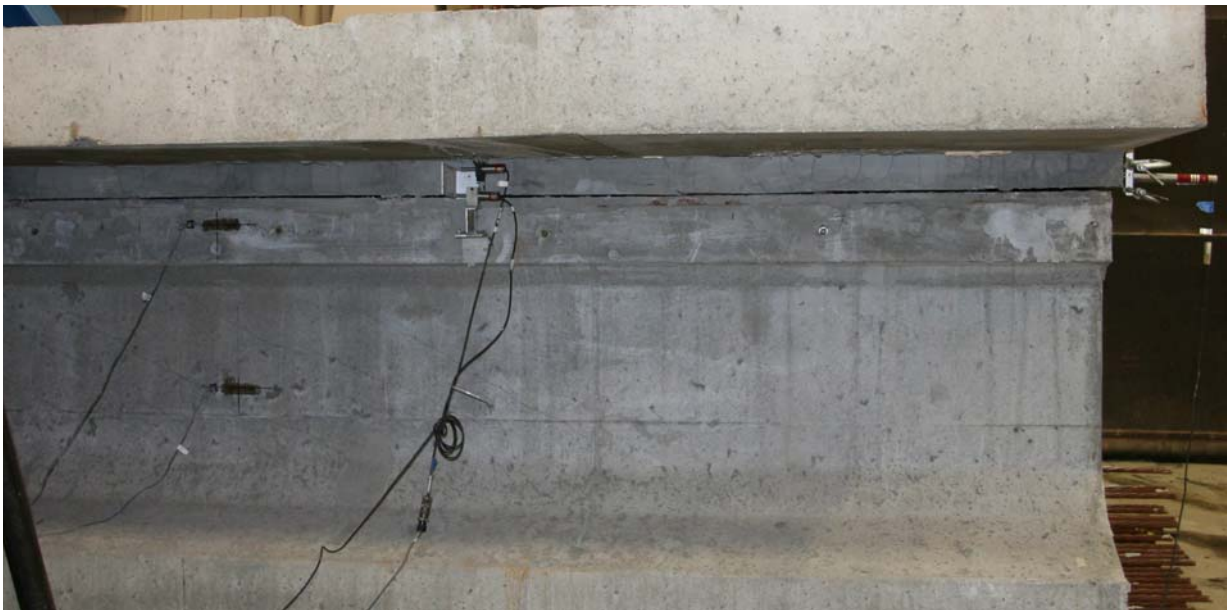

Figure 49. Photo. Haunch connection on south face at east end of test specimen when applied shear load in east end was equal to 1846 kN (415 kips).

Figure 50. Photo. Haunch connection on south face at east end of test specimen immediately after completion of test.

Figure 51. Photo. East end and north face of test specimen immediately after completion of test.

Figure 52. Photo. Midspan north face of test specimen immediately after completion of test.

Figure 53. Photo. Emulated steel girder composite connection after completion of test and removal of haunch/deck.

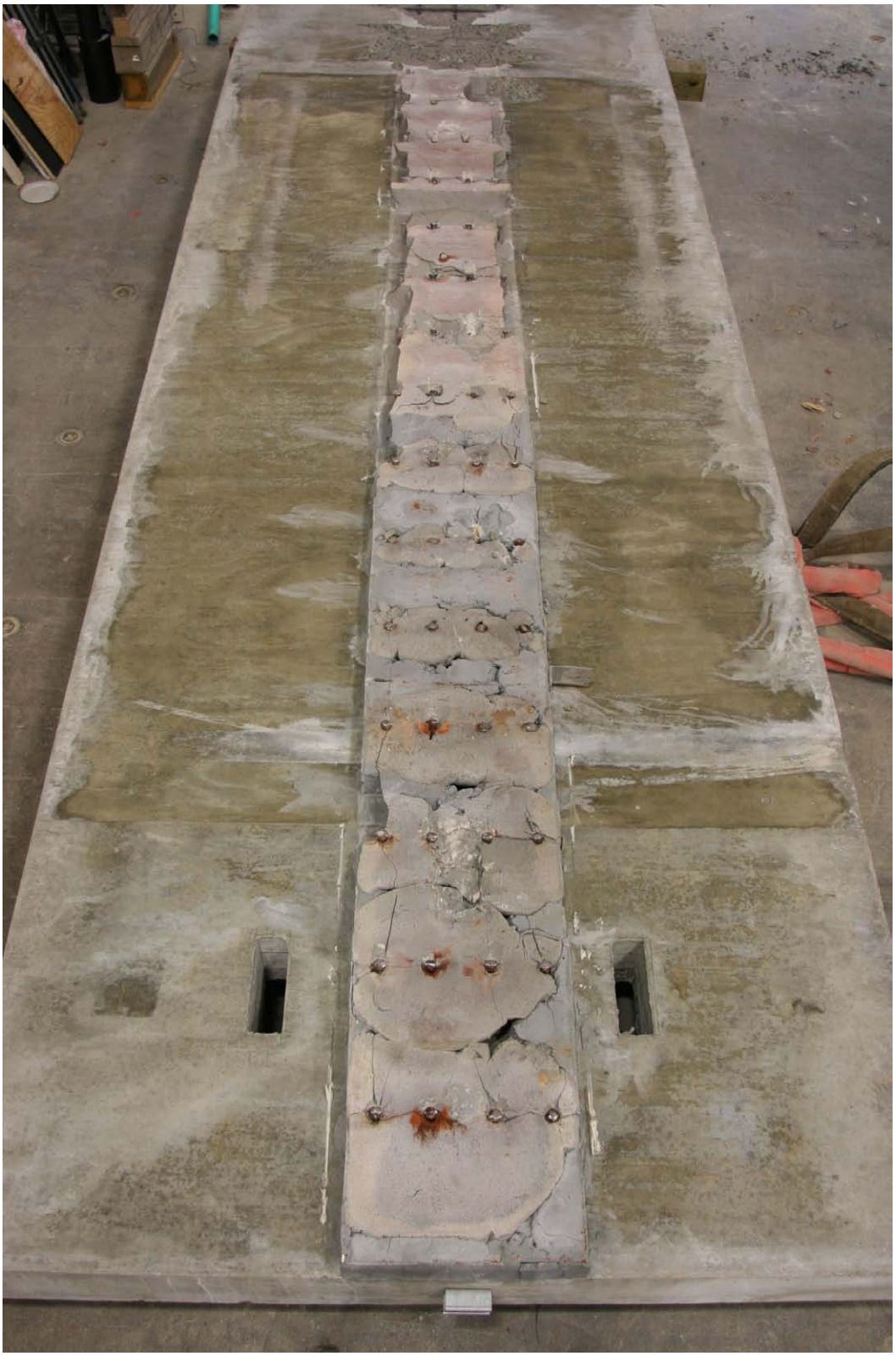

Figure 54. Photo. Emulated steel girder composite connection after completion of test and removal of haunch/deck.

Figure 55. Photo. Easternmost steel plate on top of girder within emulated steel girder composite connection.

Figure 56. Photo. Easternmost two rows of shear studs emanating from conventional grout and precast deck.

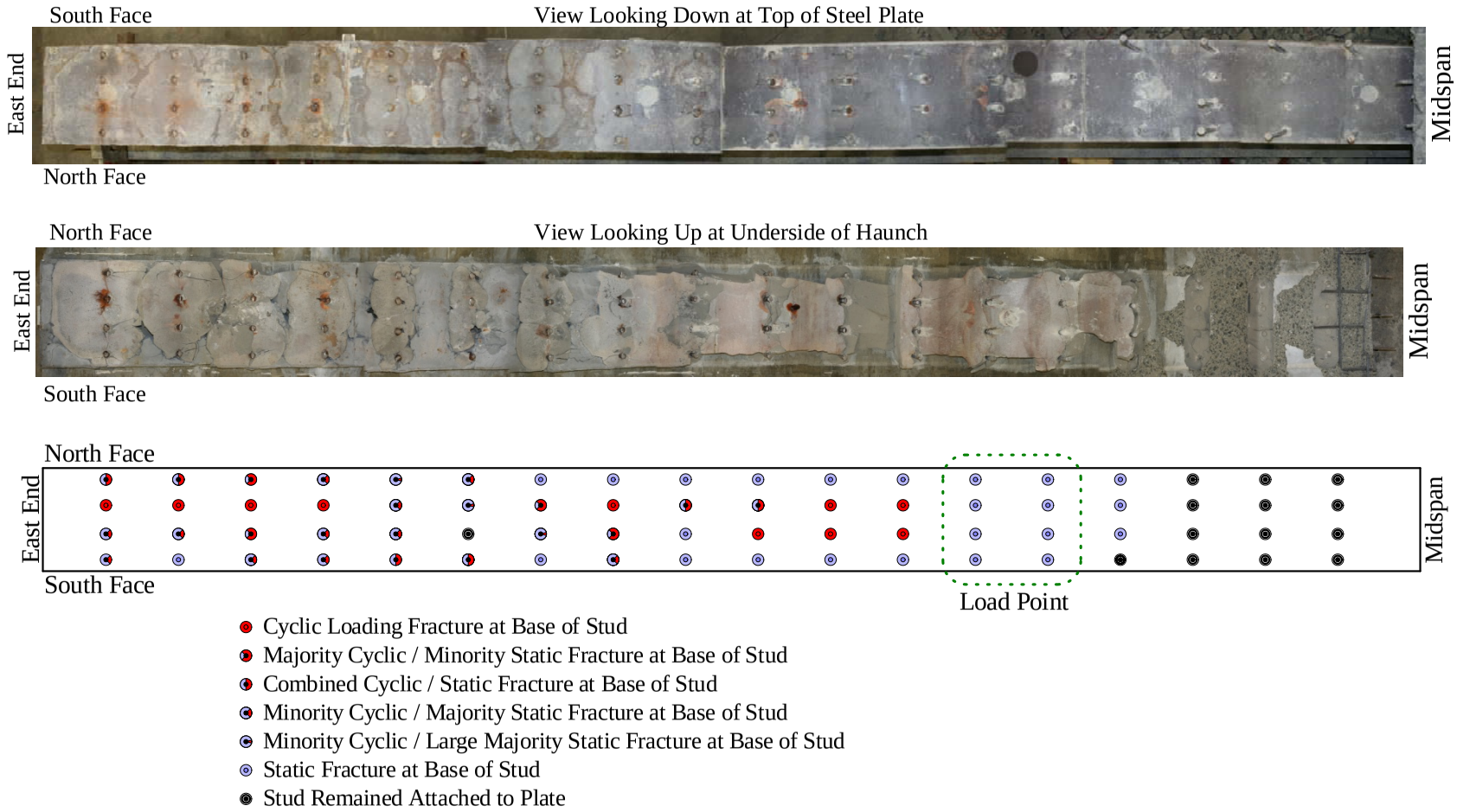

Figure 57. Illustration. Disposition of shear studs after conclusion of structural testing on conventional haunch specimen.

CHAPTER 5. DISCUSSION OF RESULTS

INTRODUCTION

The analysis and synthesis of the results developed in this research program are presented in this chapter. The results relating to the horizontal interface shear performance under cyclic and static loading are discussed first. The performance of the field-cast monolithic UHPC within the novel connection is then discussed. Next, the horizontal shear performance of the concrete girder interface with the field-cast haunch is summarized. The assessment of the performance of the steel studs, with specific focus on the likely poor welding of the studs to the plates, is then presented. Finally, the restrained shrinkage cracking performance of the UHPC and the conventional grout is discussed.

HORIZONTAL INTERFACE SHEAR — CYCLIC LOAD PERFORMANCE

The primary objective of this research project was to assess the performance of a novel UHPC composite connection used for attaching precast bridge deck elements to superstructure members. This objective was met through the full-scale testing of a pair of specimens under cyclic and static loadings. The loadings simulated and exceeded the loads which a comparative bridge, namely the two-span continuous NYSDOT Bridge SBEBR with 63.6 m (209 ft) spans and 2 m (79 inch) deep girders, was designed to carry according to the AASHTO LRFD Bridge Design Specifications. The two test specimens included a conventional specimen with conventional composite connection details and a UHPC specimen with the novel connection details.

The novel UHPC connection details succeeded in resisting all structural loads to which they were subjected throughout the testing program. The initial cyclic loads, which were applied to the test specimen for over two million cycles, generated horizontal shear stresses within the connection which exceeded the design shear fatigue capacity. Figure 58 shows the design and applied horizontal shear fatigue ranges normalized by unit length. Note that the design values are based on the assumption of behavior emulating steel stud fatigue performance as detailed in Section 6.10.10.2 of the AASHTO LRFD Bridge Design Specifications. Subsequent loadings at factors of 1.33, 1.66, and 2.0 times the initial load range for more than two million, two million, and five million additional cycles, respectively, were then completed. No damage was observed within the UHPC composite connection or in the adjoining steel connectors throughout the duration of this testing.

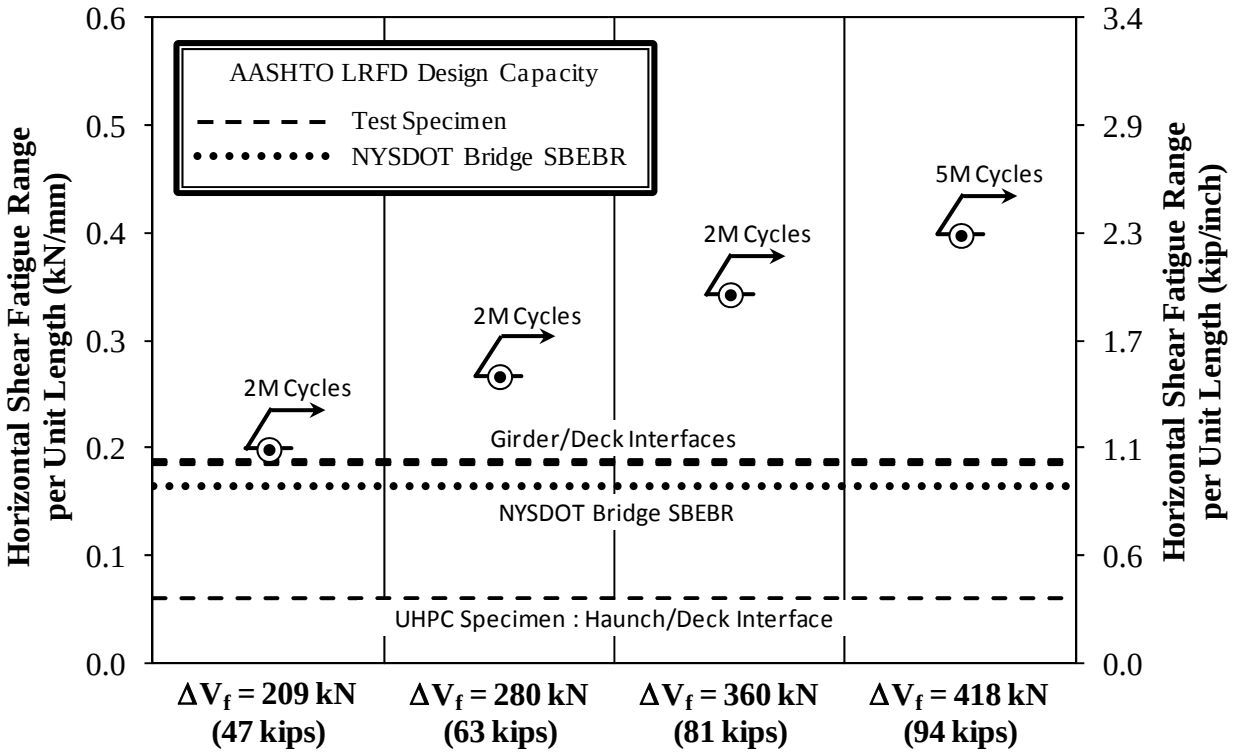

Figure 58. Graph. Design values of horizontal shear fatigue range in relation to applied shear ranges.

The conventional connection detail specimen also succeeded in completing this full suite of cyclic load applications. However, as the cyclic testing progressed, it was apparent that degradation of the connection between the emulated steel girder top flange and the haunch was occurring. Indications of this degradation are apparent in Figure 59 which shows the horizontal movement observed along this interface for both test specimens throughout the entire cyclic loading. The performance of the two specimens is very similar throughout the initial cyclic load range. The only significant difference, the fact that the conventional specimen exhibited greater movement near the support, can be attributed to the poor grout consolidation which occurred in this area of this specimen. The relative change in behavior between the two specimens becomes apparent during the second load range. The conventional specimen begins to show increasing movement per load as compared to the UHPC specimen. This increasing movement can be attributed to progressive deterioration of the composite connection along this interface. The increased rate of deterioration continues and grows larger as the cycling progresses through the conclusion of this phase of the study. Regardless, the overall performance of the conventional specimen did meet the design requirements.

Potential reasons for the comparatively lesser performance of the conventional connection include:

- poor grout consolidation in the easternmost 2.4 m (8 feet) of the composite connection,
- poor quality welding of the shear studs to the steel plate,
- different stud spacing and clustering leading to increased stresses on some studs, and/or
- different grout modulus of elasticity leading to changes in local stresses at the bases of the studs.

Due to indications that the shear studs may have failed prematurely due to poor welding practices, an additional assessment of these shear studs was completed. The results of this assessment are presented later in this chapter.

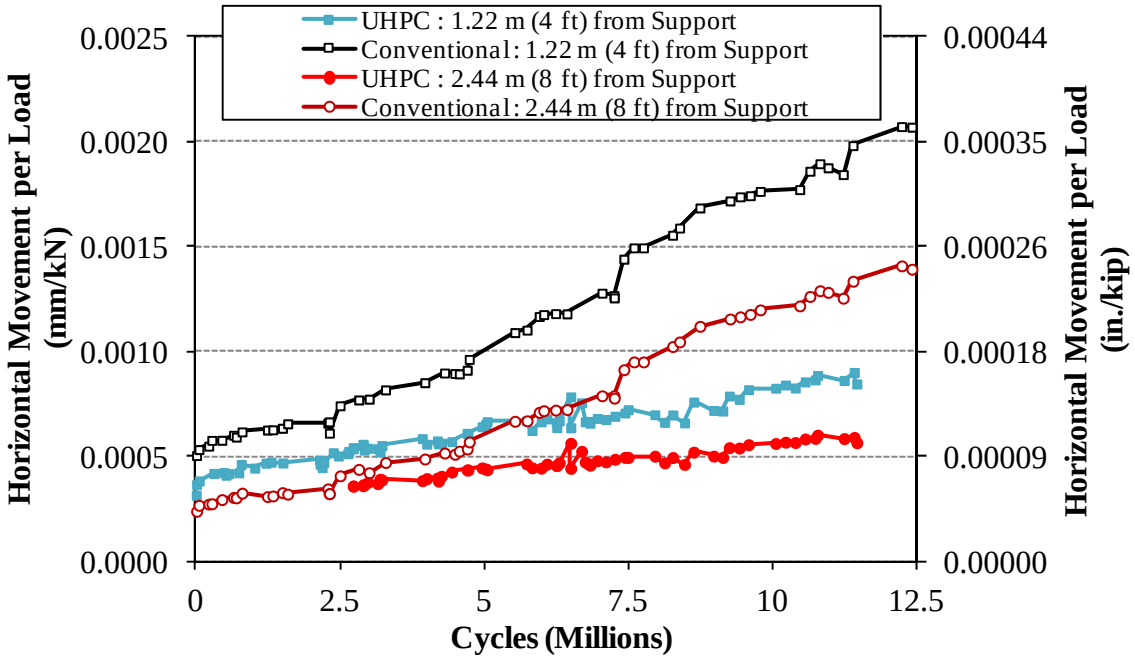

Figure 59. Graph. Comparison of horizontal movement across haunch in test specimens emulating the composite connection to a steel girder.

HORIZONTAL INTERFACE SHEAR — STATIC LOAD PERFORMANCE

After the completion of the cyclic loading program, each test specimen was subjected to static loading which culminated in failure of the test specimen. The UHPC test specimen carried a peak applied shear load of 2215 kN (498 kips) which corresponds to a horizontal shear per unit length of 2.1 kN/mm (12.0 kip/inch). At this load, the prestressed girder began to fail in a combination of horizontal and vertical shear in the web and top flange of the girder. Horizontal shear distress was also observed in the precast deck elements adjacent to the haunch. No damage was observed within the UHPC connection or in the discrete elements connecting thereto.

The conventional test specimen carried a peak applied shear load of 1980 kN (445 kips) which corresponds to a horizontal shear per unit length of 1.83 kN/mm (10.45 kips/inch). At this load, the composite connection at the emulated steel girder to haunch interface failed with nearly all of the studs in the shear span detaching from the steel plate at their bases. Note that the post-test assessment of the stud failure surfaces indicated that 10 of the studs had completely detached and 23 had partially detached during the cyclic loading, leaving a reduced number of studs to carry the horizontal shear during the static loading.

Figure 60 provides a graphical summary of the results of the static tests. This figure shows the AASHTO LRFD design capacities for the critical horizontal shear interfaces. Both specimens significantly exceeded the minimum interface capacities. In the UHPC specimen, the horizontal shear at failure exceeded the design capacity of the steel crossing the emulated steel girder/haunch interface by 66% and of the steel crossing the haunch/deck interface by 240%. In the conventional specimen, the horizontal shear at failure exceeded the design capacity of the steel crossing the emulated steel girder/haunch interface by 45%.

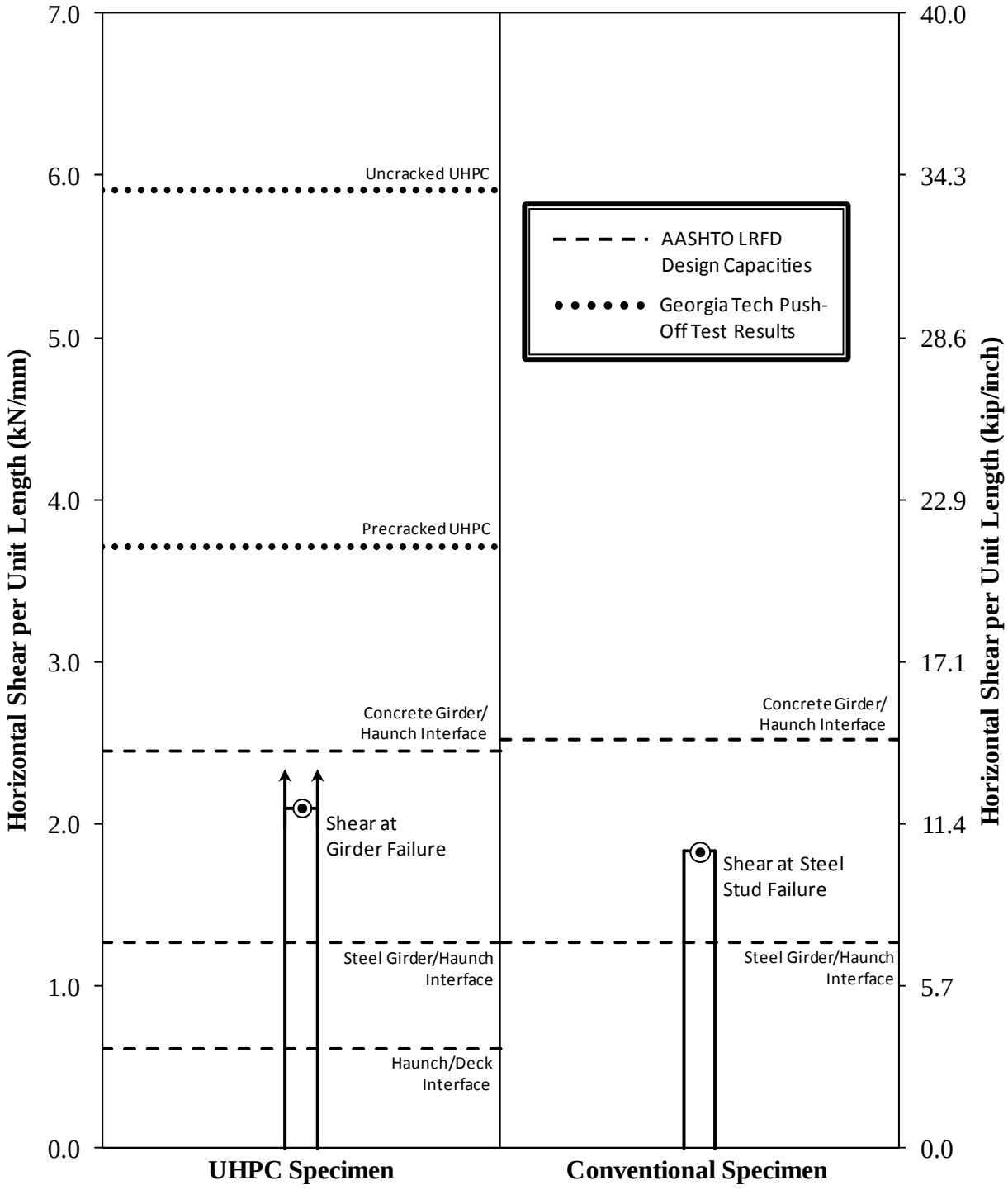

Figure 60. Graph. Horizontal shear per unit length at failure of test specimen in relation to design values and Georgia Tech push-off test results.

HORIZONTAL INTERFACE SHEAR OF MONOLITHIC UHPC

The horizontal static shear capacity of monolithic UHPC is a critical parameter in the performance of this type of novel connection. The testing completed herein provides some insight into the performance of these connections. Specifically, the loading regime implemented generated high horizontal shear fatigue load ranges as well as high levels of static horizontal shear load within the connection. These tests demonstrated that this type of connection detail can provide a minimum level of capacity under each of these loading scenarios.

In order to assess the performance of monolithic UHPC subjected to horizontal shear, the minimum shear plane within the connection must be determined. Figure 61 shows three potential shear planes for the emulated steel girder portion of the test specimen. Plane "A", with a cross-sectional length of 445 mm (17.5 inches), defines the shear plane immediately below the bottom mat of reinforcement. Plane "B", with a cross-sectional length of 337 mm (13.25 inches), defines the shear plane surrounding the pair of studs. Plane "C", with a cross-sectional length of 368 mm (14.5 inches), defines the shear plane surrounding each individual line of studs. In this test program, plane "B" defines the minimum shear plane.

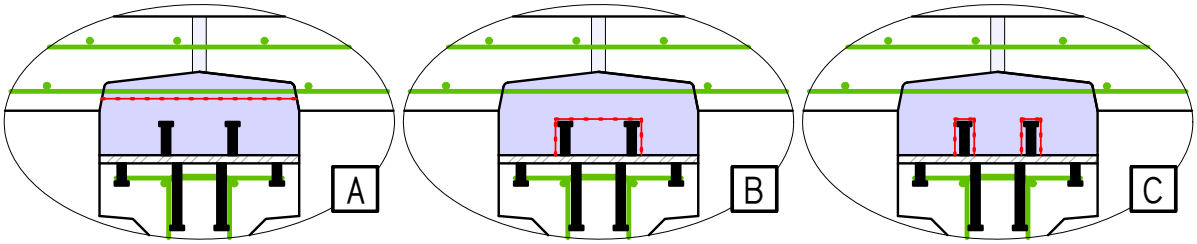

Figure 61. Graph. Minimum shear planes for horizontal shear transfer in the UHPC composite connection of the emulated steel girder portion of the test specimen.

The peak cyclic load applied to this specimen generated a horizontal shear fatigue load range of 0.398 kN/mm (2.275 kips/inch). Dividing by the minimum shear plane cross-sectional length results in a horizontal shear stress range of 1.16 MPa (168 psi). Through more than five million cycles at this stress range and more than six million cycles at lower stress ranges, no damage was observed within the UHPC composite connection.

The peak static load applied to this specimen generated a horizontal shear load of 1.83 kN/mm (10.45 kips/inch). Dividing by the minimum shear plane cross-sectional length results in a horizontal shear stress of 5.44 MPa (789 psi). No damage was observed in the UHPC composite connection under this loading. For reference, recall the push-off tests on monolithic UHPC reported by Crane.[(5)] The uncracked monolithic UHPC shear stress capacity was observed to be 17.5 MPa (2550 psi) and the precracked UHPC shear stress capacity was observed to be 11 MPa

(1600 psi). These results are also shown in Figure 60 after being converted into horizontal shear per unit length along the minimum shear plane.

PERFORMANCE OF PRECAST CONCRETE GIRDER COMPOSITE CONNECTION

The test results pertaining to the portion of each of the two test specimens which simulated the composite connection between a precast concrete girder and a field-cast grout haunch are instructive in assessing the performance of this type of connection. Consistent with common practice, the freshly placed concrete on the top surface of the precast girder was intentionally roughened prior to the setting of the concrete. When cementitious grout is cast against this roughened surface, a physically interlocked and chemically bonded interface is formed.

The bond between the precast girder and the grout haunch remained intact throughout the cyclic and static loadings of both test specimens. From this observation, two results can be developed. First, the highest cyclic load range generated a horizontal shear fatigue load of 0.398 kN/mm (2.275 kips/inch) along the length of the shear span which lasted for over 5 million cycles. Since this interface did not break during this loading, it is clear that the concrete bond was capable of resisting this level of fatigue loading.

Second, the loads applied to these test specimens during static loading to failure also did not result in debonding along this interface. The peak induced horizontal shear load in the UHPC connection was 2.1 kN/mm (12.0 kips/inch), and the peak induced horizontal shear load in the conventional grout connection was 1.83 kN/mm (10.45 kips/inch). For comparison, the provisions in section 5.8.4 of the LRFD Bridge Design Specifications indicate that the concrete cohesion component of the resistance of this interface to horizontal shear would be 0.882 kN/mm (5.04 kips/inch). However, it must be recognized that the interface shear resistance as detailed in these provisions assume a simultaneous addition of both the steel and concrete components of the resistance. Since the steel is unlikely to resist significant loads prior to debonding of the concrete interface, careful consideration must be given to any thought of modifying the concrete or steel contributions within this provision framework.

ASSESSMENT OF STUD WELDS

The failures of shear studs on the eastern portion of the conventional composite connection specimen raise questions with regard to that particular connection detail. As such, an assessment of these stud weld connections was conducted. It must be noted that all of the stud welding completed as part of this study was completed by a local subcontractor to the precast component manufacturer. It could not be confirmed whether all appropriate stud welding installation and testing procedures were followed.

The detailed assessment was conducted by engineering staff at the Turner-Fairbank Highway Research Center with assistance from Dr. Adonyi at LeTourneau University. Dr. Adonyi's

report on the stud failures is provided in Appendix A. A summary of his report and the information gathered at TFHRC is presented below.

At the conclusion of the testing of the conventional composite connection specimen, it was apparent that the shear stud to steel plate welded connection has failed. The majority of the shear studs, especially near the end of the beam, had separated from the steel plate and remained in the deck panel. The base of these studs remaining in the deck panel were exposed, leaving them open for observation. Other shear studs near midspan of the beam remained intact and connected to the steel plate.

The failure investigation consisted of visually examining the shear studs in the deck panel and the steel plate. Advanced analysis procedures including metallography, hardness tests, and fractography were also performed on selected samples. Based on the investigation, it was determined that poor weld quality of the shear stud welds contributed to early failure of these studs and thus of the conventional connection specimen.

Observation of the base of the studs in the deck panel revealed the majority of the studs had failed in the steel plate rather than in the stud itself. This was apparent because the weld connecting the stud to the steel plate was intact, leaving some of the steel plate metal connected to the base of the stud. Figure 62 shows a typical transverse row of studs in the panel and a close-up of one of these studs.

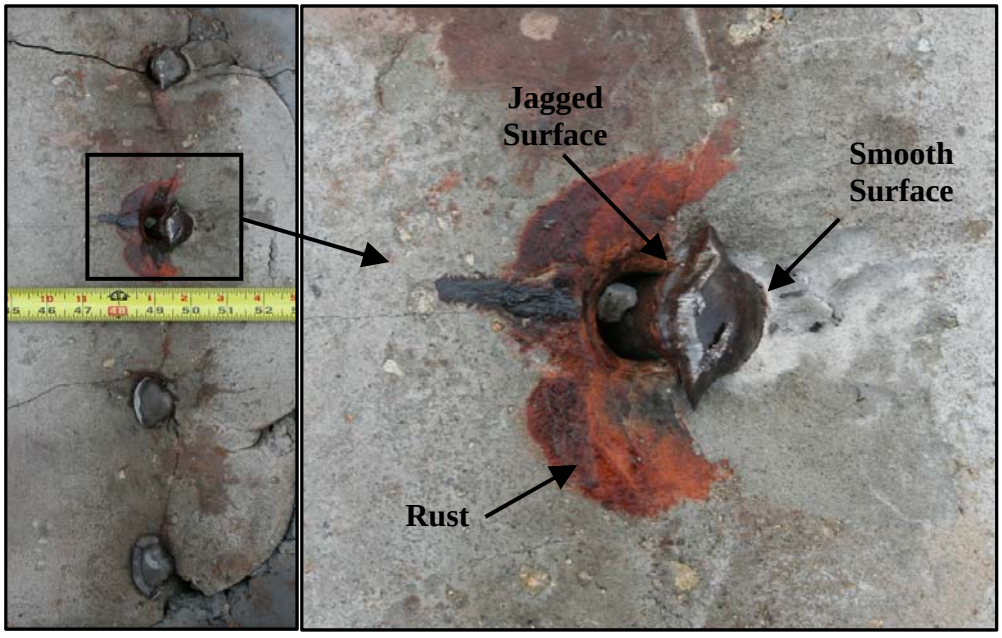

Figure 62. Illustration. Failure surface of typical shear stud in deck panel.

Several key observations are illustrated in Figure 62. The right (midpsan) side of the stud is smooth and dull, indicating partial fracture (possibly due to fatigue cracking) which would have occurred before and/or during cyclic loading. The left (east) side of the stud is jagged, which would suggest some form of brittle fracture during static loading. There is also a great deal of rust present around the stud, which is a sign of two metal surfaces rubbing together. This amount of rust was determined to be greater than that of typical fretting accompanied by metal fatigue, likely suggesting there were cracks present before any cyclic load induced fatigue cracking could have begun. The large amount of fretting also likely destroyed some of the fractographic evidence of the early cracking.

A visual examination of the steel plate confirmed the failure occurred in the base metal. This was seen from the divots left in the steel plate when the shear studs were torn away from the steel plate. These divots are visible in Figure 63, which shows where a typical row of shear studs would have been welded to the steel plate and a close up of one of these divots.

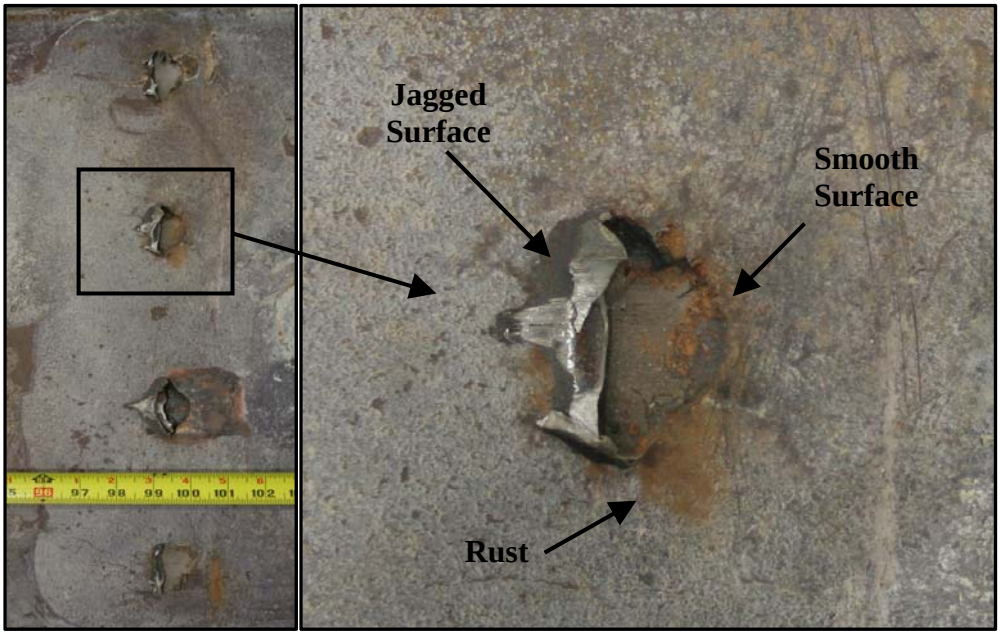

Figure 63. Illustration. Failure surface of typical divot in steel plate.

As shown in Figure 63, the divot displayed similar characteristics to the typical shear stud in Figure 62. Similar to that of the shear stud, the right side of the surface appears smooth, suggesting cracks which occurred before or during cyclic loading. The left side is jagged, indicating fracture during static loading. There is also a large amount of rust present, again suggesting there was cracking prior to any cyclic load induced crack growth.

In addition to visual examination, more advanced analyses, including metallography, hardness testing, and fractography, were performed on failed specimens from the test. The two types of

specimens included five cores of the steel plate at the shear stud welds and four welded ends of the shear studs removed from the concrete panel. Each of the five cores was extracted from near midspan of the beam. This location was chosen because the shear studs were still in place and could easily be cut off before coring the specimens. The four shear studs were removed from near the east end of the concrete panel due to relative ease of removal.

To aid in understanding the following discussion, Figure 64 is presented to show a typical cross section of a good quality shear stud weld. The different regions of a stud weld are shown in the figure and will be referred to as such in the sections to follow. A heat affected zone (HAZ) is the portion of a base metal around a weld in which its microstructure and chemical properties change due to the large amount of heat produced during the welding process.

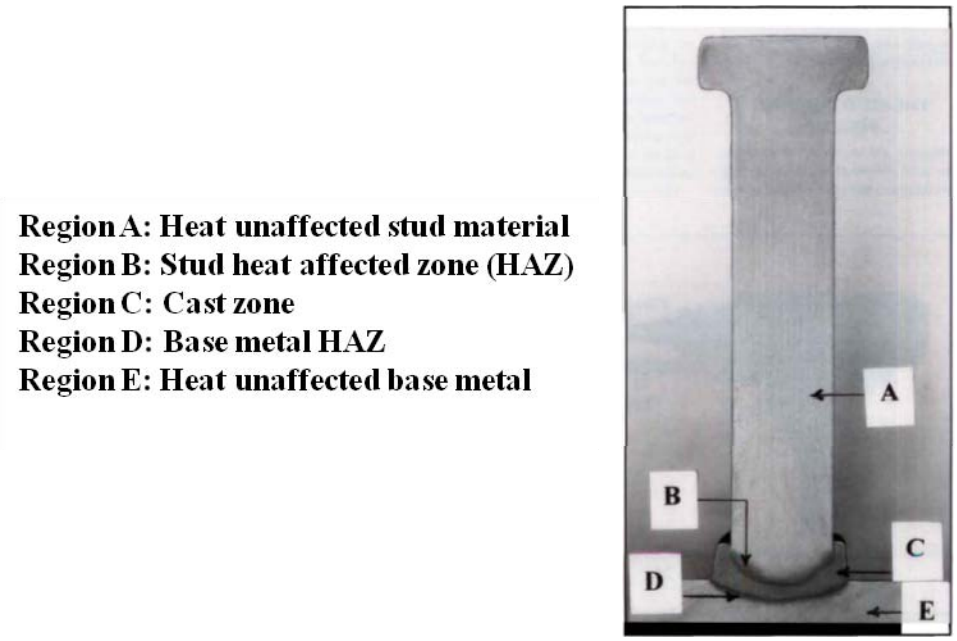

Figure 64. Illustration. Typical stud weld cross section (from Chambers 2001 [13]).

Based on the examinations of the failed specimens, it seemed likely that hydrogen induced cracking caused pre-cracks to be present before the onset of cyclic loading. Hydrogen induced cracking is also known as “cold” cracking and typically occurs within 24 to 48 hours after welding. It is caused by the presence of atomic or diffusible hydrogen, a susceptible brittle microstructure, and residual tensile stresses. It occurs only in welding processes where an arc plasma is present, which was the case for the stud welds in this experiment.

Due to the large amount of heat produced during this type of welding, water and hydrocarbon molecules are dissociated into atomic hydrogen, oxygen, carbon, etc. Hydrogen atoms can then become entrapped in the weld before diffusing out in a solid state after welding is complete. This

diffusion takes hours to days to complete, thereby producing localized ruptures when hydrogen atoms merge into molecules.

A chemical analysis was performed on two of the core samples to determine the average composition of the alloys found in the steel plate base metal. The analysis of the steel plate, likely A572 Grade 50 steel, revealed a rather high carbon equivalent of roughly 0.50%. A carbon equivalent of this level could have decreased both the weld quality and the ductility in the steel plate.

The lack of weld consistency and quality was apparent in the large differences between two sets of Vickers hardness tests performed on the HAZ of the stud and steel plate. Tests on one of the failed studs revealed that although the HAZ of both metals had borderline high hardness values, they were roughly equal, which is likely representative of those studs that did not fail. However, in another set of tests the HAZ of the steel plate had a large hardness value which was nearly twice that of the stud HAZ. Excessive HAZ hardness can be indicative of the high carbon equivalent found in the steel plate. This excessive hardness may have accelerated fatigue crack growth in the steel plate.

Select cross sections of the stud welds were polished, etched, and examined under a scanning electron microscope. These cross sections showed distinct changes in crack morphology, from the jagged hydrogen induced pre-cracking to the smooth fatigue crack that propagated independent of the microstructure. An example of a cross section of a failed stud is presented in Figure 65.

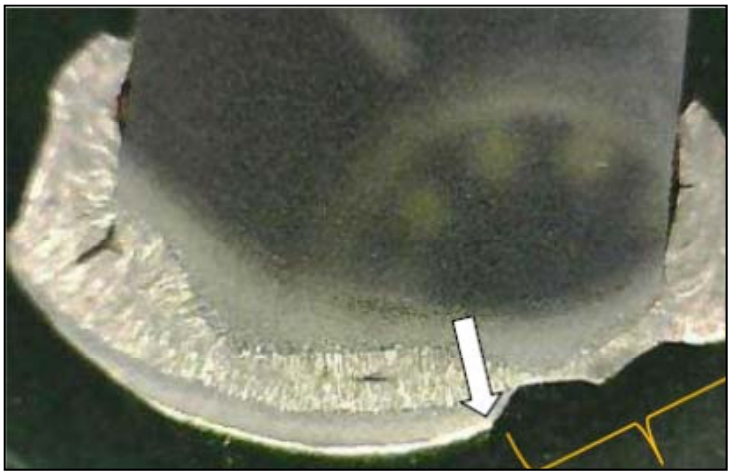

Figure 65. Photo. Cross section of shear stud weld showing change in crack morphology.

The arrow in Figure 65 signifies the location where the crack changes from a fatigue crack to the hydrogen induced pre-existing crack. To the left of the arrow, the failure surface is smooth indicating fatigue crack growth during the cyclic loading. To the right of the arrow, the failure

surface is more rough and jagged, which would indicate hydrogen induced pre-cracks which were present prior to the cyclic loading. These findings are similar to those observed in Figure 62 and Figure 63. The porosity and slag inclusions seen in the weld should also be noted, further demonstrating the poor weld quality.

Figure 66 presents a cross section of a core sample in which the stud remained intact. Recall that this stud was located near midspan and thus experienced reduced shear loading. The arrow in this figure indicates the ductile failure initiation in the stud HAZ, which is the preferred failure mode of a stud with good quality welding. There are also no porosities or slag inclusions seen in this cross section. It should be noted that although this weld is considered adequate, there is excessive flash (cast zone) shown on the right side of this weld. Excessive flash was found to be present in other stud welds as well.

Figure 66. Photo. Cross section of adequate shear stud weld.

Based on the entire stud weld forensic assessment, it is apparent that pre-existing flaws resulting from the poor quality of stud welds contributed to the failure of the conventional connection specimen. Specifically hydrogen induced cracks, excessive flash, and slag inclusions contributed to the poor weld quality. Cyclic load induced crack growth was accelerated by the pre-existing cracks and the excessive HAZ hardness. The large amounts of fretting between the fracture surfaces made it difficult to determine at what stage of loading the failures occurred. For future composite bridge studies, it is recommended all shear studs be welded and inspected according to AASHTO/AWS D1.5M/D1.5:2010 Bridge Welding Code [14] prior to any testing.

RESTRAINED SHRINKAGE CRACKING OF FIELD-CAST GROUTS

The field-cast haunch situated between the precast girder and precast deck panels presents an ideal situation for assessing the restrained shrinkage cracking behavior of the conventional grout

and the UHPC. The cracking of the haunch of each specimen was assessed after the specimen was prepared for cyclic testing. As such, the assessment of the UHPC was first completed three weeks after the UHPC had been cast. Note that the precast elements were four weeks old at the time of the UHPC casting. Continued assessment of the UHPC was then completed periodically to determine whether additional shrinkage cracking had occurred and/or whether deterioration due to cyclic loading was occurring. Neither behavior was apparent during the eight weeks of cyclic loading.

The assessment of the conventional grout was first completed 18 weeks after the grout had been cast. Note that the grout was cast when the precast elements were six weeks old. The assessment of the conventional grout was then completed periodically throughout the cyclic testing up through an age of 28 weeks after grout casting.

The cracking observed on the north face of the haunch of each specimen was recorded. Note that the exposed haunch on the UHPC composite connection specimen was 101.6 mm (4 inch) tall, and the exposed haunch on the conventional composite specimen was 76.2 mm (3 inch) tall. In both cases, the total exposed length of haunch was 12.19 m (40 feet). Also, note that the 6 m (19.75 foot) long precast deck panels were joined at midspan by a 152.4 mm (6 inch) wide UHPC non-contact lap splice connection.

Figure 67 shows the cracking observed on the north face of the haunch of the UHPC composite connection specimen. These cracks were not visible with the naked eye. They were identified through the use of a volatile alcohol-based spray which acted as a penetrating fluid allowing crack indications to temporarily become apparent on the surface of the haunch. For reference, the illustration also includes vertical divisions on 152 mm (6 inch) intervals and a horizontal division at midheight of the exposed portion of the haunch.

A portable optical microscope was used to measure the width of these cracks. All observed cracks expressed widths smaller than the minimum observable size, indicating that the cracks were smaller than 0.008 mm (0.0003 inch) wide. The observed cracking pattern did not change during the cyclic testing, indicating that this shrinkage cracking had stabilized prior to the UHPC achieving a compressive strength of 152 MPa (22.1 ksi) at 21 days after casting.

Figure 68 shows the cracking observed the north face of the haunch of the conventional connection specimen on. Given the poor grouting in the east end of the haunch, shrinkage cracking in this region is not considered within this portion of the study. The shrinkage cracks in this specimen were visible with the naked eye. The use of the volatile alcohol-based spray did not lead to the identification of any additional cracks. For reference, the illustration also includes vertical divisions on 152 mm (6 inch) intervals and a horizontal division at midheight of the exposed portion of the haunch.

In general, the shrinkage cracks observed of the north face of this haunch were measured to be approximately 0.1 mm (0.004 inch) wide. Some cracks on the east end of the specimen were observed to widen during the cyclic loading; however, this widening is attributed to cyclic deterioration of the connection, not increased shrinkage of the grout. Cracks observed elsewhere in the haunch did not widen during cyclic loading.

Photographs of the cracks observed in the haunches of the test specimen are illustrative of the type of cracks observed. Figure 69 shows a shrinkage crack on the north face of the haunch of the conventional grout specimen near the west end of the girder. The shrinkage crack is immediately to the right of the pencil mark indicating its location, and to the left of the penny which is provided for scale. Figure 70 shows two of the cracks in the UHPC haunch, also on the north face of the haunch near the west end of the girder. These two cracks are adjacent to the pencil marks but cannot be seen in the photo due to their small widths. For comparison, Figure 71 provides a photograph of the side of the precast deck where the small width map cracking of the surface of the precast concrete is apparent. This sort of cracking is common in conventional concrete and is related to the drying shrinkage of the cementitious paste.

Ignoring the regions of the UHPC haunch which were not fully restrained by the precast girder and deck elements, it was determined that the shrinkage cracks in the UHPC haunch were spaced at approximately 100 to 135 mm (4 to 5.3 inch). Under the assumption of a 100 mm (4 inch) crack spacing and 0.008 mm (0.0003 inch) wide cracks, a total of 75 microstrain of shrinkage can be assumed to be displayed within the cracks. Any remaining shrinkage strains would have been carried within uncracked regions of the UHPC, thus indicating that the strains in this area of the haunch did not surpass the tensile cracking strain of the UHPC.

Ignoring the regions of the conventional grout haunch which were not fully restrained by the precast girder and deck elements, it was determined that the shrinkage cracks in this haunch were spaced at approximately 135 to 270 mm (4.3 to 10.6 inch). Under the assumption of a 270 mm (10.6 inch) crack spacing and 0.1 mm (0.004 inch) wide cracks, a total of 375 microstrain of shrinkage can be assumed to be displayed within the cracks. Any remaining shrinkage strains would have been carried within uncracked regions of the grout, thus indicating that the shrinkage strains in this area of the haunch did not surpass the tensile cracking strain of the grout.

Comparing the results from the two test specimens, it is apparent that both the non-shrink conventional grout and the UHPC expressed restrained shrinkage cracking. The shrinkage of the conventional grout resulted in cracks that were visible with the naked eye and amounted to approximately 375 microstrain within cracks of heavily restrained regions. The shrinkage of the UHPC did not result in naked-eye visible cracks, and amounted to approximately 75 microstrain of shrinkage within cracks of the heavily restrained regions. Potential factors leading to the reduced shrinkage cracking damage in the UHPC may include reduced shrinkage of the UHPC, greater tensile cracking strength of the UHPC, and/or tensile creep relief of the UHPC during shrinkage.

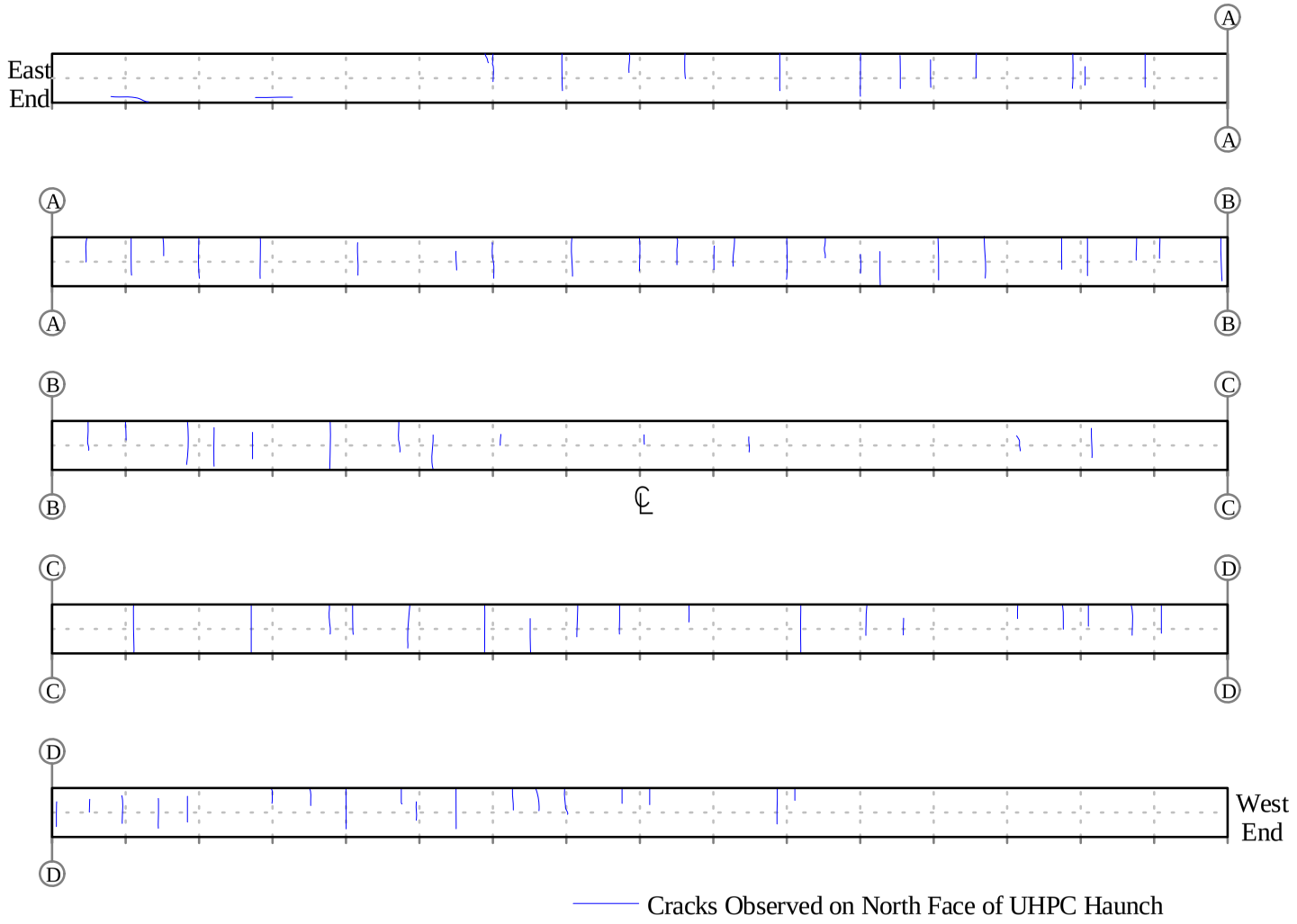

Figure 67. Illustration. Shrinkage cracking observed in haunch of UHPC composite connection specimen prior to start of cyclic testing.

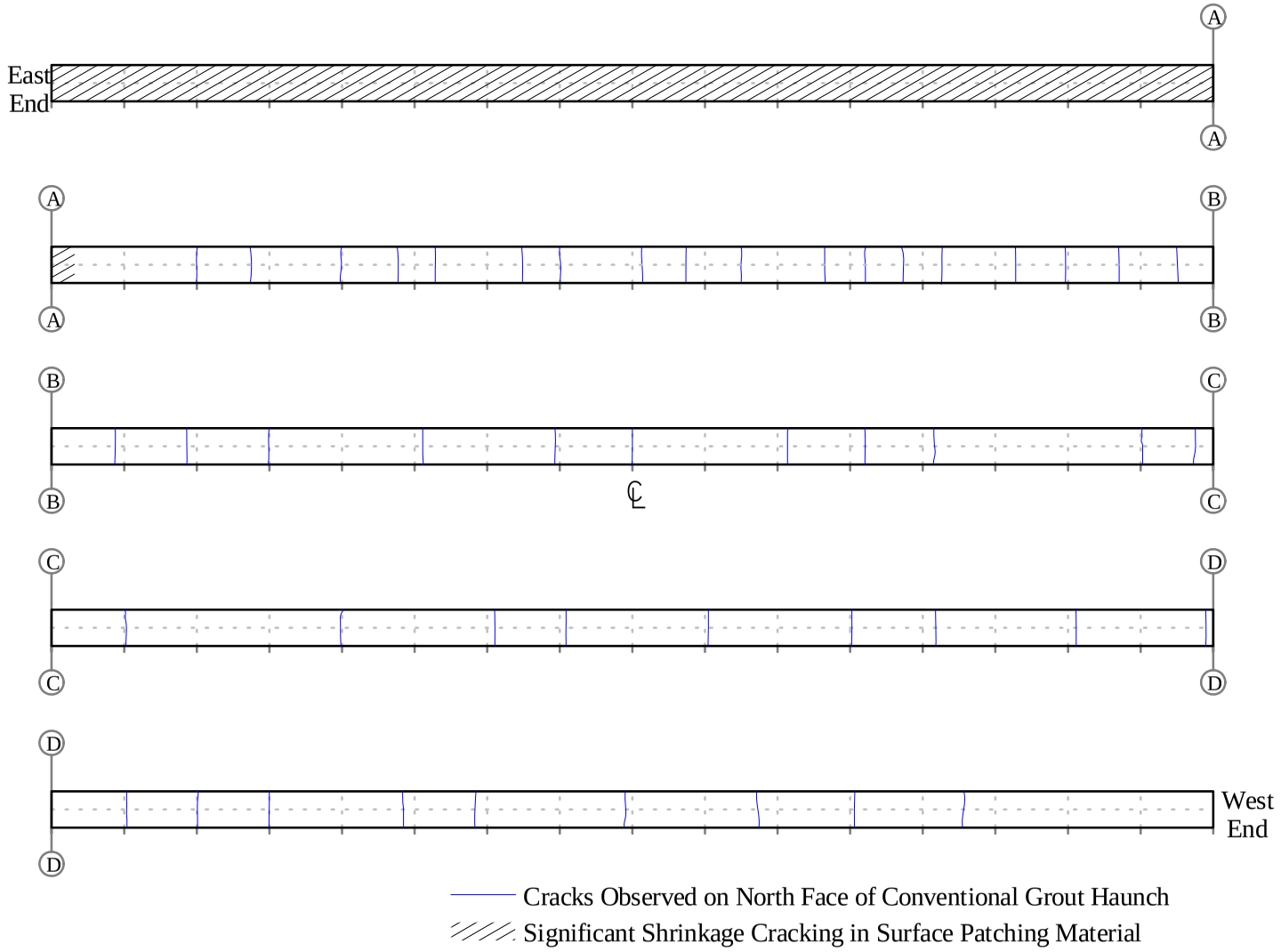

Figure 68. Illustration. Shrinkage cracking observed in haunch of conventional composite connection specimen prior to start of cyclic testing.

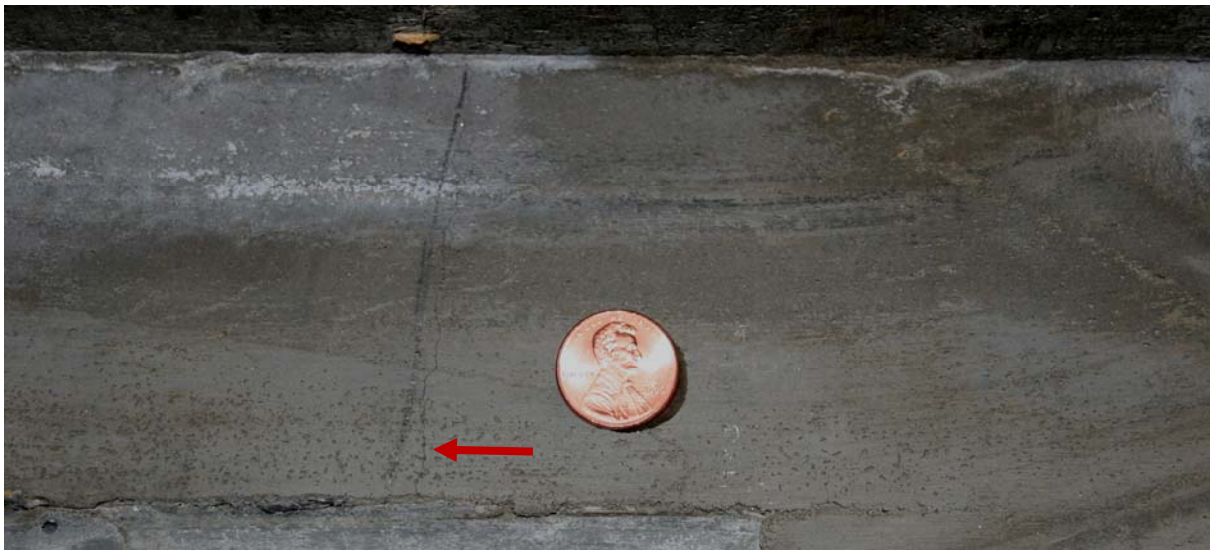

Figure 69. Photo. Shrinkage crack in haunch on north face near west end of conventional grout test specimen.

Figure 70. Photo. Shrinkage cracks in haunch on north face near west end of UHPC test specimen.

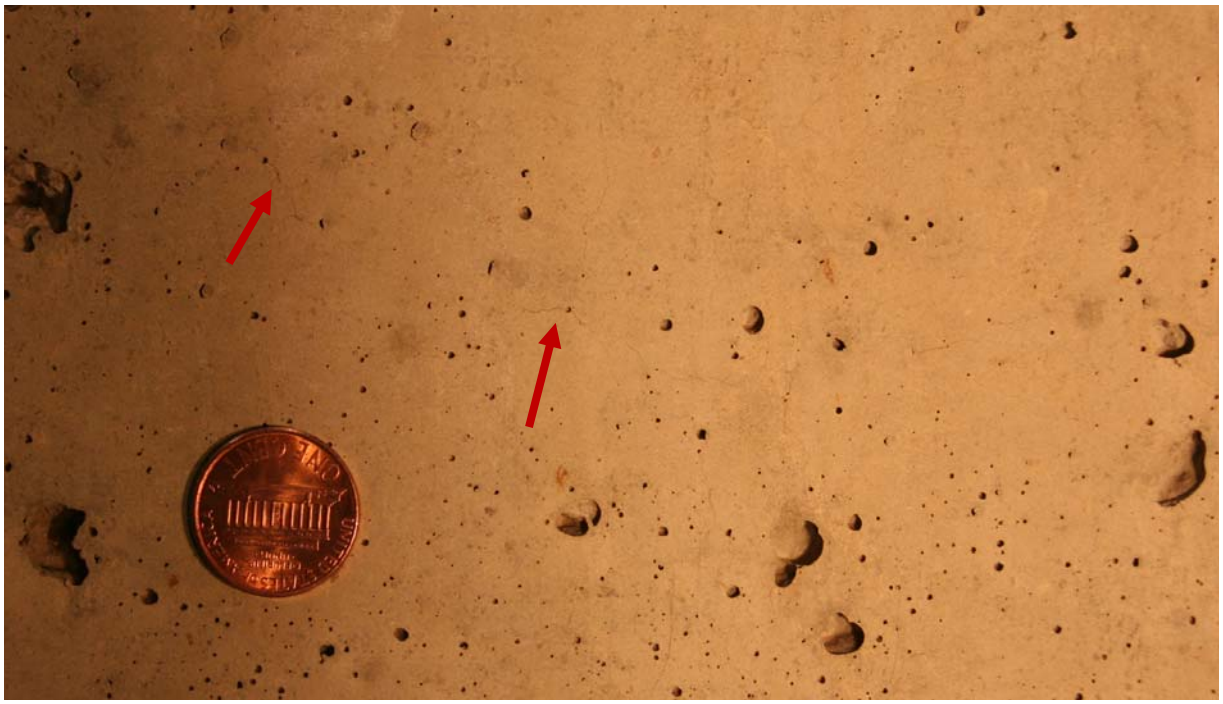

Figure 71. Photo. Surface finish and shrinkage cracks on formed side of precast concrete deck panel.

CHAPTER 6. CONCLUSIONS AND RECOMMENDATIONS

INTRODUCTION

The research program discussed herein focused on assessing the structural performance of a novel UHPC composite connection for joining precast concrete deck panels to supporting girders. Conclusions, recommendations, and a proposed direction for future research are presented below.

CONCLUSIONS

The following conclusions are presented based on the research presented in this report.

1. Field-cast UHPC is capable of appropriately completing the composite connection between precast deck panels and supporting bridge girders.
    a. The novel composite connection can withstand loads greater than those required by the AASHTO LRFD Bridge Design Specifications[1].
    b. The novel composite connection displayed performance which surpassed the performance of the companion test specimen with conventional composite connection details.
    c. Monolithic, field-cast UHPC within a composite connection was demonstrated to be capable of carrying at least 1.16 MPa (168 psi) of cyclic horizontal shear stress through more than 5 million cycles of loading.
    d. Monolithic, field-cast UHPC within a composite connection was demonstrated to be capable of carrying at least 5.44 MPa (789 psi) of static horizontal shear stress.
2. Construction of bridge systems using the field-cast UHPC composite connection can be completed using technologies and materials already available in the U.S. bridge market.
    a. With this novel connection system, the haunch connection becomes simplified, with no interference between the girder composite connectors and the precast deck panel reinforcement.
    b. Neither precast deck panel full-depth blockouts nor clustering of girder connectors is required. Along the length of the girder, an exposed bottom mat of deck reinforcement and evenly spaced girder connectors provide for the composite connection. Extended rebar in the concrete girder and shear studs in the emulated steel girder were demonstrated to perform appropriately at the girder/haunch horizontal shear interface.
    c. The field-cast UHPC was demonstrated to easily flow for 6.1 m (20 feet) through the designed connection, leading to simultaneous emanation of UHPC from periodic vent holes along the length of the deck. With a practical limit of 3 m (10 feet) on the spacing of deck-level connections between precast panels, placing UHPC into a haunch connection should not be a hurdle.

3. Field-cast UHPC in a composite connection displays limited shrinkage cracking within fully-restrained areas of a haunch.
    a. Tight cracks which were smaller than 0.008 mm (0.0003 inch) wide and not visible to naked eye were observed at approximate spacing of 100 to 135 mm (4 to 5.3 inch) within the UHPC specimen haunch. These cracks could amount to up to 75 microstrain of shrinkage, with any other shrinkage strains being carried through the inherent tensile strength of the UHPC.
    b. Non-shrink cementitious grouts commonly used in bridge construction can exhibit significant shrinkage and can crack when cast in association with restrained components. The non-shrink grout used in the conventional connection specimen displayed visible restrained shrinkage cracks in the haunch. A total of at least 375 microstrain of shrinkage was observed within cracks on the surface of the haunch in restrained regions of the conventional grout test specimen.

4. The intentionally-roughened surface at the top of a precast concrete girder provides good resistance to interface shear through surface bonding and physical interlocking with the haunch grout.
    a. This interface did not debond under cyclic loading in either test specimen. The highest cyclic load range induced a horizontal shear stress range of 0.398 kN/mm (2.275 kips/inch) along this interface for over 5 million cycles.
    b. The interface did not debond under static loading in either test specimen. The peak induced horizontal shear load in the UHPC connection was 2.1 kN/mm (12.0 kips/inch), and the peak induced horizontal shear load in the conventional grout connection was 1.83 kN/mm (10.45 kips/inch). For comparison, the provisions in section 5.8.4 of the LRFD Bridge Design Specifications indicate that the concrete cohesion component of the resistance of this interface to horizontal shear would be 0.882 kN/mm (5.04 kips/inch).

5. UHPC can exhibit significantly higher compressive strength than conventional grouts.
    a. Under ambient curing conditions, the UHPC compressive strength at 21 days surpassed 150 MPa (21.8 ksi), at 97 days surpassed 185 MPa (26.8 ksi), and at 270 days surpassed 200 MPa (29.0 ksi).
    b. The conventional grout compressive strength at both 28 and 106 days was approximately 55 MPa (8.0 ksi).

RECOMMENDATIONS

Based on the findings of this study, a set of limited recommendations can be provided to practitioners and researchers interested in engaging the UHPC composite connection detail. These recommendations are conceptual guidance, not formal design specifications.

Figure 72 provides generic, conceptual composite connection details relevant to the research presented herein. The first and third details are very similar to the details tested in this study. Reliance on the tensile and shear performance of the field-cast UHPC is a prerequisite for engaging these concepts. The second and fourth details require lesser reliance on the tensile and

shear performance of field-cast UHPC, while still engaging the rheological properties of the UHPC. The second and fourth details do not completely eliminate connector interference issues, but instead marginalize this issue by providing large spaces for the intermeshing of the connectors.

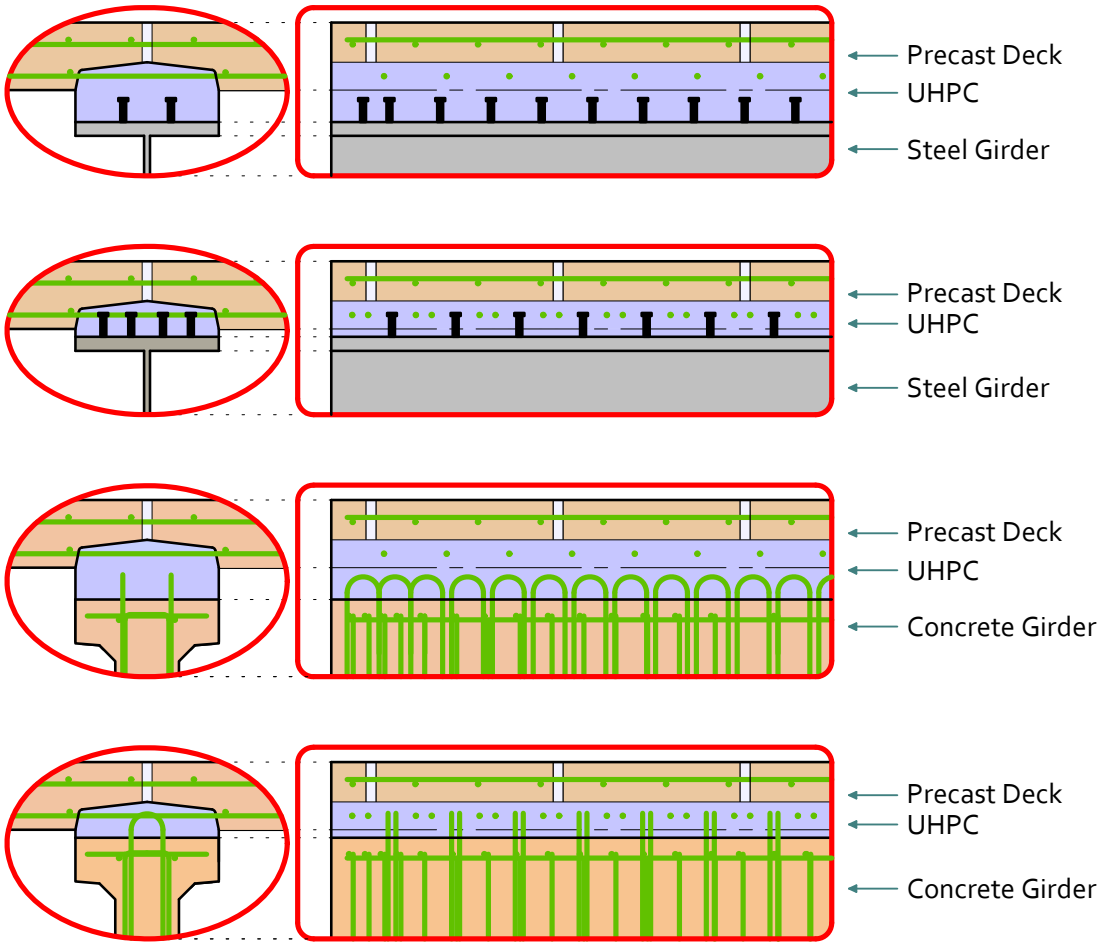

Figure 72. Illustration. Example composite connection details which emanate from the research presented herein.

Existing provisions of the AASHTO LRFD Bridge Design Specifications[2] should be retained and engaged as appropriate in the design of this detail. Relevant provisions include those in 6.10.10 pertaining to the design of shear stud connectors on a steel girder and those in 5.8.4 pertaining to the design of the connection to precast concrete girders.

It must be recognized that requirements for extension of girder composite connectors into the deck will not be met if all aspects of this novel composite connection concept are engaged.

Roughening of the interface surfaces of precast concrete elements provides significant benefit in terms of enhancing the interface resistance to horizontal shear stresses. Roughening of the top flange of a precast concrete girder, as is common practice, was demonstrated to provide good

interface shear performance. Precasting a roughened surface into interface on the underside of the precast concrete deck panel would likely provide similar benefit. A roughened surface at this location would decrease the demand on the bottom mat reinforcing bars crossing this interface and would likely disperse shearing stresses more uniformly into the connecting elements. Potentially, this could delay the type of local horizontal shear failures observed in the concrete deck at the transverse rebar locations at the conclusion of the UHPC specimen static test to failure.

The test results indicate that using greater numbers of smaller bars for the bottom mat reinforcement of the deck is likely beneficial. Larger bars create larger local stresses in the conventional deck concrete, potentially resulting in local failure of that concrete. Similarly, providing longitudinal reinforcement adjacent to the blockout and immediately above the bottom mat of reinforcement is also likely beneficial to the performance of the overall connection.

The horizontal shear resistance of the UHPC must be explicitly considered when designing this type of connection. This test program demonstrated that the monolithic UHPC in the connection was capable of carrying at least 1.16 MPa (168 psi) of cyclic horizontal shear stress and at least 5.44 MPa (789 psi) of static horizontal shear stress. Determination of horizontal shear capacity of any detail must consider the minimum shear plane engaged within the detail. This minimum shear plane is heavily dependent on the geometry of the connection and the arrangement of the composite connection connectors emanating from the adjoining prefabricated elements. It may be possible to increase the minimum shear plane through careful arrangement of these connectors.

Quality control is necessary to insure that the prefabricated components are staged properly and that the field-cast UHPC is mixed and cast properly. As compared to conventional concrete, the greater reliance on the inherent structural performance of UHPC requires that the UHPC is mixed and cast according to the design. Field modifications of predefined mixing proportions or casting procedures are not advised. UHPC rheological indicators are frequently used to ensure appropriate mixing and can predict likely success in filling the hidden composite connection voids which are inherent to this novel connection detail. It is advisable to ensure that the UHPC emanating from vent holes in the deck has retained an appropriate rheology and contains an appropriate volume of steel fiber reinforcement.

FUTURE RESEARCH

Although this research project has demonstrated the viability of the UHPC composite connection concept, the limited scope did not allow for development of an LRFD-based formulation of detailed design guidance. Additional experimental and analytical investigations are needed in order to fully develop this concept into a set of stand-alone design recommendations.

Further study in this topic area is currently underway within the FHWA Infrastructure Research and Development Program. A study investigating the limits of stud clustering for steel girder composite connections was initiated in late 2011. As this study matures, it is likely that it will be expanded to investigate performance measures relevant to the novel UHPC composite connection detail concept.

The development of detailed guidance on the novel UHPC composite connection detail concept will require investigation of a number of topics. These include:

- determination of the ultimate horizontal shear capacity of UHPC in a composite connection configuration,
- assessment of the propensity of the UHPC in this detail to suffer fatigue damage, and possibly the determination of limits on the fatigue resistance,
- determination of the impact that the higher elastic modulus of UHPC might have on the fatigue resistance of steel stud connectors which attach the UHPC to the top flange of a steel girder,
- determination of the fatigue and static ultimate capacity of bottom mat reinforcing bars which bridge the interface between the field-cast UHPC and the precast concrete deck panel,
- determination of the appropriate cohesion factors for prediction of the bond capacity of UHPC cast against a roughened precast concrete surface, and
- determination of UHPC mix design parameter impacts on the performance of the composite connection.

ACKNOWLEDGEMENTS

The research which is the subject of this document was completed through the Transportation Pooled Fund Program via project TPF-5(217) *Structural Testing of UHPC Connections Between Precast Bridge Deck Elements*. The research was funded by the U.S. Federal Highway Administration and the New York State Department of Transportation. In-kind support was also provided by NYSDOT, the Precast Concrete Association of New York, and Northeast Prestressed Products, LLC. The author gratefully acknowledges this support.

The research project discussed herein could not have been completed were it not for the dedicated support of the federal and contract staff associated with the FHWA Structural Concrete Research Program. Special recognition goes to Dr. Matthew Swenty, Dr. Gary Greene, Dr. Linfeng Chen, each of whom provided structural engineering support throughout various phases project, and to Jason Provines who assisted with the assessment and documentation of the shear stud weld failures. Recognition also goes to Tim Tuggle, Brian Story, Kevin Deasy, and Paul Ryberg, all technicians in the FHWA Structural Testing Laboratory, for their assistance in completing the experimental testing program.

REFERENCES

1. Graybeal, B., "Construction of Field-Cast Ultra-High Performance Concrete Connections," U.S. Department of Transportation, Federal Highway Administration, FHWA-HRT-12-038, April 2012, 8 pp.
2. AASHTO, *AASHTO LRFD Bridge Design Specifications, 4th Edition*, American Association of State Highway and Transportation Officials, 2009.
3. Graybeal, B., "Ultra-High Performance Concrete," U.S. Department of Transportation, Federal Highway Administration, FHWA-HRT-11-038, March 2011, 8 pp.
4. Graybeal, B., "Material Property Characterization of Ultra-High Performance Concrete," Federal Highway Administration, Report No. FHWA-HRT-06-103, August 2006, 186 pp.
5. Crane, C.K., "Shear and Shear Friction of Ultra-High Performance Concrete Bridge Girders," Ph.D. Dissertation, Georgia Institute of Technology, August 2010.
6. Hegger, J., S. Rauscher, and C. Goralski, "Push-Out Tests on Headed Studs Embedded in UHPC," *Proceedings*, 1st International Symposium on Ultra High Performance Concrete, Kassel, Germany, September 2004, pp. 425-434.
7. Hegger, J., and S. Rauscher, "UHPC in Composite Construction," *Proceedings*, 2nd International Symposium on Ultra High Performance Concrete, Kassel, Germany, March 2008, pp. 545-552.
8. Jungwirth, J., G. Seidl, V. Schmitt, and D. Ungermann, "Utilization of UHPC in Composite Structures – Lightweight Composite Structures (LCS)," *Proceedings*, 2nd International Symposium on Ultra High Performance Concrete, Kassel, Germany, March 2008, pp. 887-894.
9. ASTM C39, "Standard Test Method for Compressive Strength of Cylindrical Concrete Specimens," American Society for Testing and Materials Standard Practice C39, Philadelphia, PA, 2001.
10. ASTM C496, "Standard Test Method for Splitting Tensile Strength of Cylindrical Concrete Specimens," American Society for Testing and Materials Standard Practice C496, Philadelphia, PA, 2002.
11. Graybeal, B., "Practical Means for the Determination of the Tensile Behavior of Ultra-High Performance Concrete," *Journal of ASTM International*, V. 3, No. 8, December 2006, 9 pp.
12. ASTM C109, "Standard Test Method for Compressive Strength of Hydraulic Cement Mortars (Using 2-inch or [50-mm] Cube Specimens)," American Society for Testing and Materials Standard Practice C109, Philadelphia, PA, 2011.
13. Chambers, H.A., "Principles and Practices of Stud Welding." *PCI Journal*, pp. 46-58. 2001.
14. AASHTO, *Bridge Welding Code, Report AASHTO/AWS D1.5M/D1.5:2010, 6th Edition,* American Association of State Highway and Transportation Officials, American Welding Society, Washington D.C., 2010.

APPENDIX A

Forensic Assessment of Shear Stud Failure

Yoni Adonyi, Ph.D., P.E.
Omer Blodget Professor of Welding and Materials Joining Engineering
LeTourneau University

SUMMARY

Select Drawn Arc Stud welds were examined using metallography and fractography methods. Our analysis confirmed most conclusions made by FHWA experts regarding the stud weld failure mechanism, but also revealed the existence of pre-existing flaws. Based on the amount of rust on the fracture surfaces, we believe some studs became partially detached early – due to hydrogen cracking likely within 48 hours from welding – especially on the first four rows on the East End. Other areas showing hydrogen-induced cracking and poor quality welds were found in transverse cross sections. The consequent fretting between the detached rust particles and the divot surface during cyclic loading did indeed destroy some of the fractographic evidence of this early failure.

While the role of early failure of the inadequate stud welds on overall test performance is unclear, improvement in stud weld quality and repeatability could be accomplished in the future by completing Weld Procedure Specification before stud welding on the part. Performing hammer knock-out destructive testing on all suspect studs after 48 hours from welding and re-welding the poor quality ones would ensure better shear connection. Following the instructions on Stud Welding, Section 7, AASHTO/AWS D1.5M/D1.5:2010 Bridge Welding Code[(14)] is recommended.

BACKGROUND

Nine (9) broken and cored specimen were received from FHWA R&D Labs in McLean, VA. While the samples were not identified, they reportedly were removed from a steel/concrete composite test beam where the 3/4" (18.75 mm) diameter studs were used as shear connectors between a ¾" (19 mm) thick steel plate and the reinforced concrete. See Fig. A1 and A2 reproduced from Figure 57 in main body of report.

Fig A1. Reproduction of a portion of Figure 57 from main body of report.

After fatigue cycling and monotonic overload, almost all 72 studs were found to have failed, with the exception of 13 that remained attached on the midspan side, arrows.

Based on visual examination, the 18 rows in columns of 4 studs were categorized in six modes of failure, as shown in Fig. A2.

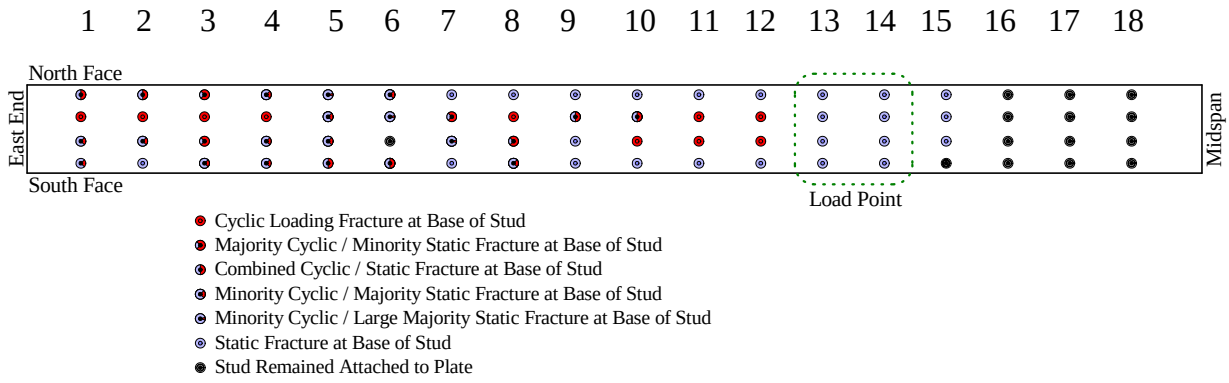

Fig. A2. Reproduction of a portion of Figure 57 from main body of report.

Note the extensive amount of oxidation shown in Fig. A3. This figure shows Rows 1 and 2 from Fig. A2.

Fig A3. Close-up of the detached stud welds, so called 'divots'.
[Reproduced from Figure 56 of main body of report.]

The view of the samples received at LETU is shown below. While the exact origin of the stud welds was unclear, the approximate column and row numbers are shown.

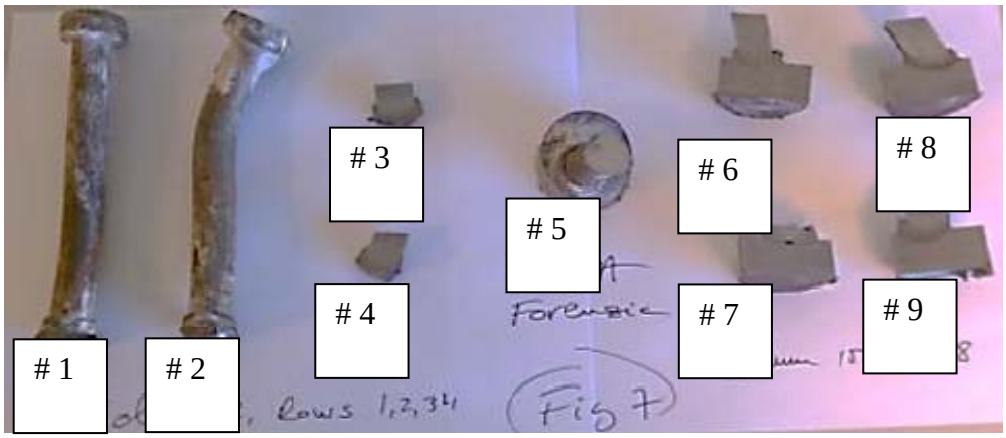

Fig. A4. View of the ¾" studs, core and fracture surfaces received, showing the LETU ID#.

Problem Definition

It is our understanding that the stud welding procedure was not qualified or tested per AWS D 1.5M: 2010 and the sequence of welding was also unknown. Nevertheless, the poor and inconsistent quality of the stud welds was obvious even at low magnification, as evidenced by lack of heat-affected zone (HAZ) symmetry, excessive flash and root porosity, as well as ceramic inclusions from the ferrule. As the fractures appeared to follow the HAZ/base metal boundary, the possible role of stud weld quality on fatigue failure was to be established.

OBJECTIVES

The purpose of this work was to independently assess the stud weld failure modes and recommend corrective action if their quality might have affected the performance of the concrete/steel structure fatigue test.

METHODOLOGY

Select fracture surfaces were examined using the Scanning Electron Microscope. Metallography samples were mounted, polished, etched, and subsequently examined using optic and electron microscopy. Hardness testing was also performed on two samples.

RESULTS AND DISCUSSION

To set the stage for this analysis, a brief overview of Drawn Arc Stud Welding and Hydrogen-Induced Cracking (HIC) follows, as regular stud welding is not normally susceptible to HIC.

1. Drawn Arc Stud Welding Overview

Stud welding belongs to the group of Electric Resistance Welding (ERW) Processes in which Joule heating is used to melt adjoining parts. Typically, very high currents (10-20 kA) are applied for very short times (5-10 ms) to create a 'nugget' between the stud and the base metal, at which point an axial forging pressure is applied to the stud in order to consolidate the weld. Differently from the ERW process, when the stud diameter exceeds ½" (3/4" in this case), more energy is required to make a weld; hence an electric arc plasma has to be established instead of only resistive heating. Accordingly, the Drawn Arc Stud welding uses a welding gun capable of making an initial contact between the stud and the plate, followed by a retraction (drawn back) of the stud by about ¼" to establish an electric arc. A few milliseconds later, the stud is plunged back toward the plate, ejecting most molten and resolidified metal in the process. Hence, this becomes a brief arc weld without any shielding gas.

A small ceramic cylinder called a "ferrule" is used to contain the molten metal, as well as to protect it from atmospheric contamination. After welding is completed, this ceramic typically breaks off like slag in Shielded Metal Arc welding upon cooling, as its Coefficient of Thermal Expansion (CTE) is much lower than the metal's. Accordingly, this type of stud welding can be as susceptible to hydrogen-induced cracking, slag inclusions, porosity and solidification cracking as any arc welding process such as SMAW or GMAW.

2. Hydrogen-Induced Cracking (HIC)

This type of cracking is also known as "cold" or "delayed" cracking because it typically takes one to two days to appear. It is known to be caused by the simultaneous presence of 1) atomic or diffusible hydrogen, 2) susceptible brittle microstructure and 3) presence of residual tensile stresses. It only occurs in welding processes where an arc plasma is present, capable at 30,000°F to dissociate water or hydrocarbons into atomic hydrogen, oxygen, carbon, etc. As part of this hydrogen can be entrapped in the weld, it can diffuse out in solid state after welding is complete, driven by solubility differences between phases. This diffusion takes hours to days, hence localized ruptures can start when hydrogen atoms merge into molecules.

3. Steel base plate analysis: chemical composition and metallography

Spectrographic analysis on the base metal included in the core samples #8 and #9 showed the following average composition, apparently of an A572 grade 50 steel:

C%	Mn%	S%	P%	Si%	Cr%	Ni%	Cu%	Mo%	Al%	V%	Nb%
0.26	1.11	0.007	0.008	0.18	0.11	0.15	0.26	0.04	0.03	0.04	0.006

The rest of residuals were: B=0.00025%, Co=0.010%, Ti=0.007%, Ca=0.0024%, W=0.012%

The carbon equivalent (IIW) calculation shows a CE= C +(Mn+Si)/6 + (Cr+Mo+V)/5+ (Cu+Ni)/15 value of CE=0.26+1.117/6+0.19/6+0.19/15=0.44+0.038+0.012=0.49%

This represents a rather high hardenability of CE ~ 0.50% and explains the reason for the high Vickers hardness found in some of the stud weld HAZ, plate side, Fig A5.

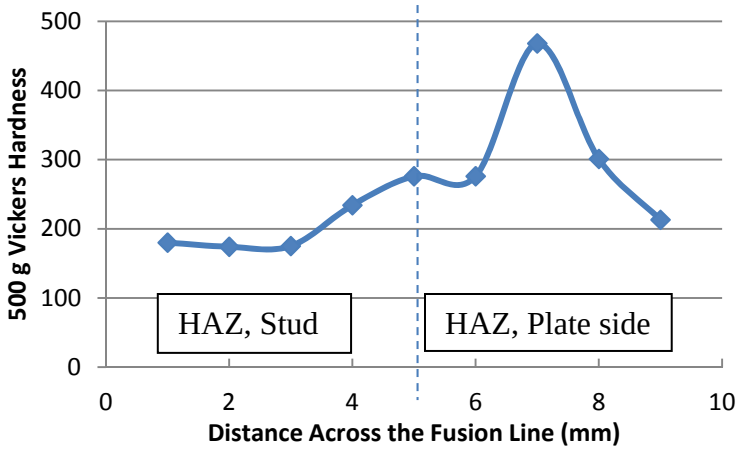

Fig A5. Hardness profile, LETU Sample # 3

However, to emphasize the inconsistencies in welding, the HAZ hardness distribution did not always show the spike, see Fig. A6 pertaining to Sample #4.

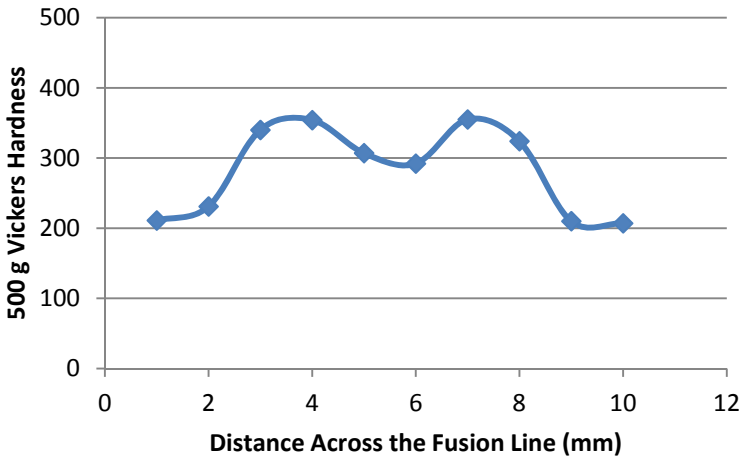

Fig. A6. Hardness profile across weld #4. Notice similar HAZ hardnesses on both the stud- and plates side of the stud weld.

In this case, both the stud and plate HAZ's had borderline high (350 HV) hardness, but were more even. It can be assumed that this HV profile was representative of those studs that did not fail.

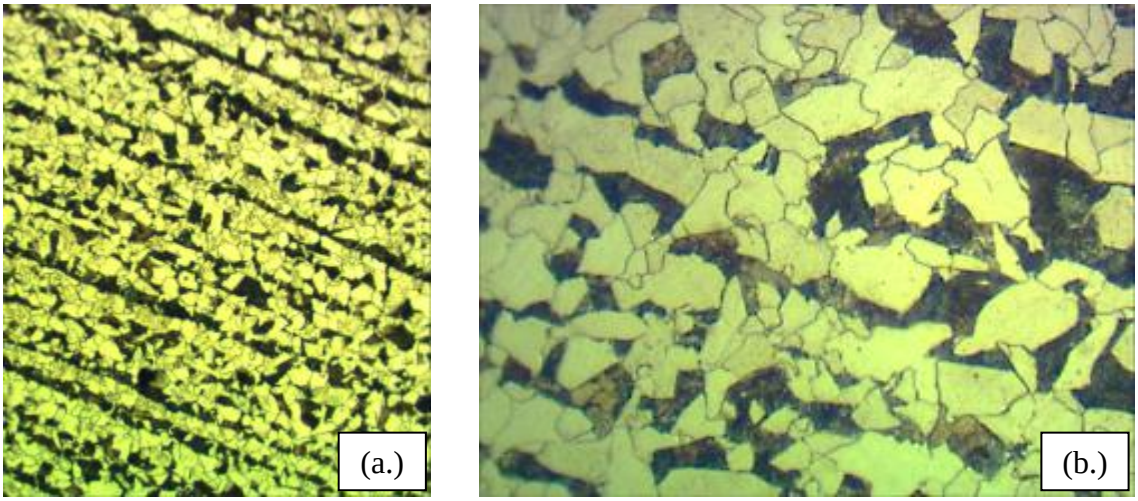

Fig A7. Base metal microstructure showing typical pearlite/ferrite microstructure, a) 100 X and b) 500 X magnification

Fractography

Several cross sections examined showed an abrupt change in crack morphology, from a typical jagged hydrogen-induced pre-existing crack to a smooth fatigue crack that propagated independent of microstructure.

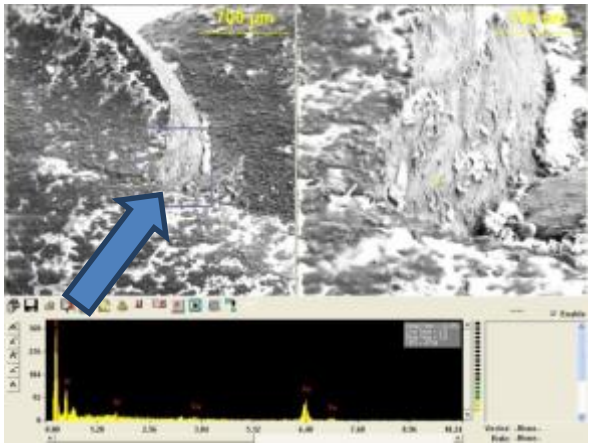

Fig. A8. SEM fractograph showing a transition between cleavage and fatigue type failure at arrow.

Metallography

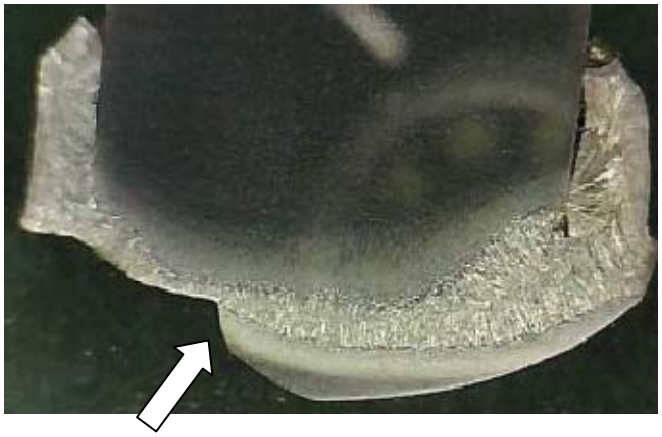

Fig. A9. The same transition in crack morphology as in Fig. A8, this time in a cross section, Sample S-2.

The initial fractured stud showing typical jagged hydrogen induced crack (pre-existing) to the left, turning into a smooth fatigue crack at the point highlighted by the arrow. Failure must have propagated from the left corner to the right corner.

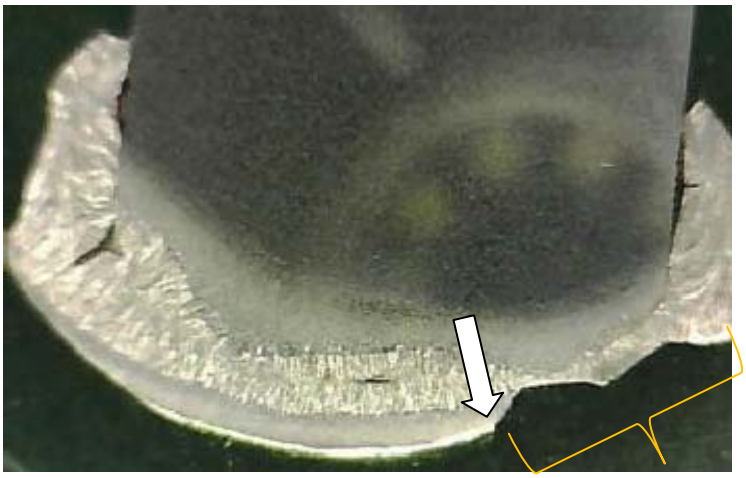

Fig. A10. Same as Fig. A9, this time Sample S-3.

Same scenario as in Sample S-2, with the pre-existing crack on the right, turning into a fatigue crack to the left at the point marked by the arrow. In this cross section the failure initiated to the left and propagated to the right. Also note the porosity and slag inclusions in the weld.

Fig. A11. Sample S-1. Asymmetrical, but adequate weld. Note ductile failure initiation near the stud HAZ, arrow, representing the preferred mode of failure for cases wherein the stud welds has good quality.

CONCLUSIONS

1. The average quality of most stud welds evaluated was inadequate, presenting excessive flash, root porosity and hydrogen induced cracking. Indeed, it appears that only 13 out of 72 studs (18%) remained intact after the final overload.

2. Pre-existing cracks and excessive HAZ hardness accelerated the fatigue crack growth. It is estimated that 38% of the studs (or 28 of 72) were already detached more than half of their cross section at the very start of testing, as also evidenced by the excessive rusting found around the divots. Discounting the surviving studs, this percentage is even higher at 47% or 28 / 59.

3. The fatigue crack propagation followed the stress redistribution path and did not have anything to do with the HAZ or base plate microstructure, as expected.

It is difficult to say how much these inadequate welds might have offset the entire assembly fatigue test results, as localized stresses were clearly different at each location. Nevertheless, because of the high percentage of stud welds showing pre-existing cracks, future stud welding should comply with Section 7, AASHTO/AWS D1.5M/D1.5:2010 Bridge Welding Code [14].

This page intentionally left blank.